博士論文

Formation and geotectonic implications for Low-pressure/High-temperature type metamorphic rocks in southwest Japan: Constraints on the Seto Inland Sea, Yamaguchi Prefecture

（低圧高温型変成岩の形成と地質構造区分の意義：山口県瀬戸内地域からの制約）

2025 年 9 月

LU ZEJIN

山口大学大学院創成科学研究科

Catalogues

List of Illustrations

1. Introduction

Convergent plate margins are characterized by the presence of high-pressure/low-temperature (High-*P/T*) and Low-pressure/High-temperature (Low-*P/T*) metamorphic rocks (Miyashiro, 1973). The High-*P/T* type Suo Belt and low-*P/T* type Ryoke plutono-metamorphic complex (Ryoke Belt, hereafter) are closely distributed in the Inner Zone of Southwest Japan (Fig. 1-1), although their metamorphic ages are different. In this manner, the traditional recognition of the zonal arrangement of SW Japan has classified every region into only one of the belts, based on the implicit assumption that each belt formed in different settings at different ages. Based on zircon U–Pb dating, Miyazaki et al. (2017) revealed that the Suo Belt in the Omuta area, Fukuoka Prefecture, northern Kyushu, underwent Low-*P/T* type metamorphism during the Cretaceous, similar to the Ryoke metamorphism. They concluded that the geographic trend of the Cretaceous Low-*P/T* type metamorphic field was oblique to the accretionary terranes in the Inner Zone of Southwest Japan. However, they have a rhetorical difficulty in defining Ryoke metamorphism because the Suo and Ryoke Belts are separated from each other in northern Kyushu, although the metamorphic rocks from the Suo Belt underwent Low-*P/T* metamorphism during the Cretaceous.

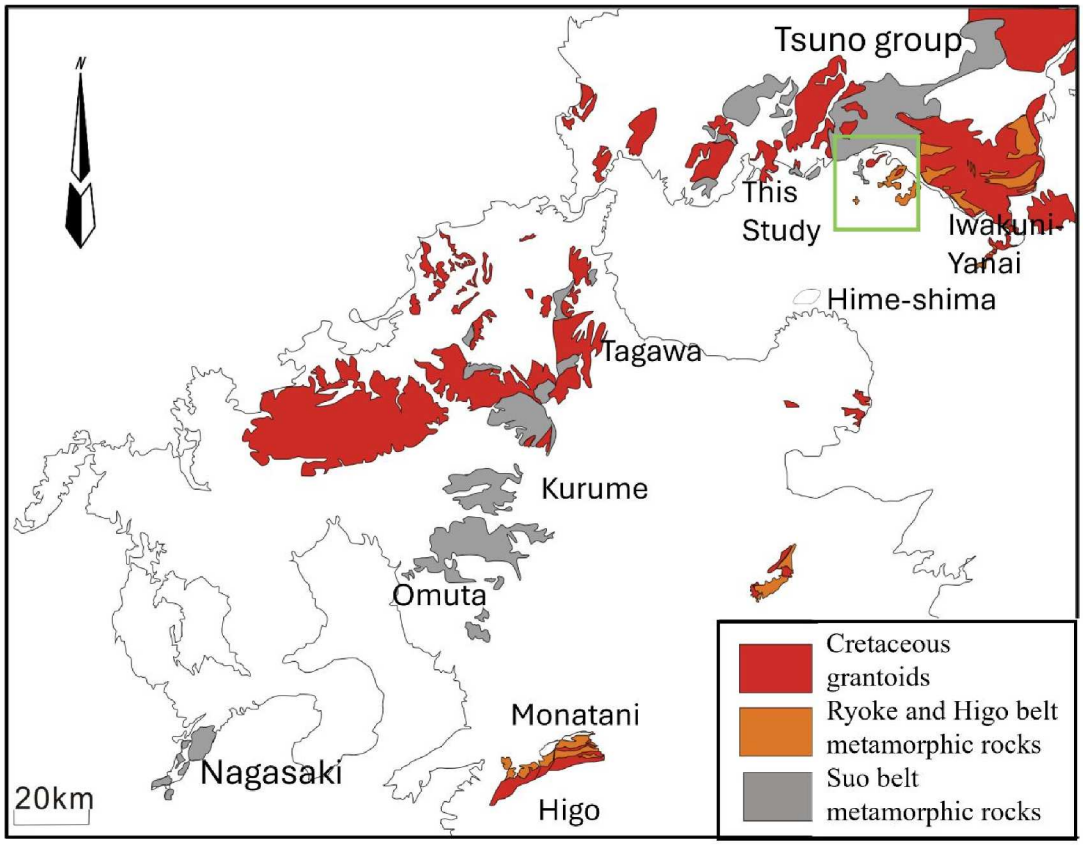

Fig. 1-1. Distribution map of the metamorphic rocks from the Ryoke Belt, the Higo Belt, the Suo Belt and the Cretaceous granitoids in the south Chugoku and north Kyushu areas. (modified from Geological Survey of Japan, AIST, 2024). The green square indicates the location of this study.

In Yamaguchi Prefecture, the Suo metamorphic rocks known as the Tsuno Group show the youngest zircon U–Pb age of ca. 260 Ma, which corresponds to the depositional age of the protoliths (Tsutsumi et al., 2000); its metamorphic age is thought to be Early Triassic (230–210 Ma) (Nishimura et al., 1989). The protoliths of the Tsuno Group (Suo Belt) are considered to belong to the Permian Nishiki Group (Akiyoshi Belt) (Nishimura, 1971). In contrast, the protolith of the Ryoke metamorphic rocks is considered to be of the Kuga Group, a Jurassic to Early Cretaceous accretionary complex belonging to the Mino-Tamba Belt (Higashimoto et al., 1983). These rocks underwent Low-*P/T* type metamorphism during the Cretaceous (Okudaira et al., 2000; Okudaira et al., 2001; Skrzypek et al., 2018). Geological information of Suo and Ryoke metamorphic rocks in Yamaguchi Prefecture is given in Table 1-1.

The Suo and Ryoke Belts are closely distributed in the southern part of the Yamaguchi Prefecture, particularly on the islets of the Seto Inland Sea. Beppu and Okudaira (2006) reported that the metamorphic rocks from Kasadojima Island underwent the Low-*P/T* type Ryoke metamorphism. In contrast, metamorphic rocks from Ozushima Island, located 6 km northwest of Kasadojima Island, belong to the Suo Belt (Fig. 1-2). This indicates that the boundary between the Suo and Ryoke Belts is located within this area (Fig. 1-2).

In this study, I describe the microstructure and metamorphic zonation of pelitic rocks from these areas using mineral assemblages and discuss the metamorphic *P-T* conditions. In addition, detrital zircon U–Pb dating was conducted to constrain the depositional ages of the protoliths, and biotite K–Ar age was identified with time for passing through the closure temperature of biotite. Compared with the other Suo Belt regions in Kyushu, it is crucial to emphasize that it belongs to the Ryoke belt, not only based on *P-T* conditions but also due to its spatial proximity. Comparison with Low-*P/T* type metamorphic rocks reveals the distribution and tectonic implications in south-west Japan. Furthermore, it

could contribute to the understanding of the Mesozoic geological developmental history of Japan. Table 1-2 shows mineral abbreviations following Warr (2021).

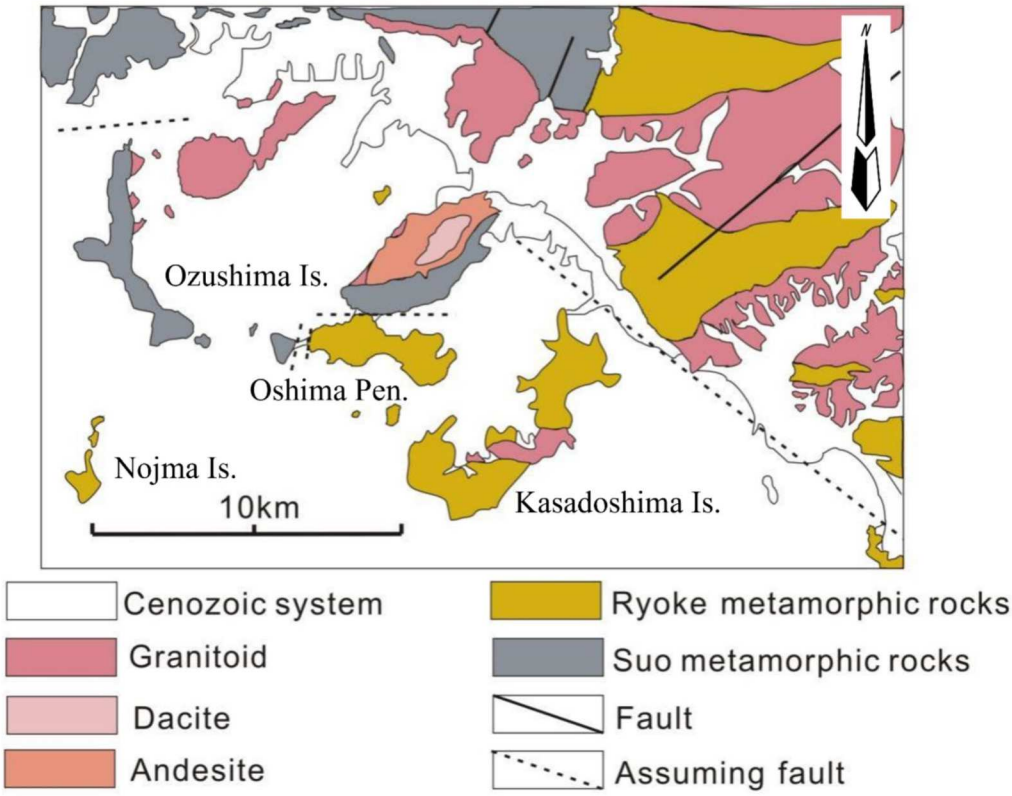

Fig.1-2. Geological map of southern Yamaguchi Prefecture (modified from Geological Survey of Japan, AIST, 2024).

Table 1-1! Geological information of Suo and Ryoke metamorphic rocks in Yamaguchi Prefecture.

	Suo	Ryoke
Protolith	Tsuno Group	Kuga Group
Depositional age	Late Permian	Jurassic
Metamorphic age	Early Triassic	Cretaceous

Table 1-2. Mineral abbreviations.

Ab	albite	Chl	chlorite	Ky	kyanite
Amp	amphibole	Cpx	clinopyroxene	Ms	muscovite
An	anorthite	Crd	cordierite	Or	orthoclase
And	andalusite	Crn	corundum	Pl	plagioclase
Bt	biotite	Grt	garnet	Qz	quartz
Cal	calcite	Kfs	K-feldspar	Sil	sillimanite

2 Nojima Island

2.1 Geological outline

Nojima Island is a narrow island in the Seto Inland Sea, south of Hofu City in southern Yamaguchi Prefecture, with a length of 1.4 km from north to south and a width of 1 km from east to west. It consists mainly of crystalline schist and basalt. Other granite veins intruding metamorphic rocks are also present. The basalts have undergone recrystallisation and are referred to in this paper as "metamorphosed basalts, metabasalt hereafter". The metabasalt is exposed mainly on the north coast through to the north-east coast, occurring as blocks in pelitic schist and directly contacting crystalline limestone at the north-eastern coast.

The crystalline schist is composed of pelitic schist, siliceous schist and calc-siliceous schist. The dominant rock type is the pelitic schist. The siliceous schist occurs as lenses in the pelitic schist. The calc-siliceous schist appears only in the northern part of the island and occurs as blocks in the pelitic schist in the vicinity of the metabasalt (Fig. 2-1-1). The crystalline schist has pervasive schistosity. The foliations of the schist generally show east-west trends with an 18–80° dipping to the north and south (Fig. 2-1-1). The metabasalt has a well-developed pillow structure, dark green and fine-grained (Fig. 2-1-2). The pillows here hang down towards the upper part and the entire outcrop is inverted. Amphibole, clinopyroxene, and Plagioclase phenocrysts can be visible to the naked eye (Fig. 2-1-3). The calc-siliceous schists are distributed mainly on the northern coast near the lithological boundary with the metabasalt. It is structurally overlaid on the upper part of the metabasalt. It shows an overall grey color and weakly has schistosity (Fig. 2-1-4). The siliceous schist is underlain by the Nojima islands and occurs as lenses or blocks in pelitic schist. It is composed of white to light grey, accumulating siliceous layers with a thickness of 1 cm to 3 cm per layer. The layers are interspersed by thin pelitic layers (Fig.

2-1-5). The foliation develops east–west oriented and 18−80° dipping to north-south. These structures are roughly parallel to the schistosity of the pelitic schists.

The dominant rock type of Nojima Island is the pelitic schist interbedded with the lenticular or blocky siliceous schist (Fig. 2-1-6). They are black to brown with significant schistosity and well-developed folding. The pelitic schist is generally enriched in biotite, which forms foliations and locally contains garnet (Fig. 2-1-7).

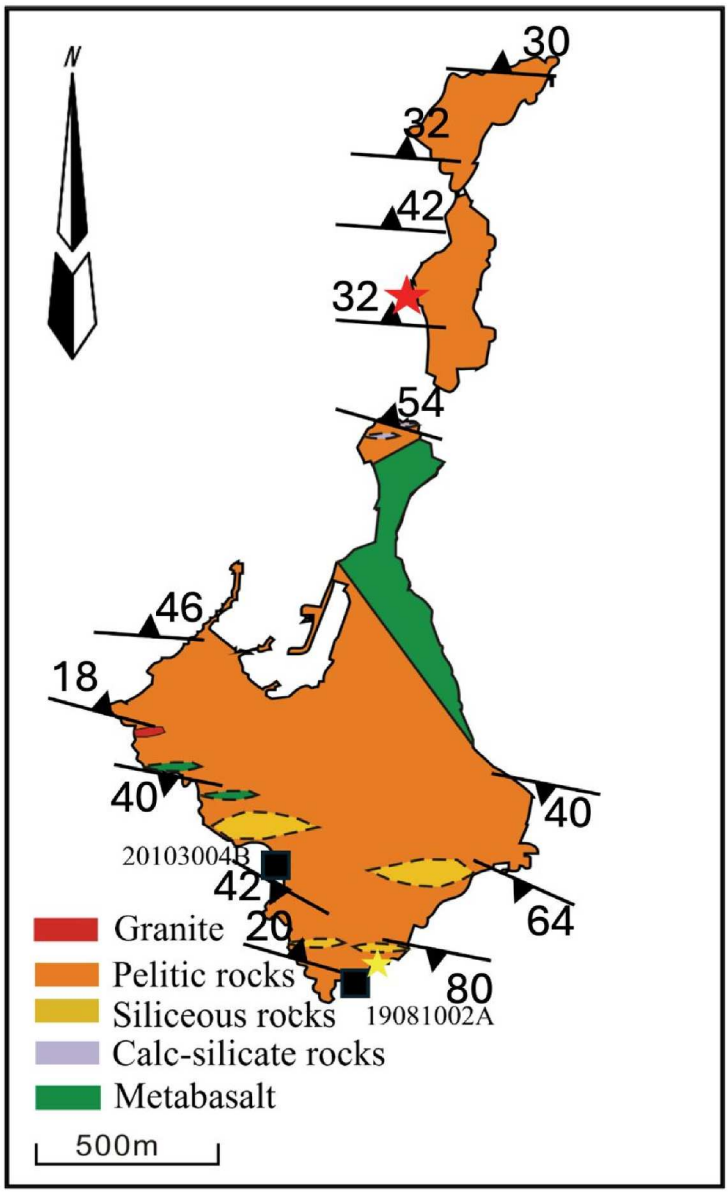

Fig. 2-1-1. Geological map of Nojima Island. The red star indicates the sampling site for zircon U–Pb dating. The yellow star indicates the sampling site for K–Ar age. The black squares indicate the sampling site for petrological investigation.

Fig. 2-1-2. Metabasalt has a well-developed pillow structure.

Fig. 2-1-3. Phenocryst structure.

Fig. 2-1-4. Calc-siliceous schist.

Fig. 2-1-5. Siliceous schist.

Fig. 2-1-6. Pelitic schist.

Fig. 2-1-7. Garnet occurs in visible grains in blackish lithofacies in pelitic schist.

2.2 Petrographical characteristics

The metabasalt exhibits well-developed porosity (Fig. 2-2-1). It contains clinopyroxene, amphibole and plagioclase as phenocrysts (probably relict minerals). Plagioclase occurs as automorphous to semi-automorphous columnar crystals with a major axis of 0.2–1 mm (Fig. 2-2-2). Crystal twinning and zonal structure are observed. Amphibole in phenocrysts often has a zonal structure, although some crystals have partially replaced clinopyroxene. The matrix consists of recrystallized fine-grained fibrous amphibole, biotite and plagioclase (Fig.2-2-3). The siliceous schist consists mainly of quartz, biotite, muscovite and small amounts of garnet (Fig. 2-2-4), rarely accompanied by Plagioclase. The constituent minerals are fine-grained. The mineral assemblages of the pelitic schist differ between the northern and southern parts of the island. The mineral assemblage in the north is characterized by quartz and plagioclase, as well as muscovite, biotite and often chlorite. Fine-grained biotite and muscovite are oriented and form schistosity (Fig. 2-2-5). In the south, the schistosity is more pronounced, due to the preferred orientation of biotite and muscovite. In addition to biotite and muscovite, garnet and small amounts of K-feldspar are present (Fig. 2-2-6).

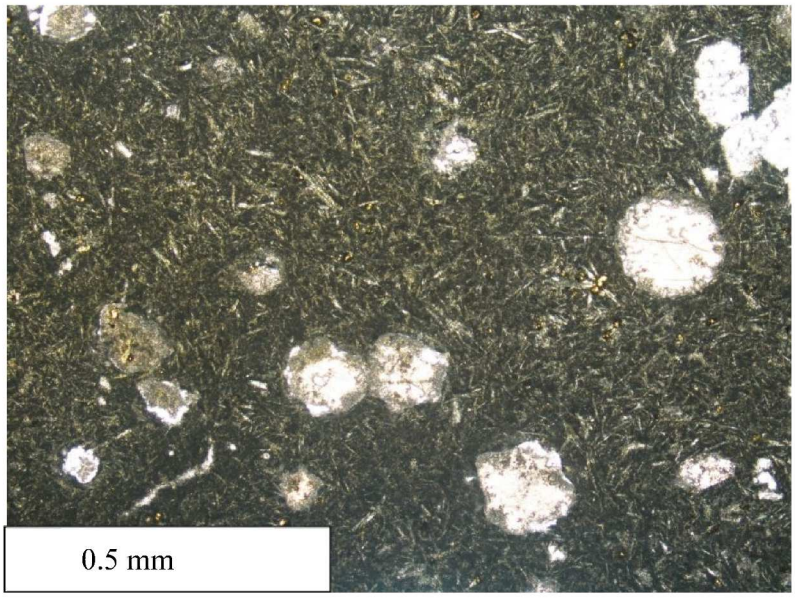

Fig. 2-2-1. Metabasalt exhibits well-developed porosity.

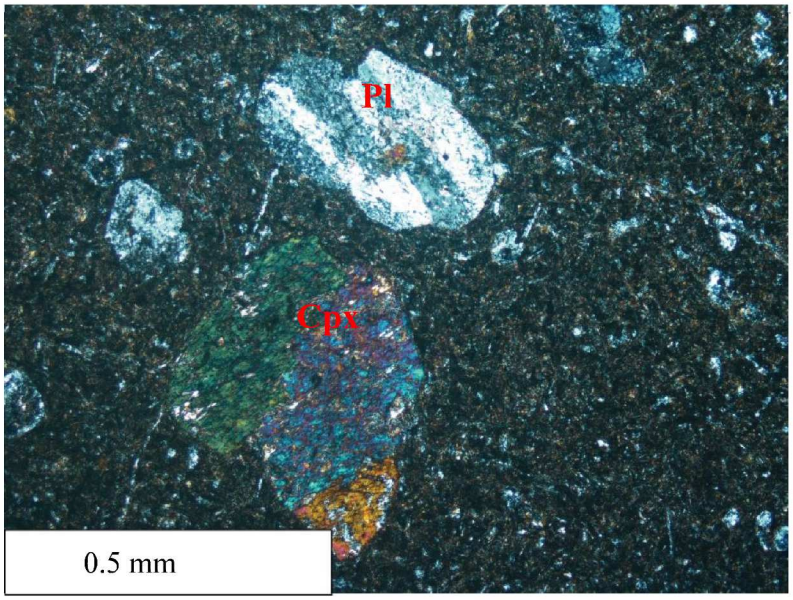

Fig. 2-2-2. Plagioclase and clinopyroxene in metabasalt.

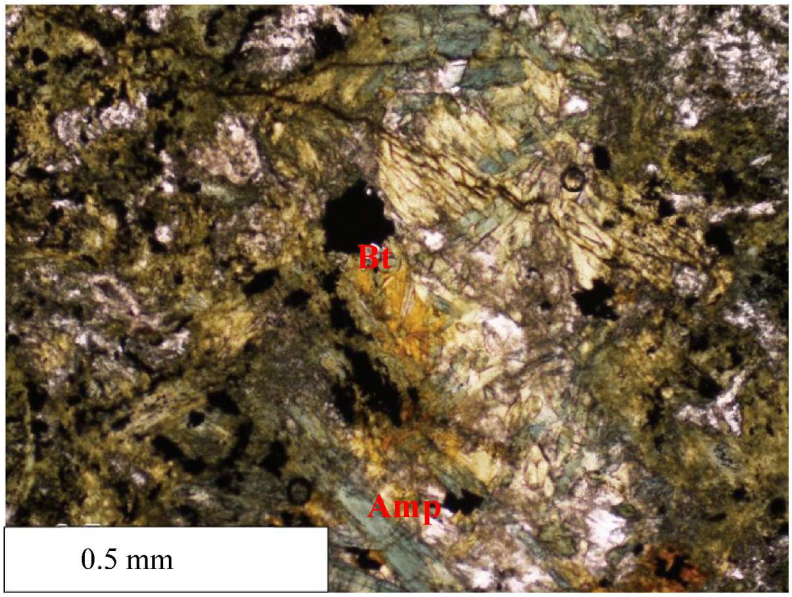

Fig. 2-2-3. Recrystallized fine-grained fibrous amphibole and biotite.

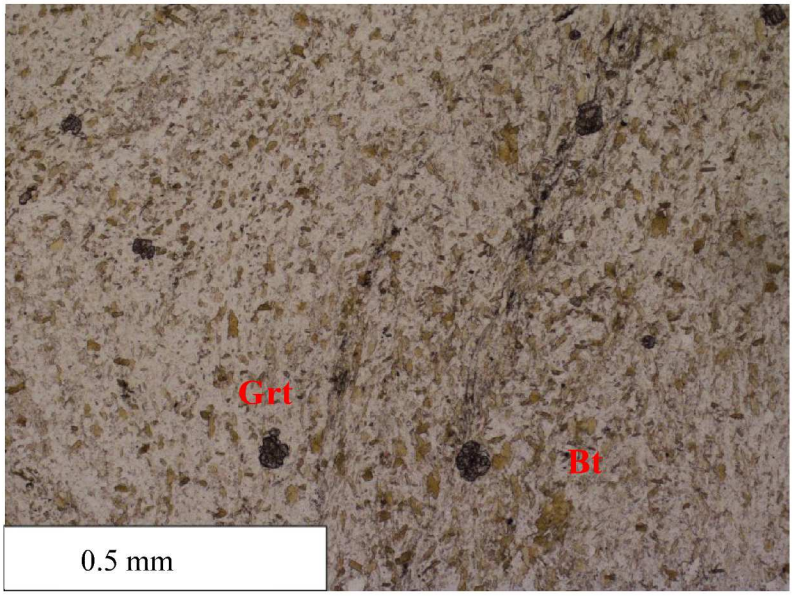

Fig. 2-2-4. Garnet in siliceous schist.

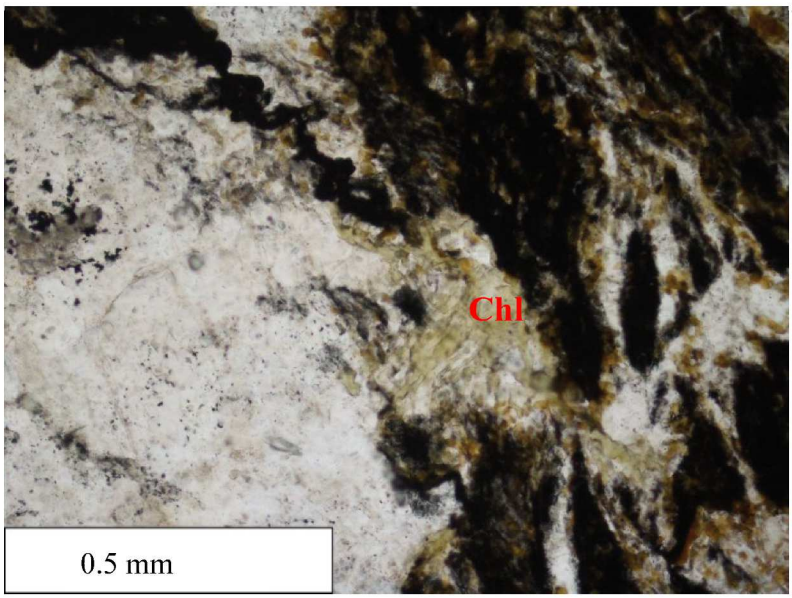

Fig. 2-2-5. Fine-grained chlorite in the pelitic schist.

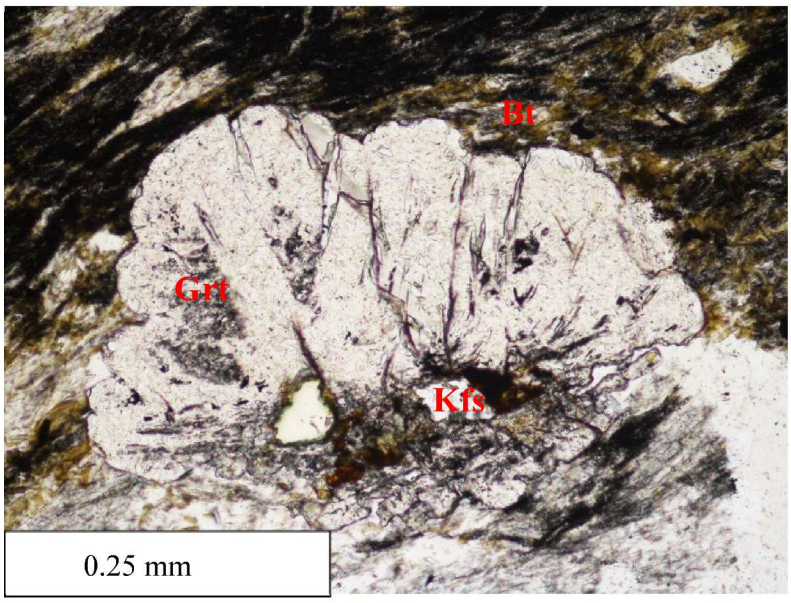

Fig. 2-2-6. Garnet in pelitic shist.

2.3 Metamorphic zoning

We defined the metamorphic zoning on Nojima Island using the mineral parageneses of the pelitic schists. Metamorphic rocks from Nojima Island can be spatially divided into the Biotite zone and Grt-Kfs zone (Fig. 2-3-1).

Bt zone

This zone is defined by the paragenesis of muscovite and biotite, and dominates the wide area from the north to the south-central parts of the island. Fine-grained chlorite occurs locally in the muscovite- and biotite-rich layers. Garnet-bearing and garnet-free mineral assemblages are also present, probably owing to differences in their bulk-chemical compositions. The main mineral assemblages are as follows:

$$\mathrm{Bt} + \mathrm{Ms} \pm \mathrm{Chl} \pm \mathrm{Grt}$$

Grt-Kfs zone

This zone is defined by the first appearance of K-feldspar, coexisting with garnet, occurring in the southern end of the island, and is represented by the following assemblage:

$$\mathrm{Bt} + \mathrm{Grt} + \mathrm{Kfs} + \mathrm{Ms}$$

The southernmost part of Nojima, where garnet and K-feldspar coexist, is thought to be the highest peak metamorphism conditions in the island. In other words, the metamorphic rocks of Nojima Island are considered to have undergone progressive metamorphism, with grade increasing from north to south.

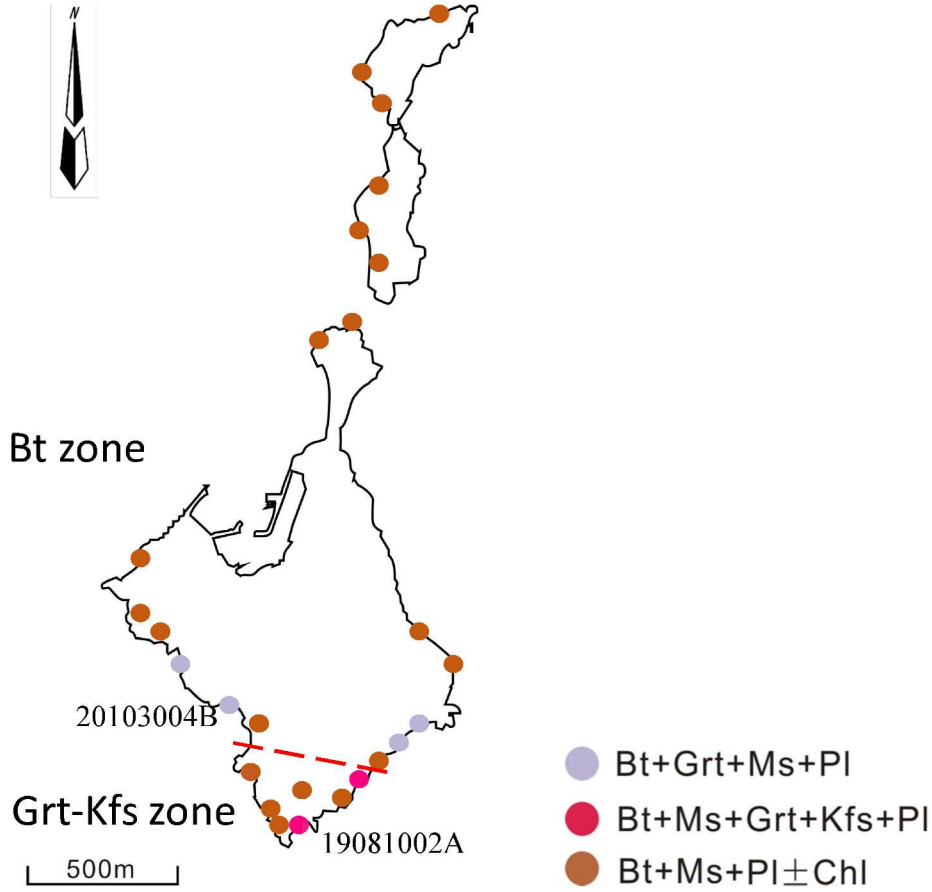

Fig. 2-3-1. The map shows the metamorphic zonation of Nojima Island. The reddish broken lines indicate the position of the inferred isograd of the metamorphic zonation.

2-4 Mineral chemistry

Mineral compositions were measured by a JXA-8230 by JEOL housed at the Center for Instrumental Analyses, Yamaguchi University. The measurement conditions were 15 kV voltage and 20 nA, and the beam diameter was normally <5 μm.

We selected the analyzed samples from the pelitic rocks in the Bt zone (20103004B) and Grt-Kfs zone (19081002A) (Figs. 2-1-1 and 2-3-1). The chemical compositions of garnet were rich in Alm (almandine) and Sps (spessartine), and poor in Prp (Pyrope) and Grs (grossular). All the garnet grains exhibited normal zoning, characterized by an increase in Fe and a decrease in Mn from the core to the rim. Figs. 2-4-1 and 2-4-2 show zoning profiles of garnet from the Bt zone and the Grt-Kfs zone, respectively. They also show the normal zoning.

Biotite was chemically homogenous in each zone. The chemical composition of biotite depends on the mineral combination. Fig. 2-4-3 shows the relationship between Ti and X_{Mg} [=Mg / (Fe+Mg)] in biotite. In the Bt zone, X_{Mg} = 0.40–0.42 is higher than those of the Grt-Kfs zone (X_{Mg} = 0.36–0.39). Ti values (per formula unit; p.f.u.) of biotite for both zones are lower than 0.11. Plagioclases were fine-grained and almost homogeneous. The chemical compositions of plagioclase remain nearly constant as X_{Ab} [Na / (Ca+Na)] = 0.857 in the Bt zone, X_{Ab} = 0.946–0.769 in the Grt-Kfs zone.

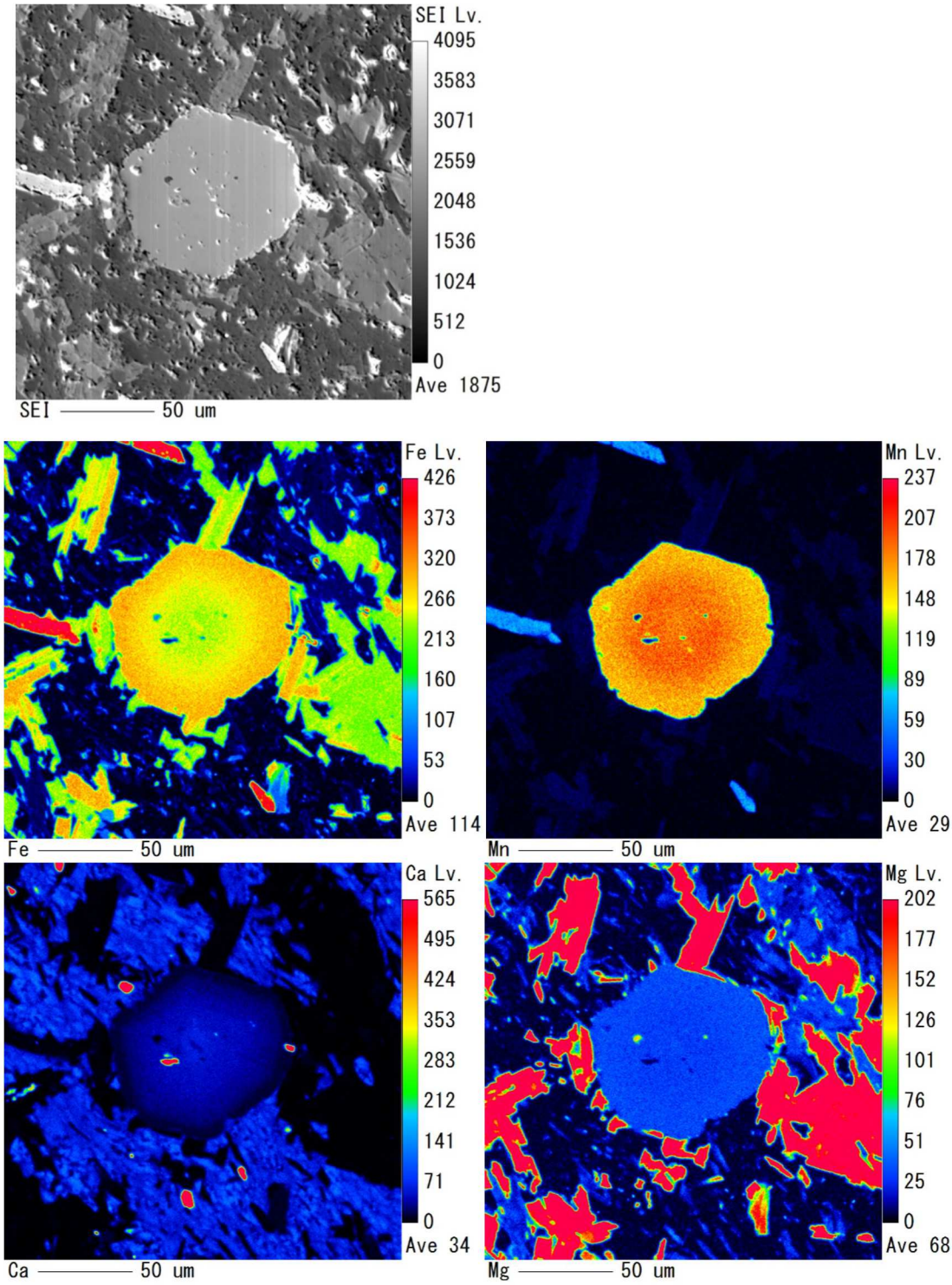

Fig. 2-4-1. Zoning profiles of garnet from 20103004B in Bt zone. SEI image and Elemental mapping.

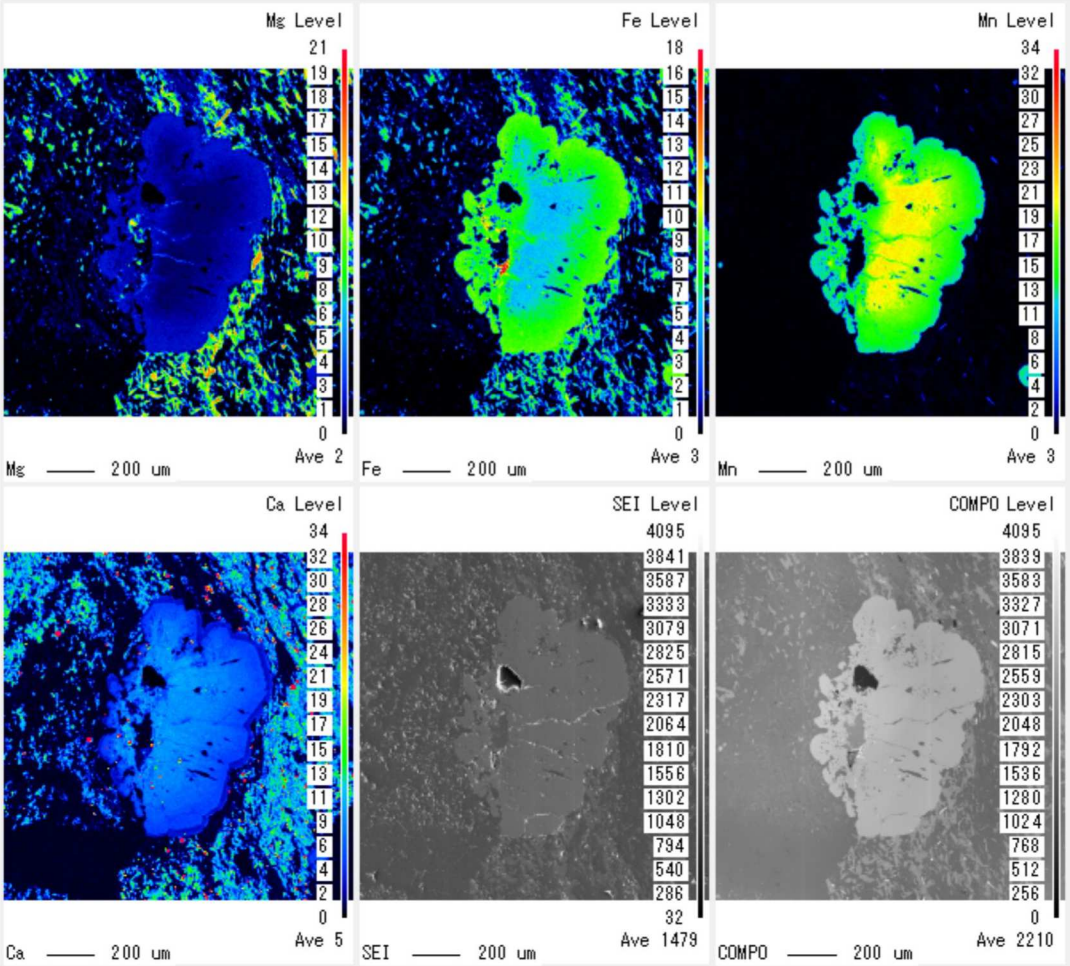

Fig. 2-4-2. Zoning profiles of garnet from 19081002A in Grt-Kfs zone. SEI, BSE image and elemental mapping.

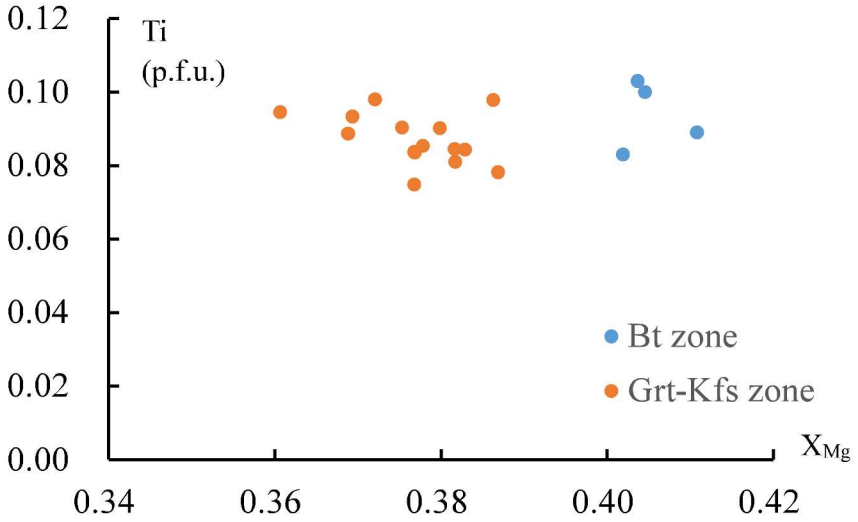

Fig. 2-4-3. Ti (O = 11, p.f.u.) vs (versus) X_{Mg}[= Mg / (Mg+Fe)] of biotite. (Grt-Kfs zone from 19081002A and Bt zone 20103004B.)

2-5 Metamorphic condition

Metamorphic pressure and temperature (*P-T*) conditions were estimated from the chemical composition of each mineral using conventional geothermobarometers. The chemical composition of the garnet (Figs. 2-4-1 and 2-4-2) with low-Mn rim is regarded as a time for the formation of peak metamorphism. The estimated metamorphic *P-T* conditions are presented in Table 2-5-2. The Grt-Bt (Ferry and Spear, 1978; Hodges and Spear, 1982) and the Grt-Bt-Pl-Qz (Hoisch, 1990) geothermobarometers were used for the temperature and pressure estimation.

Grt-Bt geothermometer based on Ferry and Spear (1978):

$K_D = X^G_{Mg} \bullet X^B_{Fe} / (X^G_{Fe} \bullet X^B_{Mg}) = Mg^G Fe^B / (Fe^G Mg^B)$ (in p.f.u.)

T (°C) = (-12454 - 0.057P(bar) / (-4.662 + 3RlnK_D) - 273.15.

Grt-Bt geothermometer based on Hodges and Spear (1983):

Where W_{CaMg} = 3300 - 1.5T,

T (°C) = (-12454 - 0.057P(bar) - 9900X_{Grs}) / (-4.662 + 3RlnK_D - 4.5X_{Grs}) - 273.15.

Barometers of Hoisch (1990) are used for R1 and R2, which are based on the net reactions among garnet, plagioclase, biotite, and quartz.

Table 2-5-1. Data set used for calibration.

Sample. No	K_{R1}	K_{R2}	X^B_{Mg}	X^B_{Fe}	X^B_{Al}	X^B_{Ti}	ΔV_{gr} (J/bar)
20103004B	312.39	35.72	0.309	0.400	0.143	0.033	-0.549
19081002A	302.24	46.35	0.290	0.435	0.143	0.031	-0.918

Where: X^B_{Mg} = Mg / 3; X^B_{Fe} = Fe / 3; X^B_{Ti} = Ti / 3; X^B_{Al} = (Al + Si - 4) / 3. (O = 11, p.f.u.)

Table 2-5-2. Calculated metamorphic *P-T* conditions.

Sample. No	FS-H			HS-H		
	T (°C)	*P*(MPa)(R1)	*P*(MPa)(R2)	*T* (°C)	*P*(MPa)(R1)	*P*(MPa)(R2)
20103004B	427	257	252	441	277	280
19081002A	515	325	325	524	337	340

FS-H: Ferry & Spear (1978)- Hoisch (1990);
HS-H: Hodges & Spear (1982)- Hoisch (1990)

To be verified, I used Ti in biotite geothermometer based on Henry et al. (2005):

T (°C) = $\{[\ln(Ti) + 2.3594 + 1.17283(X_{Mg})^3] / 4.6482e - 9\}^{0.333}$. (Ti is based on O = 22 and the p.f.u.. X_{Mg} is Mg / (Mg+Fe).)

In the Ti-saturation surface, the calibration range of this geothermometer for this expression is X_{Mg} = 0.275–1.000, Ti (O = 22) = 0.04–0.60 p.f.u., and T = 480–800 °C.

Fig.2-5-1 shows the results of Ti in biotite temperature. In Grt-Kfs zone, the temperature range is 500–550 °C, similar to the Grt-Bt geothermometer. In Bt zone, the temperature range is 500–560 °C, that is not match the Grt-Bt geothermometer. It is possible because the Bt zone is not the Ti-saturation surface. On the other hand, biotite Ti-substitution mechanisms are controlled by several factors. These also affected the results of the Ti in biotite temperature.

As a result, the *P-T* conditions of the Bt zone and the Grt-Kfs zone are estimated at 430 °C, 260 MPa, and 520 °C, 330 MPa, respectively. The metamorphic rocks on Nojima Island, therefore, clearly underwent the Low-*P/T* type metamorphism.

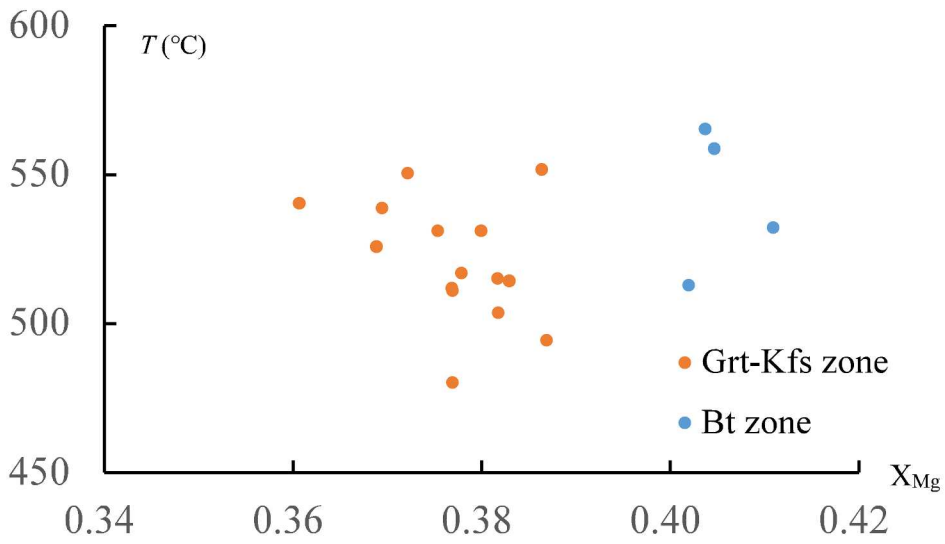

Fig. 2-5-1. Ti in biotite temperature (°C) vs X_{Mg}.

2-6 Biotite K–Ar age

The biotite K–Ar age was performed by ACT Labs Geometallurgy-MLA Dept. The result is 92.1 ± 2.1 Ma (Table 2-6-1). The age can be recognized as time for passing through the closure temperature of biotite, probably at approximately 300 ℃, suggesting the metamorphic rocks of Nojima Island were undergone by Low-*P/T* peak metamorphism at least 90 Ma.

Table 2-6-1. Biotite K–Ar age.

lithology	**location**	**K (wt%)**	**^{40}Ar rad, (ng/g)**	**^{40}Ar air (%)**	**K-Ar age (Ma)**
Metapelite	Noshima	7.12 ± 0.08	46.66 ± 0.15	5.8	92.1 ± 2.1

2-7 U–Pb age

Zircon grains from the pelitic schist, sample number 22030904, collected from the Bt zone (Fig. 2-1-1) for detrital zircon dating. Zircon extraction and zircon U–Pb dating were performed by Kyoto Fission-Track Co., Ltd., Japan. In situ U–Pb dating was carried out using a New Plasma II ICP-MS (Nu instruments, Wrexham, UK), combined with a LIGHT CONVERSION laser system equipped with a 257 nm Yb: KGW femtosecond laser at the Department of Geology and Mineralogy, Kyoto University. The laser spot size of 10 μm in diameter was used. The zircon U–Pb data and analytical conditions for LA-ICP-MS are presented in the appendix. The cathodoluminescence (CL) images were obtained using a JEOL JSM-6360 scanning electron microscope and a Gatan Mini CL system (customized by Prof. Toshiaki Shimura) at the Center for Instrumental Analyses, Yamaguchi University, Japan. The CL images were captured at an acceleration of 7–9 kV, a specimen current of 1.5–2.0 nA, and a working distance of 9mm.

Fig. 2-7-1 shows CL images of the zircon. All zircon grains were analyzed in the core parts. The isotope ratios of $^{206}Pb/^{238}U$ and $^{207}Pb/^{235}U$ were statistically analyzed using Isoplot software (Ludwig, 2012). These were plotted on Concordia diagrams (Fig. 2-7-2). All data point error ellipses are 2σ (95% confidence). Following the method of Dickinson and Gehrels (2009), the weighted mean age was calculated with 8 grains that overlap in age at 2σ, using ^{238}U–^{206}Pb ages. The result of the calculated 203.1 ± 1.6 Ma indicates the depositional age of the protolith (Fig. 2-7-3).

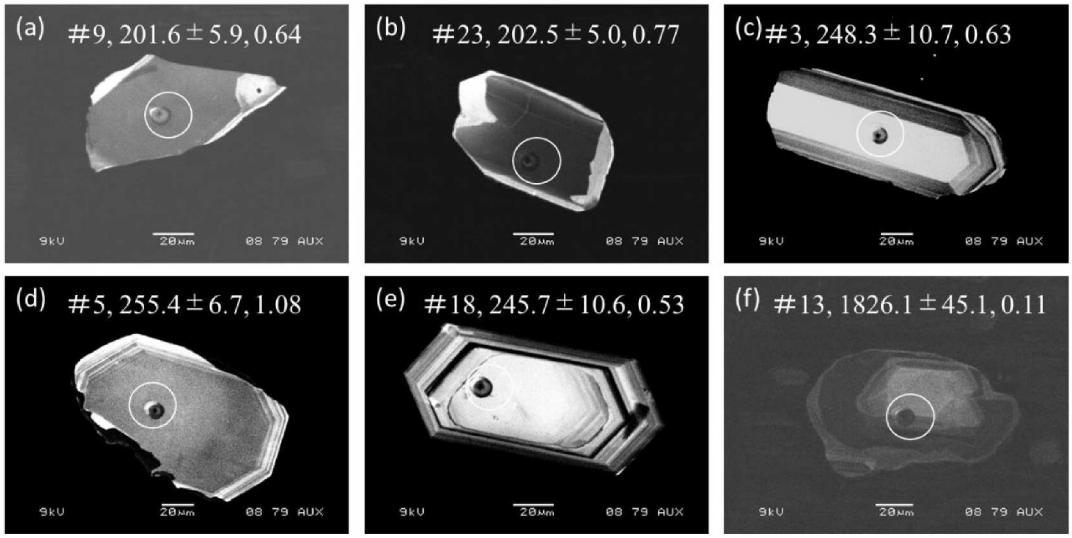

Fig. 2-7-1. Cathodoluminescence (CL) images of zircon grains. The "#" means grain number. The values with error ranges show the ^{238}U–^{206}Pb age. The right-side values indicate Th/U ratios.

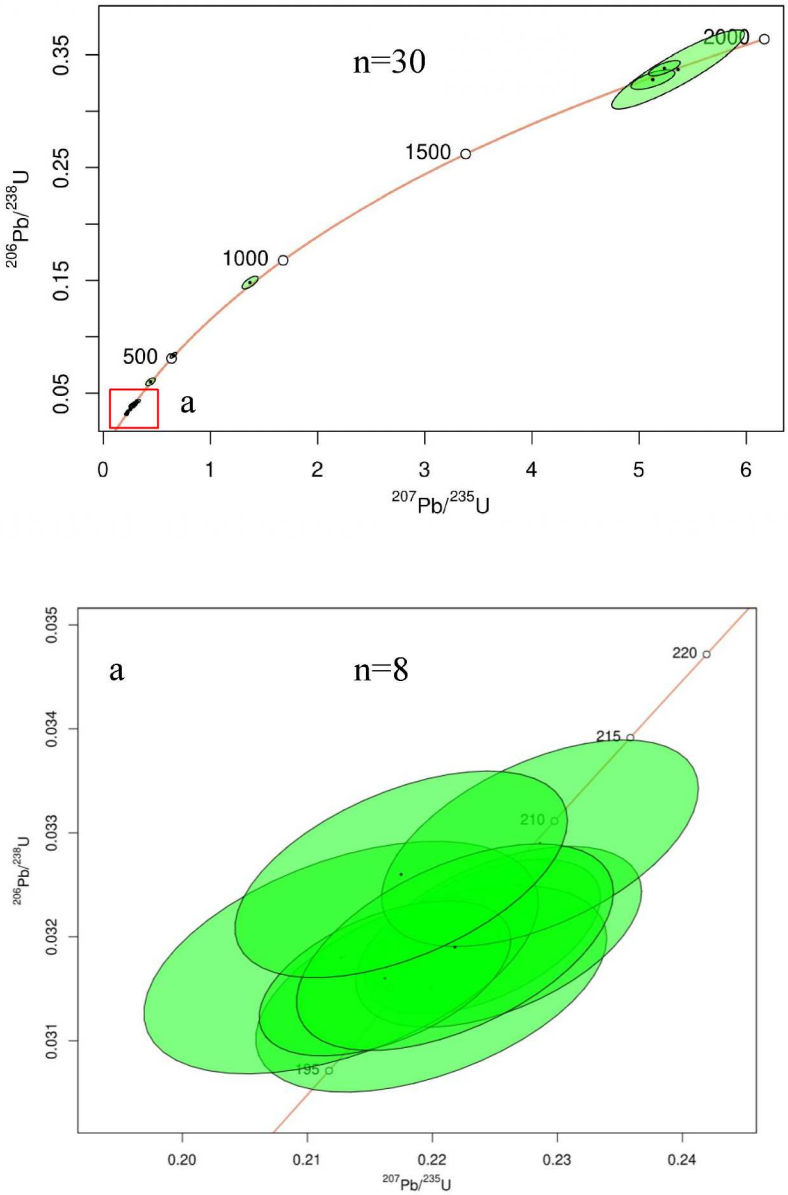

Fig. 2-7-2. Concordia diagrams for the detrital zircons (All date point error ellipses are 2σ). a: The younger age cluster.

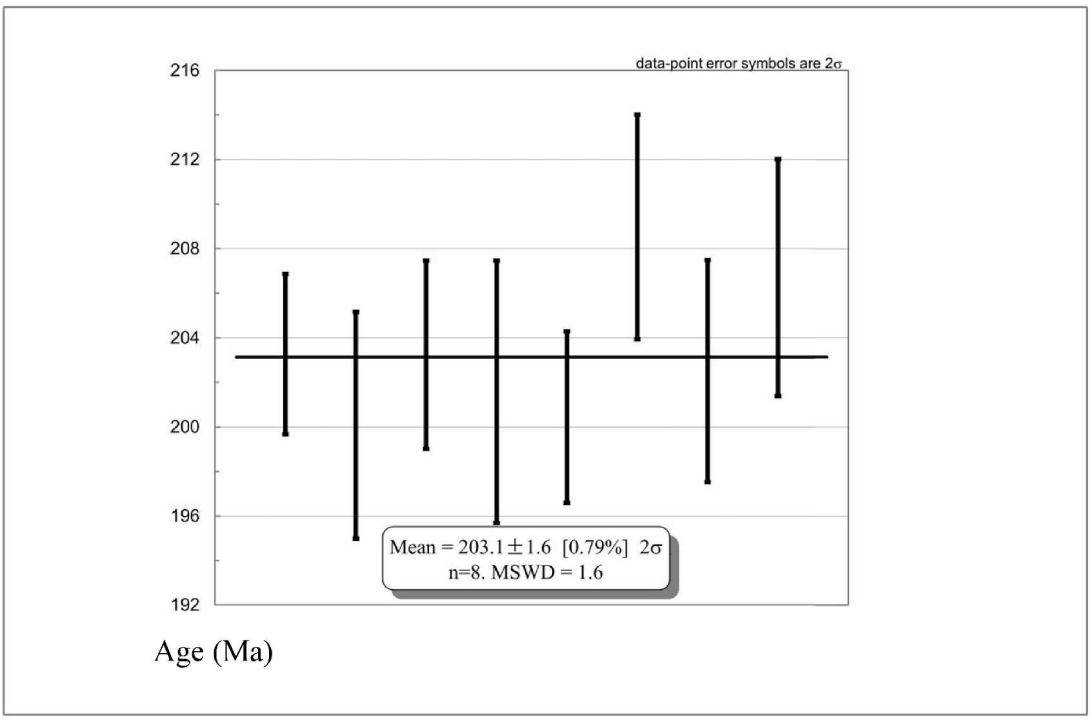

Fig. 2-7-3. The weighted mean age in Nojima Island.

2-8 Summary

The detrital zircon U–Pb dating revealed an age of 203.1 ± 1.6 Ma, as the youngest mean value from the metamorphic rocks on Nojima Island. In addition, the biotite K–Ar age is 92.1 ± 2.1 Ma. According to the protolith age and biotite cooling age, the metamorphic rocks on Nojima Island were deposited in the Jurassic age, probably correlated with the Jurassic Kuga Group, and their metamorphic age is comparable to the Cretaceous Ryoke Belt. Based on mineral paragenesis and estimated *P-T* conditions, the metamorphic rocks can be divided into the Bt zone and the Grt-Kfs zone, which underwent Low-*P/T* type metamorphism. The estimated peak metamorphic conditions of the Bt zone and the Grt-Kfs zone are 430 °C, 260 MPa, and 520 °C, 330 MPa, respectively.

3. Ozushima Island

3-1 Geological outline

Ozushima Island is a narrow island located in the Seto Inland Sea, in the central part of Yamaguchi Prefecture. It extends 3.5 km from north to south and 0.5 km from west to east (Fig. 3-1-1). The island mainly consists of metamorphic rocks with small amounts of granite stocks. Based on field research, the metamorphic rocks are composed mainly of pelitic schists (Fig. 3-1-2), accompanied by psammitic and siliceous schists (Fig. 3-1-3) and metabasalt as a block. The schistosity strikes in an east-west direction and gently dips towards the north and south. Fold structures with an E–W trending axis were also developed. In the southern part of the island, there is a NW–SE striking and 20–30° NE dipping thrust that is weakly oblique to the general foliation (Fig. 3-1-4). A granite stock intrudes into the metamorphic rocks in the northeastern part of the island (Fig. 3-1-5). The formation age of the granite is unknown; however, it is thought to belong to the Cretaceous intrusive rocks (Nishimura et al., 2012). Small diorite dikes with widths of 1–2 m occur west and south of the island (Fig. 3-1-6). Metamorphic rocks near the granite stock exhibit a granoblastic texture and were affected by contact metamorphism. As this study focused on regional metamorphism, the effects of contact metamorphism are not discussed further.

Pelitic schists often alternate with psammitic schists and exhibit microfolding with minor faults at the outcrop scale. Three deformational events were identified based on field surveys. Each stage is described in the following sections.

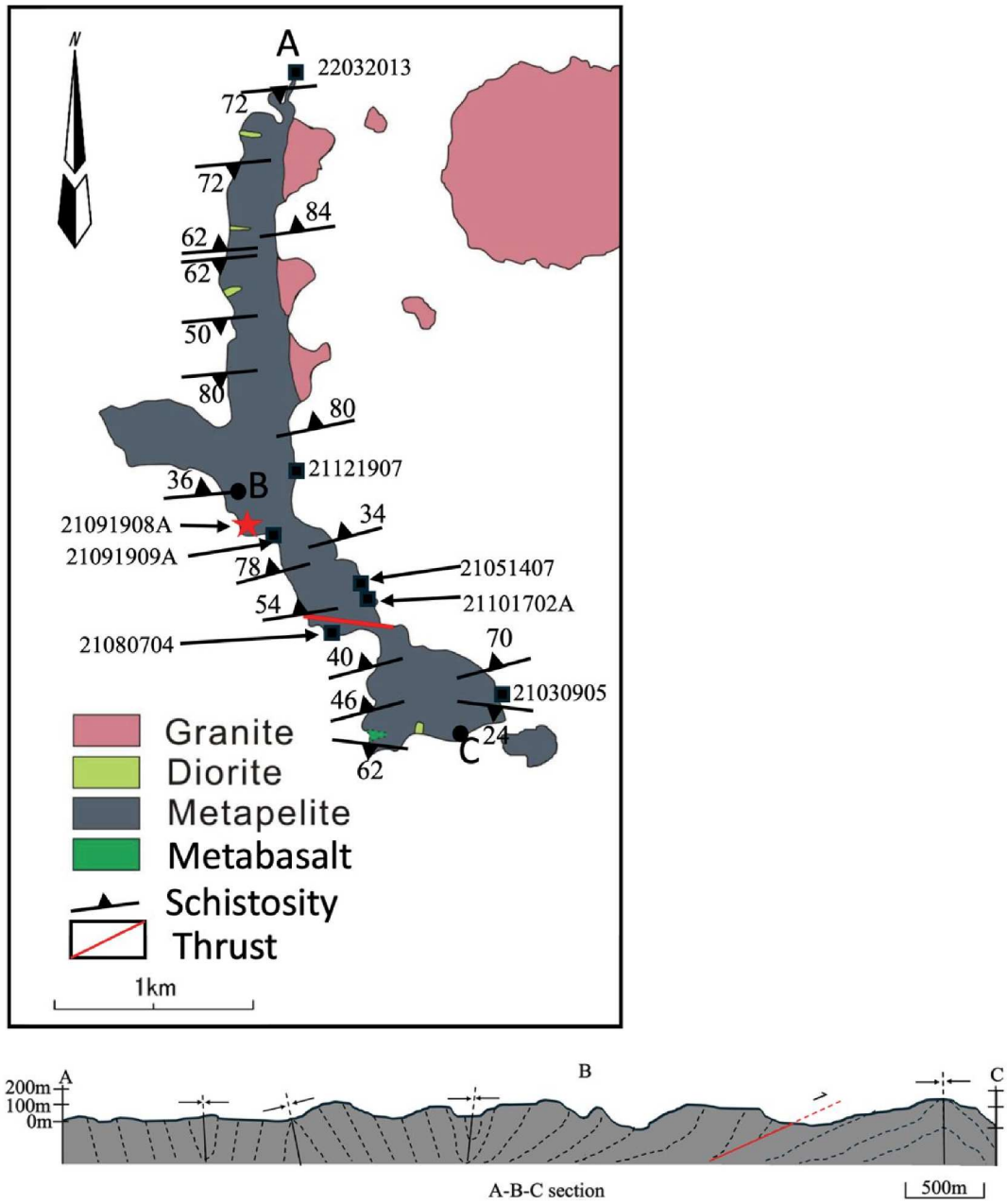

Fig. 3-1-1. Geological map of Ozushima Island. Geological cross-section along A-B-C with general structure (broken lines). The black squares indicate the sampling site. The red star indicates the sampling site for zircon U–Pb dating (21091908A).

Fig. 3-1-2. Pelitic schist. (Bedding plane of the protoliths (S0) and metamorphic foliations (S1). The S2 foliation is formed along the folded axial planes of the S1 foliation.)

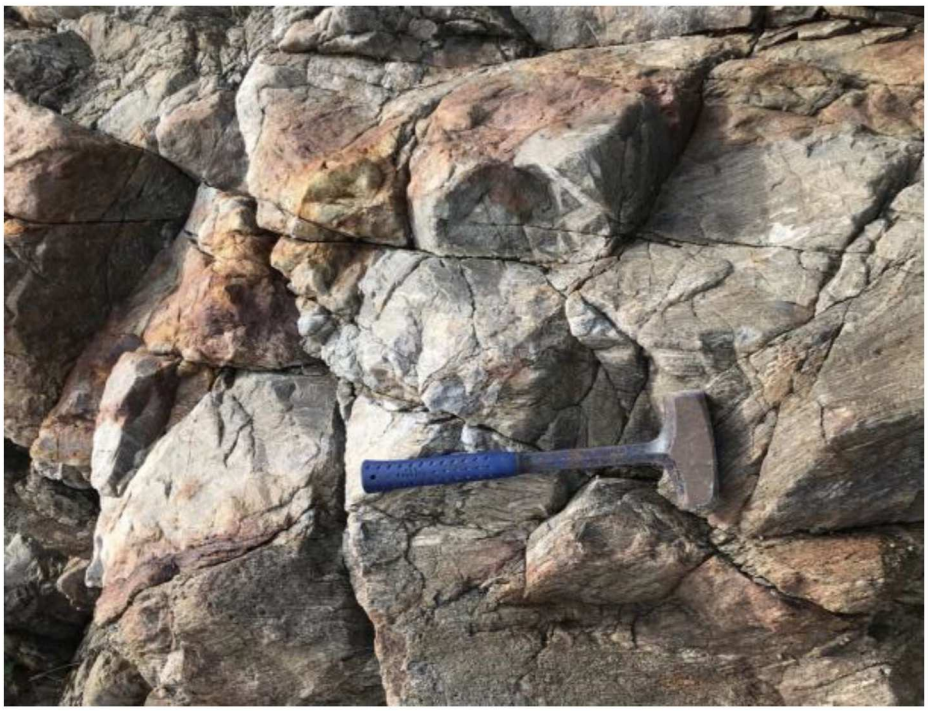

Fig. 3-1-3. Siliceous schist.

Fig. 3-1-4. The S3 foliation was locally produced along the thrust in the southern island.

Fig. 3-1-5. A granite stock intruded into the metamorphic rocks.

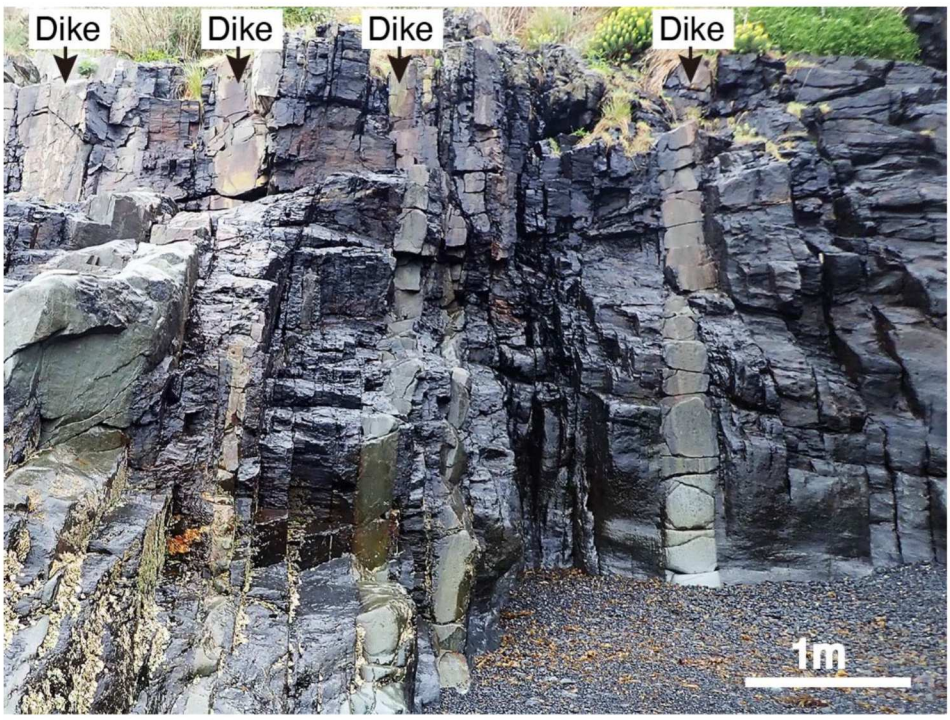

Fig. 3-1-6. Diorite dikes.

3-2 Petrographical characteristics of each deformational stage

The three stages of deformation are described as follows. Stage 1 involves the formation of metamorphic foliation (S1), parallel to the bedding plane (S0). Stage 2 forms along the folded axial planes of the S1 foliation (S2) (Fig. 3-1-2). Stage 3 involves the formation of the thrust and the thrust plane (S3) (Fig. 3-1-4). The mineral assemblages of the pelitic rocks were described for each deformational stage. Mineral paragenesis is defined by the constituent minerals that form a preferred orientation at each stage. For instance, the mineral orientations of Stages 1, 2, and 3 form the foliation of S1, S2, and S3, respectively. It is noteworthy that the main minerals of Stage 1 include andalusite, sillimanite, cordierite, garnet, corundum, and K-feldspar.

Andalusite along the S1 foliation includes fine-grained quartz and muscovite (Fig. 3-2-1). The others are surrounded by muscovite (Fig. 3-2-2). Garnet and sillimanite occurred along the S1 foliation (Fig. 3-2-3, 4). Sillimanite mostly has a fibrous shape (fibrolite) coexisting with quartz (Fig. 3-2-4) and is locally surrounded by muscovite. Corundum appears within the quartz-free domains in the pelitic schist and is locally replaced by muscovite (Fig. 3-2-5). The cordierite-bearing S1 foliation is locally cut by the muscovite-bearing S2 foliation (Fig. 3-2-6). The S3 foliation is parallel to the thrust plane (Fig. 3-1-4) and composed of biotite and chlorite (Fig. 3-2-7). North of Ozushima Island, near the granite stock, some of the pelitic rocks do not show a granoblastic texture; however, coarse Biotite grains in these rocks locally cut the foliation and were probably recrystallized by contact metamorphism (Fig. 3-2-8).

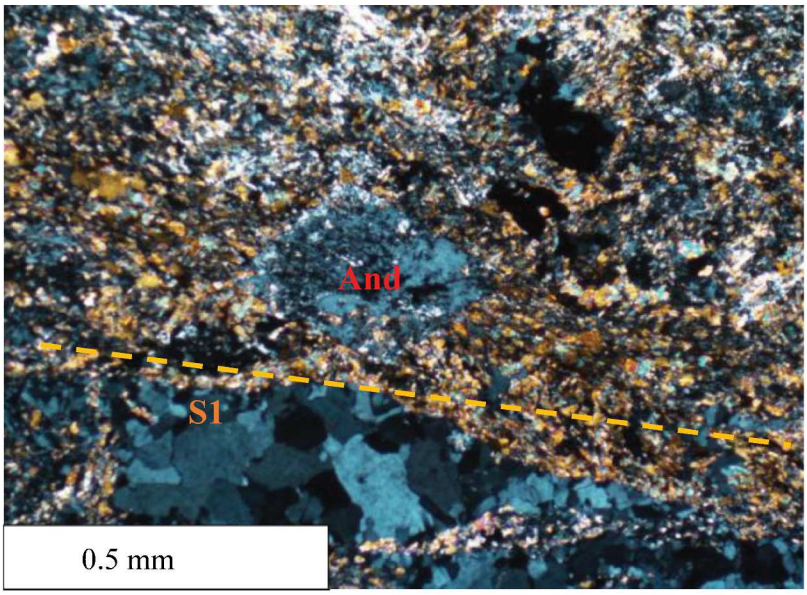

Fig. 3-2-1. Andalusite includes fine-grain quartz and muscovite (21091909A).

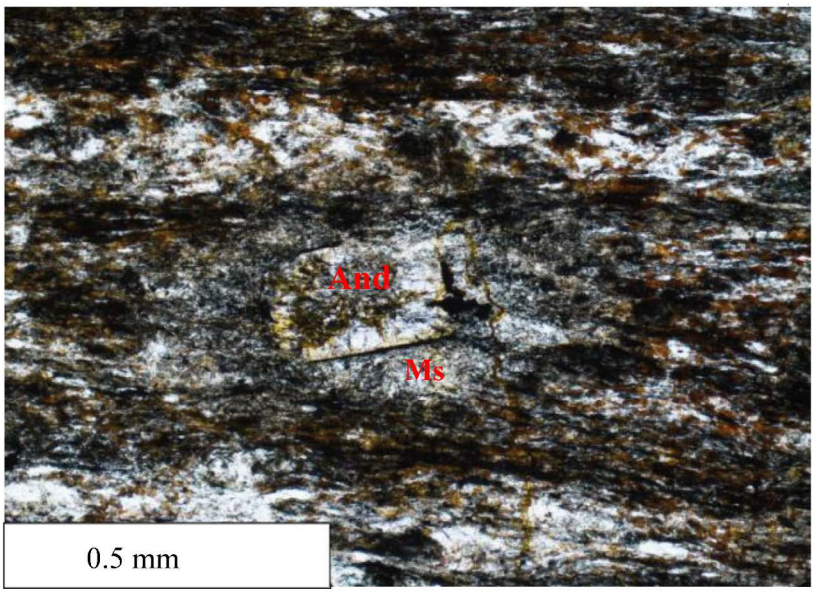

Fig. 3-2-2. Andalusite is surrounded by muscovite.

Fig. 3-2-3. Garnet occurred along the S1 foliation (21080704).

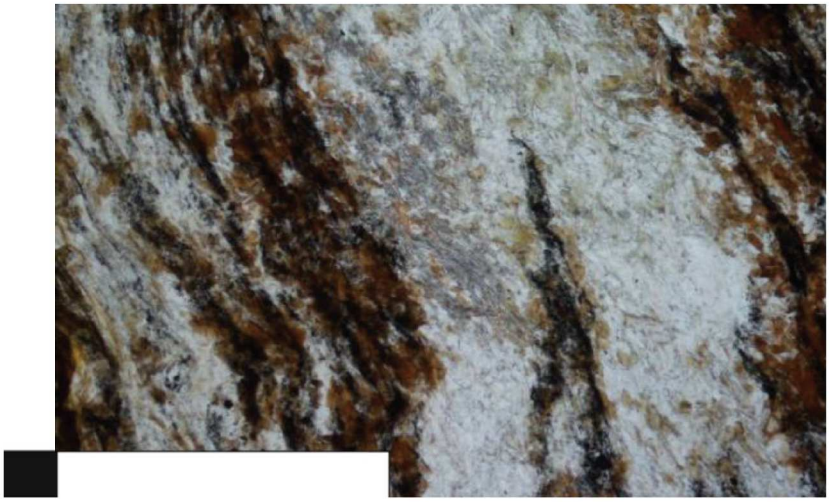

Fig. 3-2-4. A fibrous shaped (fibrolite) sillimanite exists along the foliation.

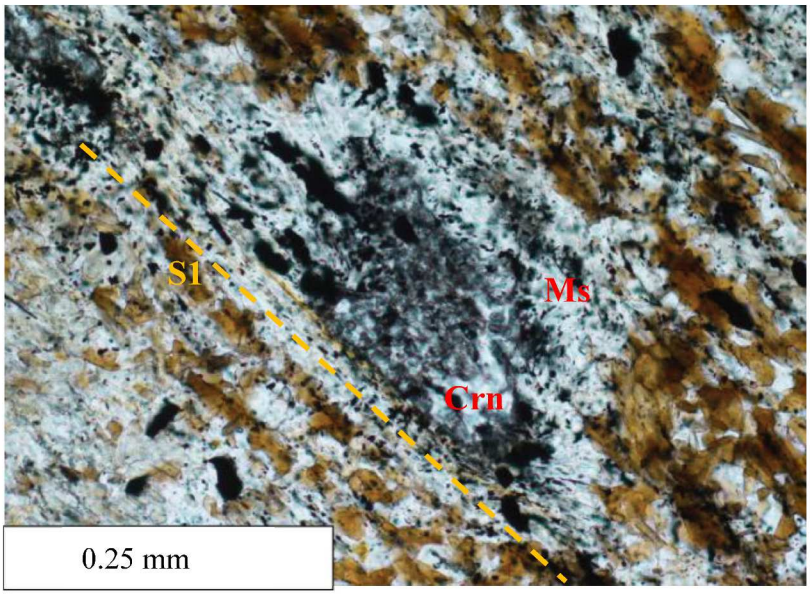

Fig. 3-2-5. Corundum is replaced by Muscovite (21101702A).

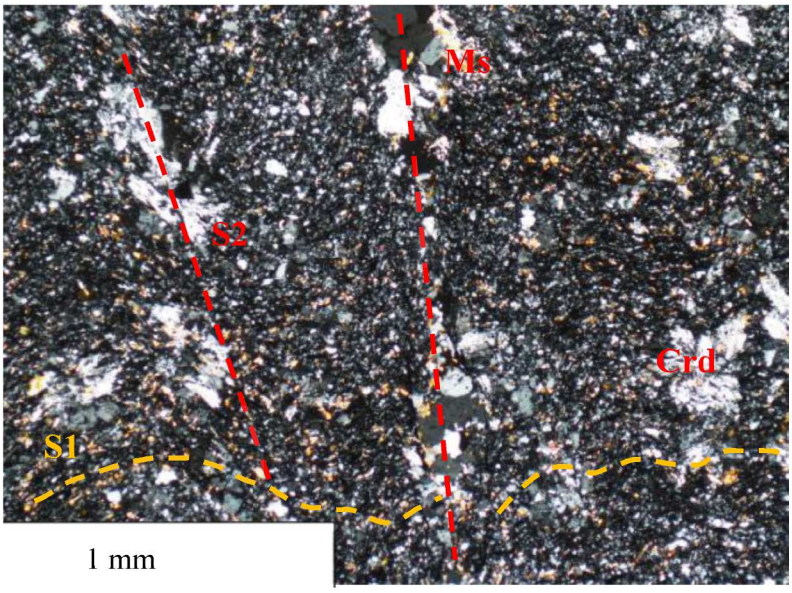

Fig. 3-2-6. The S2 foliation in Stage 2 developed along axial plane of the S1 foliation (21030905).

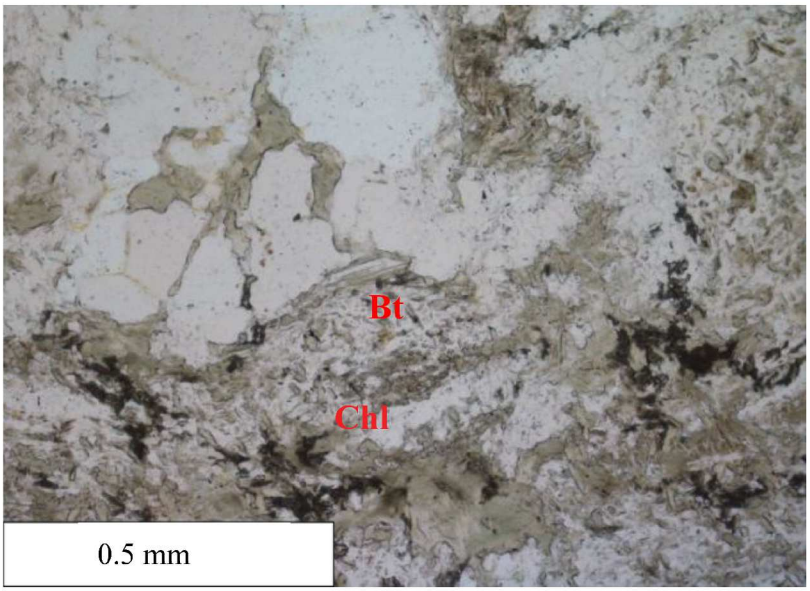

Fig. 3-2-7. Chlorite replacing biotite along the thrust plane (S3) in Stage 3.

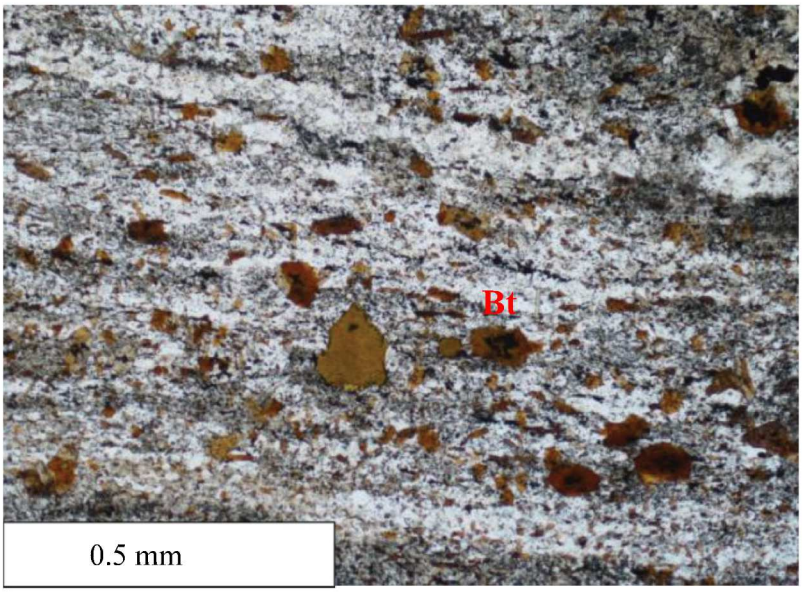

Fig. 3-2-8. Recrystallized coarse-grained biotite.

3-3 Metamorphic zoning

We defined metamorphic zoning on Ozushima Island using the mineral parageneses of the pelitic schist from the Stage 1 assemblages. The regional distribution of mineral paragenesis in Stage 1 is shown in Fig. 3-3-1. The metamorphic rocks can be spatially divided into the following three zones: Bt zone, And zone and Sil zone. In addition, the location of each zone appeared to be independent of the distribution of granite stock, with the And and Sil zones occurring repeatedly due to folding and thrusting (Fig. 3-3-1). The mineral assemblages of each zone are listed in Table 3-3-1. For clarity, the metamorphic zones studied here are labeled from north to south as Sil zone north; Sil zone (N), And zone north; And zone (N), Bt zone, And zone middle; And zone (M), Sil zone south; Sil zone (S), and And zone south; And zone (S) (Table 3-3-1, Fig. 3-3-1).

Bt zone

This zone is located in the central part of the island. It was defined by the paragenesis of muscovite and biotite. Fine-grained chlorite occurs locally in the muscovite- and biotite-rich layers. The main mineral assemblages are as follows:

$$\mathrm{Bt} + \mathrm{Ms} \pm \mathrm{Chl}$$

And zone

This zone is defined by the first appearance of Andalusite and is represented by the following assemblage:

$$\mathrm{Bt} + \mathrm{Ms} + \mathrm{And} + \mathrm{Kfs} \pm \mathrm{Crd}$$

The fine-grained andalusite (ca. 1 mm) is surrounded by muscovite flakes, suggesting that the rock had undergone retrograde metamorphism. In addition, cordierite occurs with andalusite. In this zone, an andalusite-free assemblage exists. Garnet-bearing and garnet-free mineral assemblages are also present, probably due to their bulk chemical

composition differences, coexisting with biotite, cordierite, muscovite, and K-feldspar. The cordierite includes fine-grained muscovite and chlorite.

Bt + Grt + Kfs ± Ms, Bt + Crd + Ms + Kfs

Sil zone

This zone is defined by the first appearance of sillimanite and the metamorphosed pelitic rock was recognized as gneiss by the naked eye. The southern part of this zone thrusts over the And zone. It frequently coexists with sillimanite and cordierite. In this zone, K-feldspar is ubiquitously present in all pelitic gneisses. The quartz-bearing gneisses have the following mineral assemblages:

Bt + Crd + Sil + Kfs

Corundum is present in the Quartz-free domain, coexisting with K-feldspar.

Garnet is ubiquitous in pelitic gneisses and coexists locally with cordierite. The mineral assemblage is as follows:

Bt + Grt + Kfs ± Crd

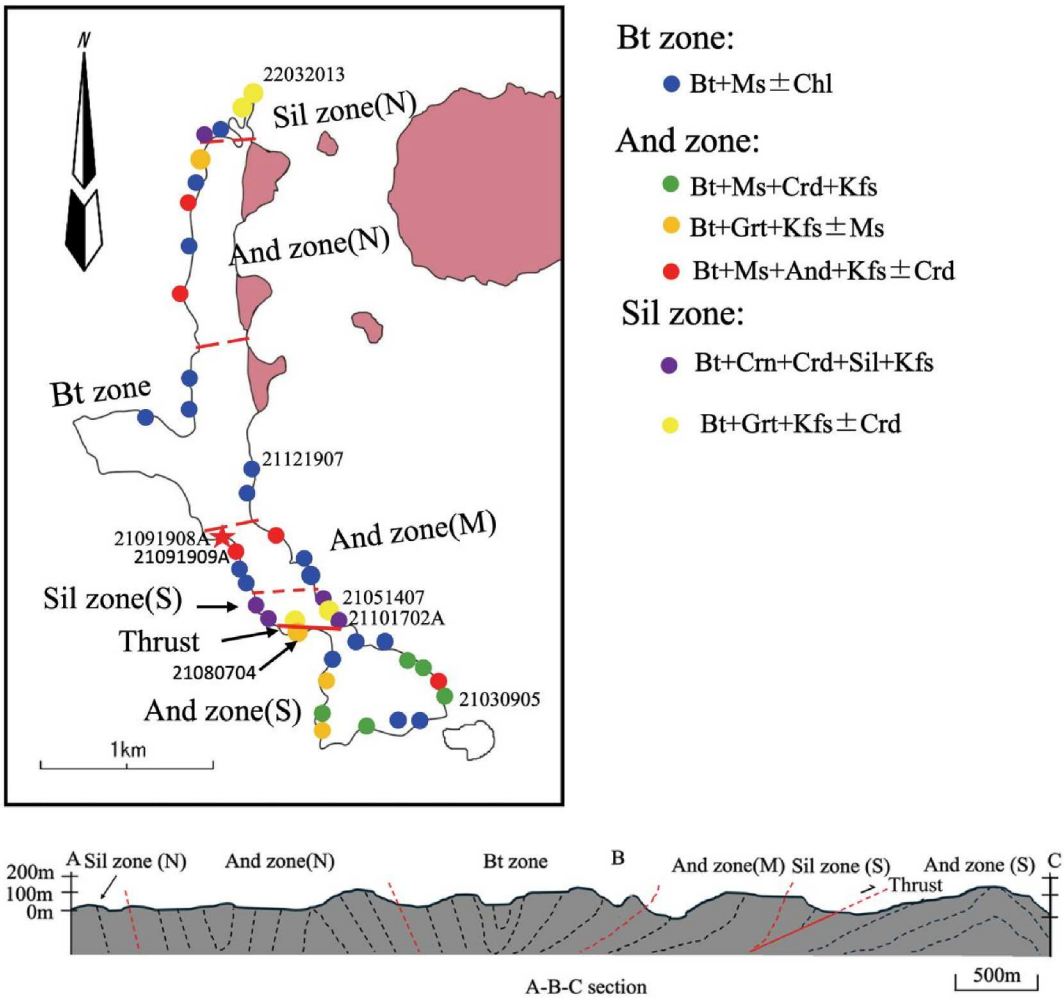

Fig. 3-3-1. Metamorphic zonation map of Ozushima Island with cross-section along A-B-C. The reddish broken lines indicate the position of the inferred isograd of the metamorphic zonation.

Table 3-3-1. Mineral assemblages of pelitic rocks of Bt, And, and Sil zones.

Sample	Zone	Chl	Ms	Bt	And	Kfs	Crd	Sil	Grt	Crn	Qz
21121907	Bt	(○)	○	○							○
21091909A	And(M)		○	○	○	○					○
21030905	And(S)		○	○		○	○				○
21080704	And(M)		○	○		○			○		○
21101702A	Sil(S)			○		○	○	○		○	
21051407	Sil(S)			○		○			○		○
22032013	Sil(N)			○		○	○		○		○

All samples contain plagioclase.

(○): Rare; ○: Present.

3-4 Mineral chemistry

Mineral compositions were measured by a JXA-8230 by JEOL housed at the Center for Instrumental Analyses, Yamaguchi University. The measurement conditions were 15 kV voltage and 20 nA; the beam diameter was typically <5 μm. We selected the analyzed samples from the pelitic rocks in the Sil zone (N) (22032013), Sil zone (S) (21051407), and And zone (S) (21080704).

Garnet was found in both And and Sil zones. The chemical compositions of Garnet were rich in Alm (almandine) and Sps (spessartine) and poor in Prp (Pyrope) and Grs (grossular). All the Garnet grains exhibited normal zoning, increasing Fe content and decreasing Mn content from the core to the rim. In Sil zone, most rim shows Alm > 60, Sps = 17.5–32.3, and Prp and Grs contents below 10 (Fig. 3-4-1). In the And zone, elemental mapping was performed to analyze the chemical zoning (Fig. 3-4-2). The chemical compositions of Garnet rim show Alm = 49.1, Sps = 39.2, Prp and Grs contents ≤ 1.0.

Biotite was chemically homogenous in each zone. In the And zone, Ti is lower than in the Sil zone, while X_{Mg} [Mg / (Mg+Fe)] = 0.40–0.45 is higher than those of the Sil zone (X_{Mg} = 0.30 – 0.35) (Fig. 3-4-3). Plagioclases were fine-grained and almost homogeneous. The chemical compositions of plagioclase remain nearly constant as X_{Ab} [Na / (Ca+Na)] = 0.883 in the And zone, X_{Ab} = 0.868 in the Sil zone (S), and X_{Ab} = 0.765 in the Sil zone (N). The chemical composition of cordierite in the Sil zone is X_{Fe} [Fe / (Fe+Mg)] = 0.51, whereas, in the And zone, cordierite contains chlorite and muscovite (Fig. 3-2-7) and shows a value of X_{Fe} = 0.48.

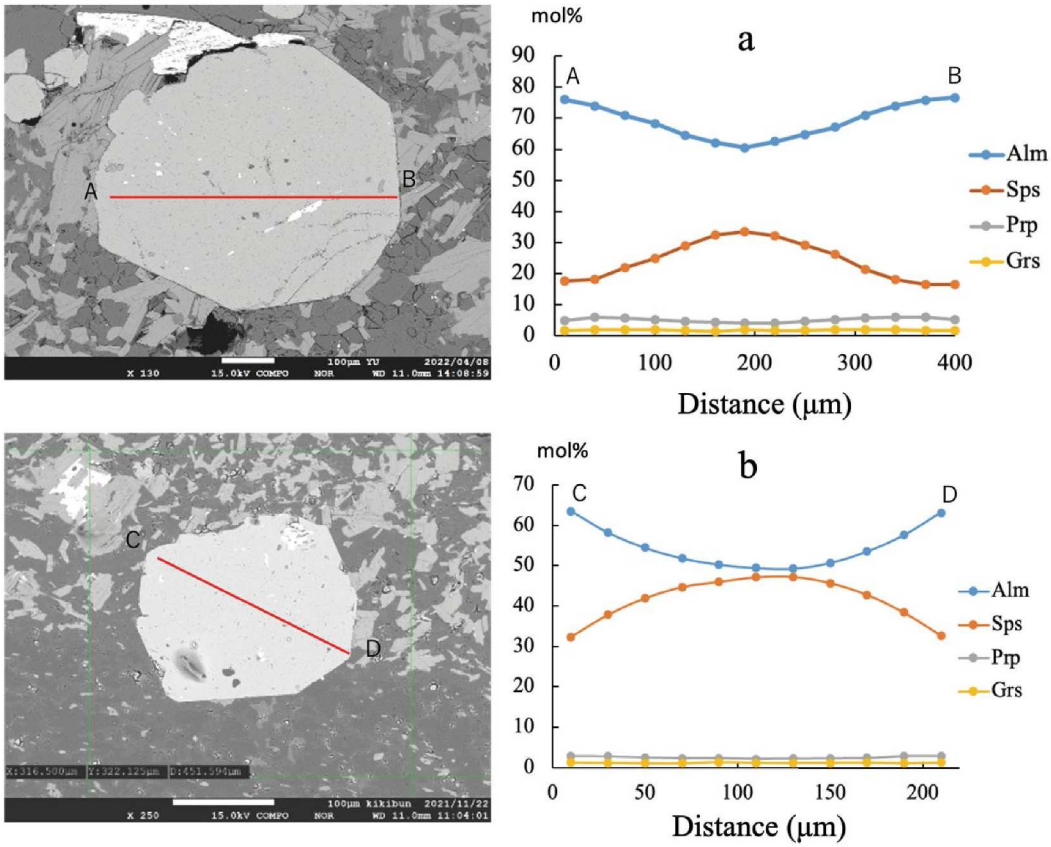

Fig. 3-4-1. Backscattered images (left) of garnet and their zoning profile (right) along A–B in a and C–D in b. a: 22032013 in Sil zone (N), b: 21051407 in Sil zone (S).

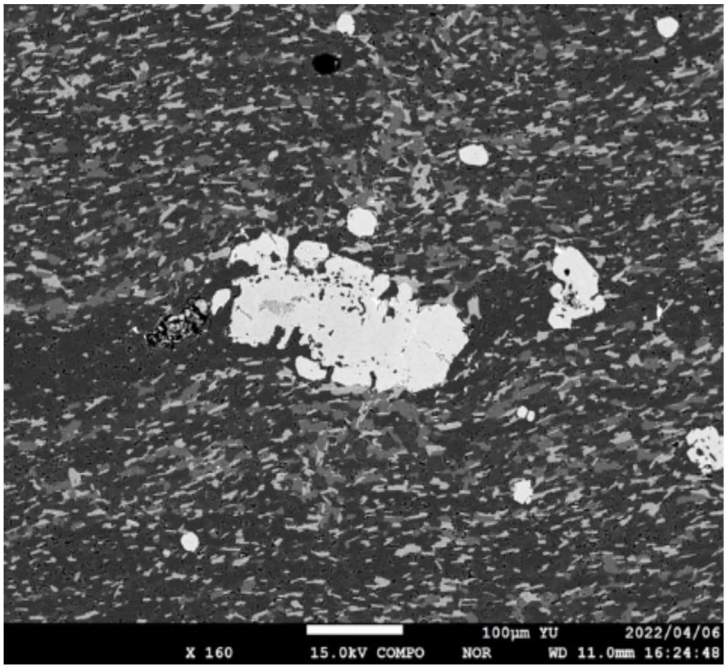

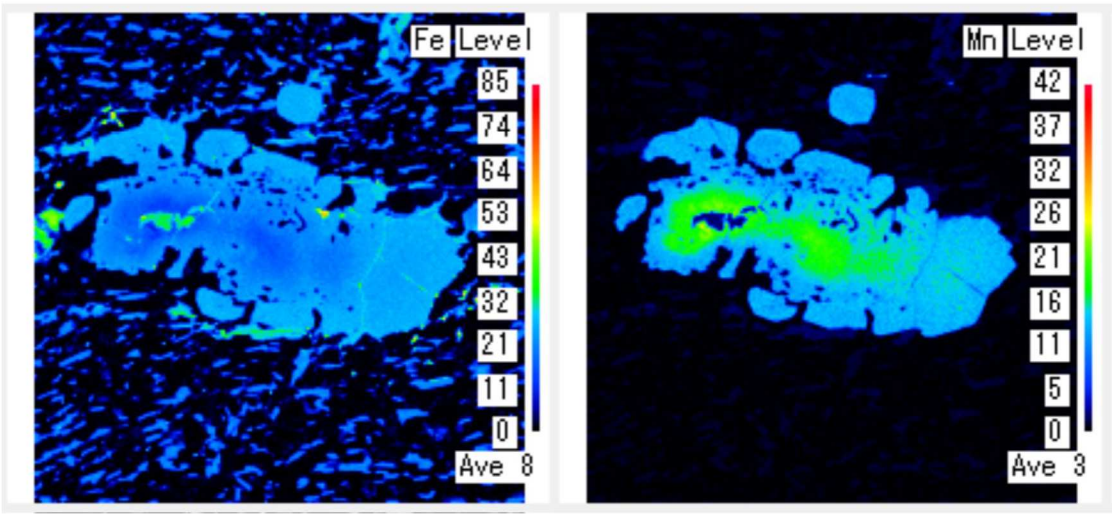

Fig. 3-4-2. Zoning profile of garnet from 21080704 in And zone(S). a: Backscattered image. b and c: Elemental mapping of Fe and Mn.

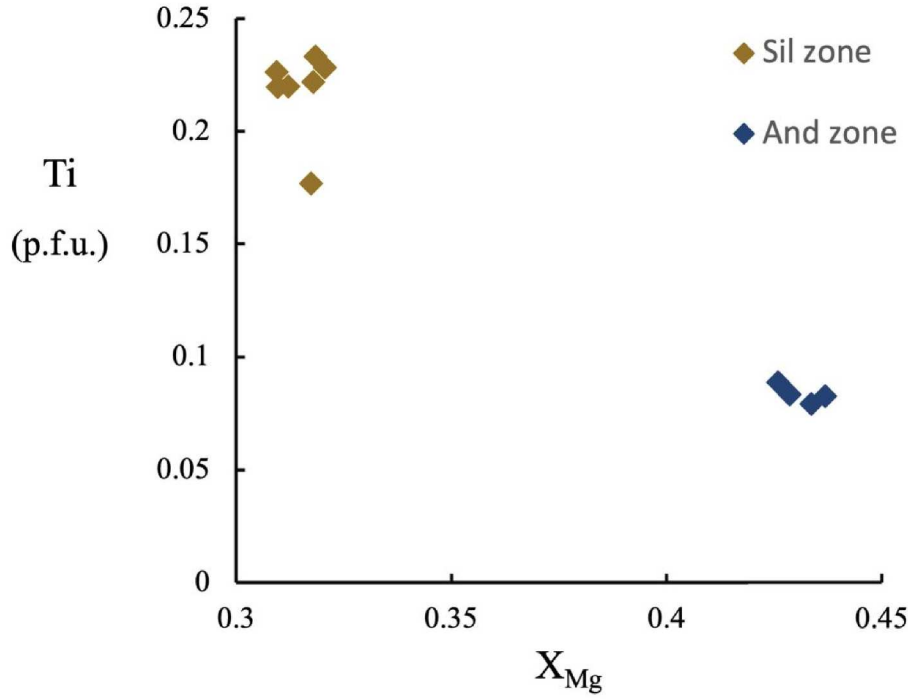

Fig. 3-4-3. Ti (O = 11, p.f.u.) vs X_{Mg} [= Mg / (Mg+Fe)] of biotite. Sil zone from 22032013; And zone from 21080704.

3-5 Metamorphic condition

Metamorphic pressure and temperature (*P-T*) conditions were estimated from the chemical composition of each mineral using conventional geothermobarometers. The chemical composition of the garnet at the low-Mn rim was regarded as peak metamorphism (Figs. 3-4-1 and 3-4-2). In addition to the above-described garnet, plagioclase and biotite were used on the geothermobarometers. In the Bt and And zones (M), Garnet was not observed in the pelitic rocks. The rocks from the And zone (N) likely underwent contact metamorphism owing to the intrusion of the granite stock (Fig. 3-2-8). Therefore, the metamorphic conditions were unlikely to be estimated in the Bt zone, and And (N) and And (M) zones.

The Grt-Bt (Ferry and Spear, 1978; Hodges and Spear, 1982) and the Grt-Bt-Pl-Qz (Hoisch, 1990) geothermobarometers were used for the temperature and pressure estimation, respectively. Ti in biotite geothermometer (Henry et al., 2005) is to be verified. The calculation method is explained in the chapter 2-5 of Nojima Island.

Table 3-5-1. Data set used for calibration.

Sample. No	K_{R1}	K_{R2}	X^{B}_{Mg}	X^{B}_{Fe}	X^{B}_{Al}	X^{B}_{Ti}	ΔV_{gr} (J/bar)
21121911	262.21	51.33	0.220	0.431	0.147	0.052	-1.145
22032013	448.03	114.23	0.271	0.429	0.124	0.057	-0.937
21080704	2077.92	340.05	0.226	0.490	0.134	0.038	-1.561

Where: X^{B}_{Mg} = Mg/3; X^{B}_{Fe} = Fe / 3; X^{B}_{Ti} = Ti / 3; X^{B}_{Al} = (Al + Si - 4) / 3. (O = 11, p.f.u.)

Table 3-5-2. Calculated metamorphic *P-T* conditions.

Sample	FS-H			HS-H		
	T (°C)	*P*(MPa)(R1)	*P*(MPa)(R2)	*T* (°C)	*P*(MPa)(R1)	*P*(MPa)(R2)
21121911	603	326	329	610	334	340
22032013	709	389	390	718	399	403
21080704	534	60	64	537	62	68

FS-H: Ferry & Spear (1978) - Hoisch (1990);
HS-H: Hodges & Spear (1982) - Hoisch (1990)

Fig.3-5-1 shows the results of Ti in biotite temperature. In Sil zone, the temperature range is 650–700 °C, in And zone, the temperature range is 500–600 °C. They are consistent within the error range.

The calculated metamorphic *P-T* conditions are listed in Table 3-5-2. The And and Sil zones would be 530 °C, 60 MPa and 600–720 °C, 330–400 MPa, respectively. These *P-T* conditions are similar to the Low-*P/T* of Kasadojima Island at 550 °C, 250 MPa (Beppu and Okudaira, 2006).

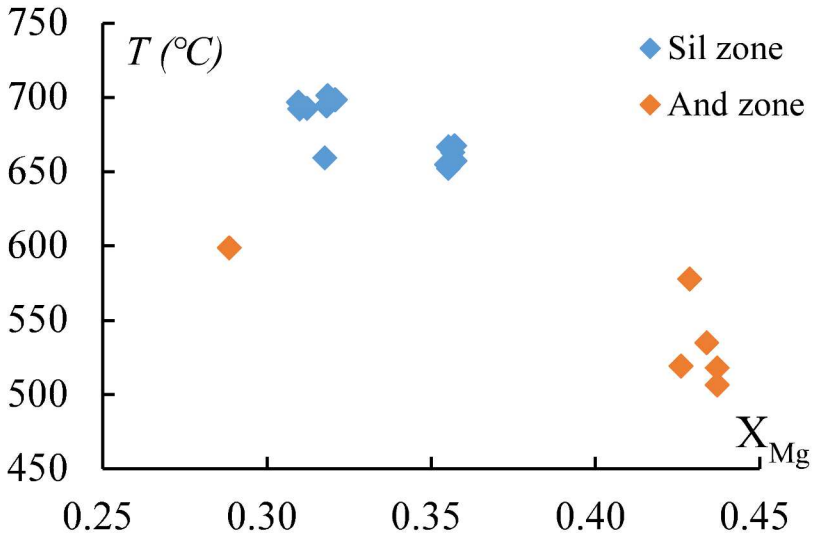

Fig. 3-5-1. Ti in biotite temperature (°C) vs X_{Mg}. (Sil zone from 22032013; And zone from 21080704.)

3-6 U–Pb age

Zircons were extracted from sample 21091908A, a psammitic schist in the And zone (M), for detrital zircon dating. Zircon extraction from the samples and zircon U–Pb dating were performed by Kyoto Fission-Track Co., Ltd., Japan. In situ U–Pb dating was carried out using a New Plasma II ICP-MS (Nu instruments, Wrexham, UK), combined with a LIGHT CONVERSION laser system equipped with a 257 nm Yb: KGW femtosecond laser at the Department of Geology and Mineralogy, Kyoto University. The laser spot size of 10 μm in diameter was used. The zircon U–Pb data and analytical conditions for LA-ICP-MS are presented in the appendix. The information about CL images is explained in the chapter 2-7 of Nojima Island.

Fig. 3-6-1 shows CL images of the zircon. All zircon grains were analyzed in the core parts. The Th/U ratios and zoning patterns of the analyzed grains were separated into two groups. One group was composed of young-aged zircon grains with oscillatory zoning and high Th/U ratios (0.21–0.96). The other one consisted of old-aged zircon grains with no zoning and low Th/U ratios (0.03–0.19). The isotope ratios of $^{206}Pb/^{238}U$ and $^{207}Pb/^{235}U$ were statistically analyzed using Isoplot software (Ludwig, 2012). These were plotted on Concordia diagrams (Fig. 3-6-2). All data point error ellipses are 2σ (95% confidence). The results showed two major components from 1900 to 1800 Ma and ca. 250 Ma. Following the method of Dickinson and Gehrels (2009), the weighted mean age was calculated with 16 grains that overlap in age at 2σ, using ^{238}U–^{206}Pb ages. The result of the calculated 250.6 ± 4.5 Ma indicates the depositional age of the protolith (Fig. 3-6-3). Consequently, the ages of the detrital zircons possess two major peaks: Paleoproterozoic and Permo-Triassic.

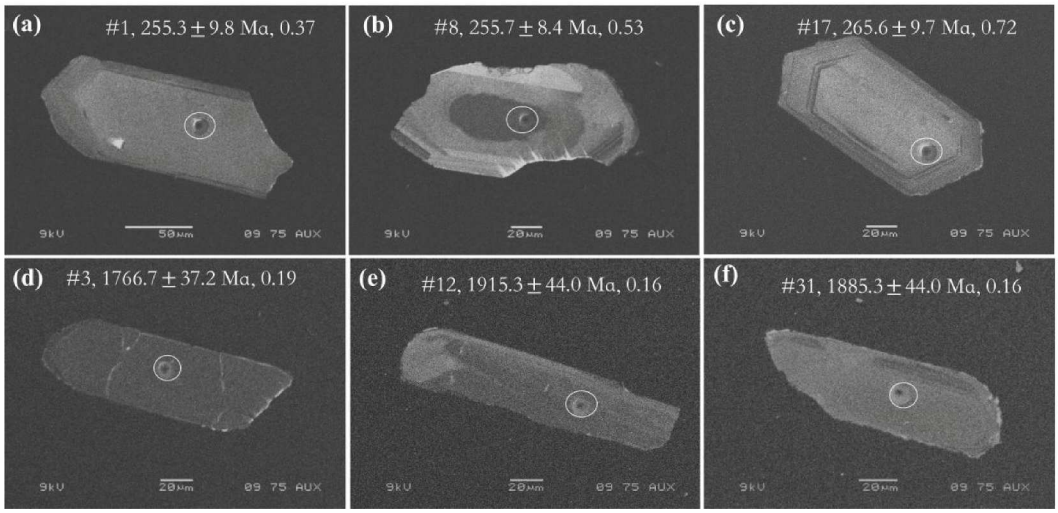

Fig. 3-6-1. Cathodoluminescence (CL) images of zircon grains. The "#" means grain number. The values with error ranges show the ^{206}Pb–^{238}U age. The right-side values indicate Th/U ratios.

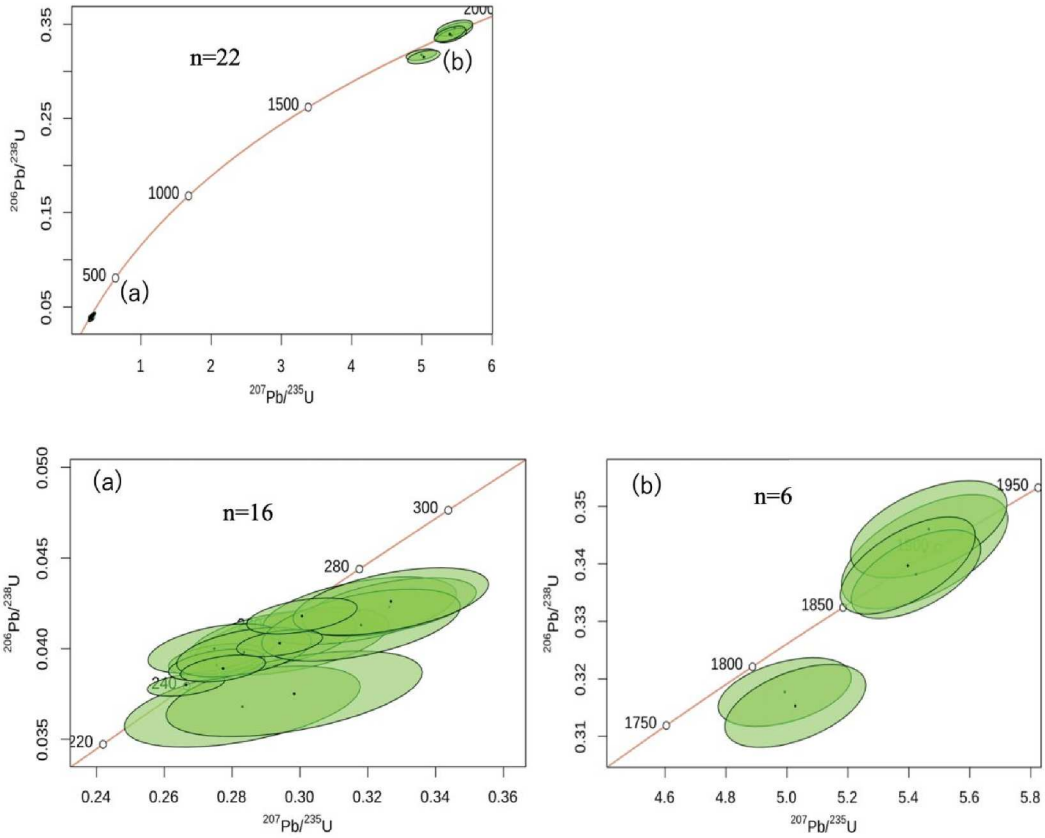

Fig. 3-6-2. Results of zircon U–Pb dating of Sample 21091908A, located in the And zone (M). Concordia diagrams for the detrital zircons (All date point error ellipses are 2σ). a: The younger age cluster. b: The older age cluster.

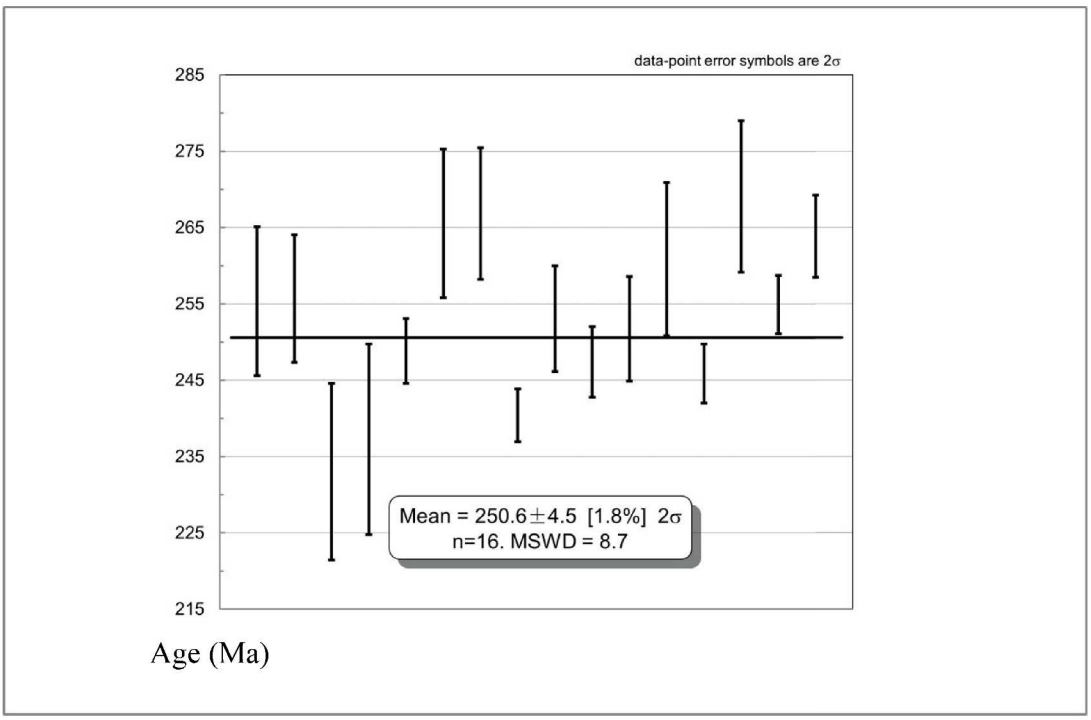

Fig. 3-6-3. The weighted mean age in Ozushima Island.

3-7 Summary

The detrital zircon U–Pb dating revealed an age of 250.6 ± 4.5 Ma, as the youngest mean value from the metamorphic rocks on Ozushima Island. According to this protolith age, the metamorphic rocks on Ozushima Island were deposited in the Late Permian and belong to the Suo Belt. Based on mineral paragenesis and estimated *P-T* conditions, the metamorphic rocks can be divided into three metamorphic zones: Bt, And, and Sil zones, which underwent Low-*P/T* type metamorphism. The peak metamorphic conditions of the And and Sil zones would be 530 °C and 60 MPa and 600–720 °C, 330–400 MPa, respectively. These *P-T* conditions are similar to those of metamorphic rocks on Ksadojima Island, which belongs to the Ryoke metamorphic belt (Beppu and Okudaira, 2006). Considering the spatial proximity of Ozushima and Kasadojima Islands, the metamorphic rocks on Ozushima Island clearly underwent the Low-*P/T* type Ryoke metamorphism.

4. Oshima Peninsula

4-1 Geological outline

Oshima Peninsula is located in the Seto Inland Sea south of Shunan City in southern Yamaguchi Prefecture, with a length of 6 km from north to south and a width of 5 km from east to west (Fig. 4-1-1). This peninsula is topographically divided into two parts, Oshima and Sukumojima Island (Fig. 4-1-1). The constituent rocks from Oshima Peninsula consist mainly of crystalline schist and metabasalt as basement rocks, and unconformable overlaying Cretaceous volcanic rocks with small amounts of granite stocks (Fig. 4-1-1).

Based on field research in Oshima, the crystalline schist is composed of pelitic schist and siliceous schist (Fig. 4-1-2). The schistosity strikes in an east-west direction and gently dips towards the north and south. Fold structures with an E–W trending axis were also developed. In Sukumojima Island, the crystalline schist is almost composed of pelitic schist (Fig. 4-1-3), and a granite stock intrudes into the metamorphic rocks in the western part of the island (Fig. 4-1-4).

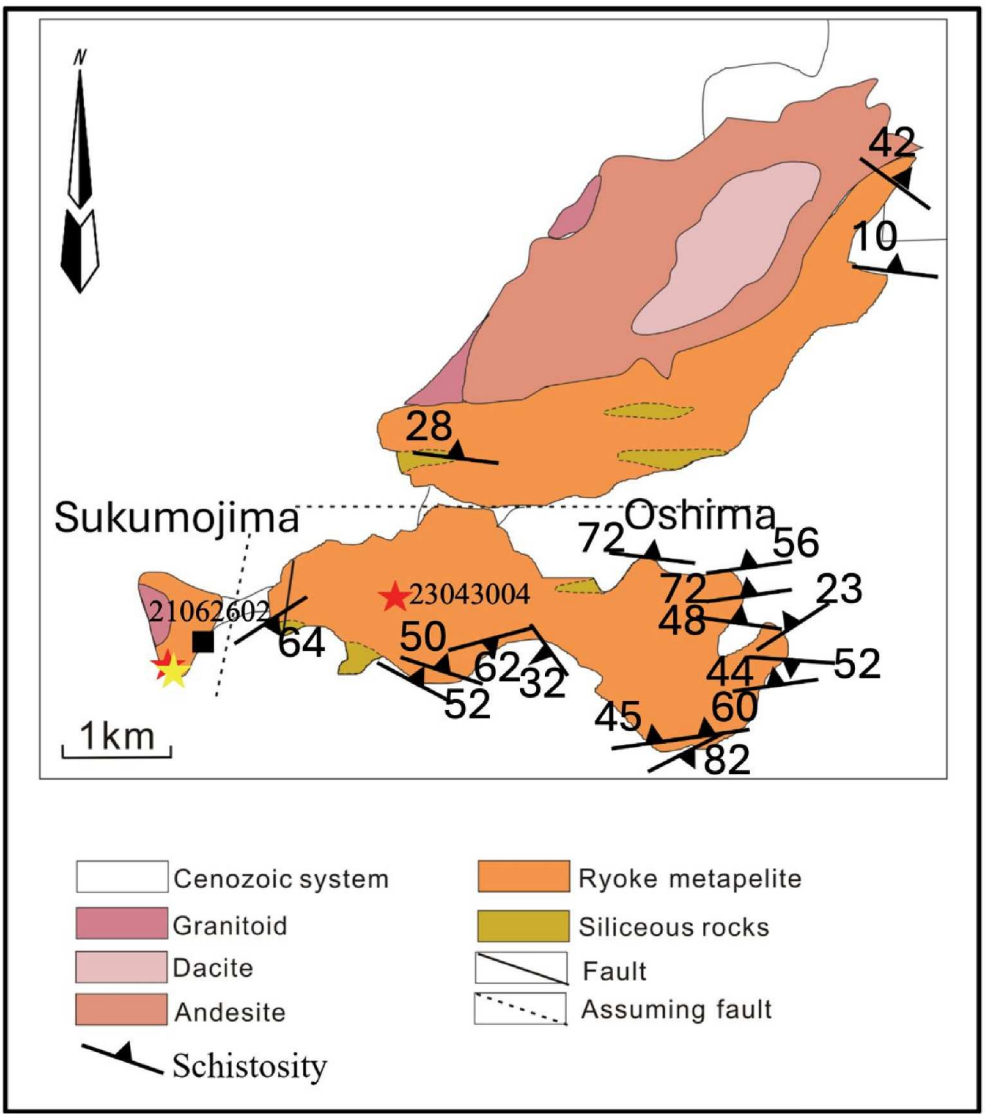

Fig. 4-1-1. Geological map of Oshima Peninsula (modified Geological Survey of Japan, AIST, 2024). The red star indicates the sampling site for zircon U–Pb dating. The yellow star indicates the sampling site for K–Ar age. The black square indicates the sampling site.

Fig. 4-1-2. Pelitic schist and siliceous schist in Oshima.

Fig. 4-1-3. Pelitic schist in Sukumojima Island.

Fig. 4-1-4. Granite stock intrudes into pelitic schist in Sukumojima Island.

4-2 Petrographical characteristics

In Oshima, the mineral assemblages of the pelitic schist differ between the northern and southern parts. Fine-grained biotite and muscovite are oriented, and they form schistosity coexisting with quartz and plagioclase, in the north (Fig. 4-2-1). In the south, the schistosity is more pronounced due to the formation of oriented biotite and muscovite grains. The mineral assemblages are mainly biotite, muscovite, garnet, cordierite, and K-feldspar (Figs. 4-4-2 and 4-4-3). In Sukumojima Island, fine-grained biotite and muscovite form schistosity. Porphyroblastic andalusite is surrounded by muscovite (Fig. 4-4-4). The fine-grained garnet exists with biotite and muscovite (Fig. 4-4-5).

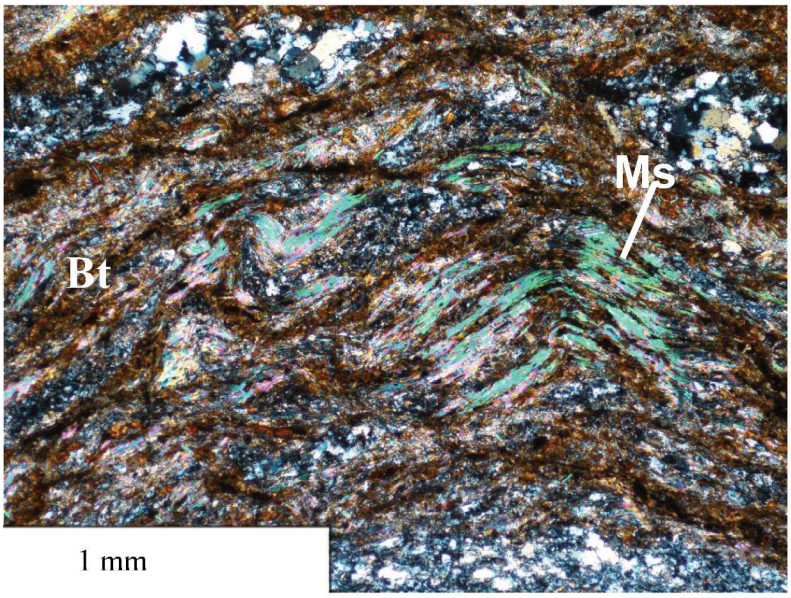

Fig. 4-2-1. Fine-grained biotite and muscovite are oriented and form schistosity in Oshima.

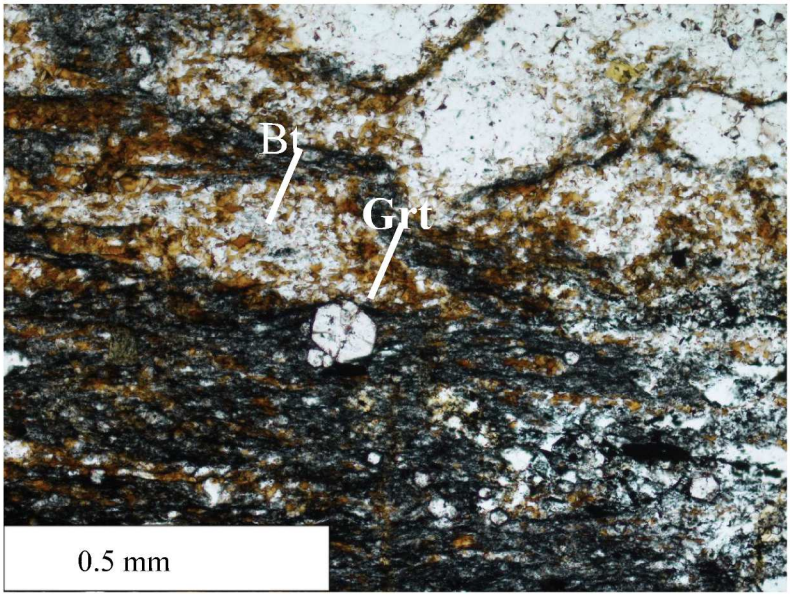

Fig. 4-2-2. Garnet in pelitic schist in Oshima.

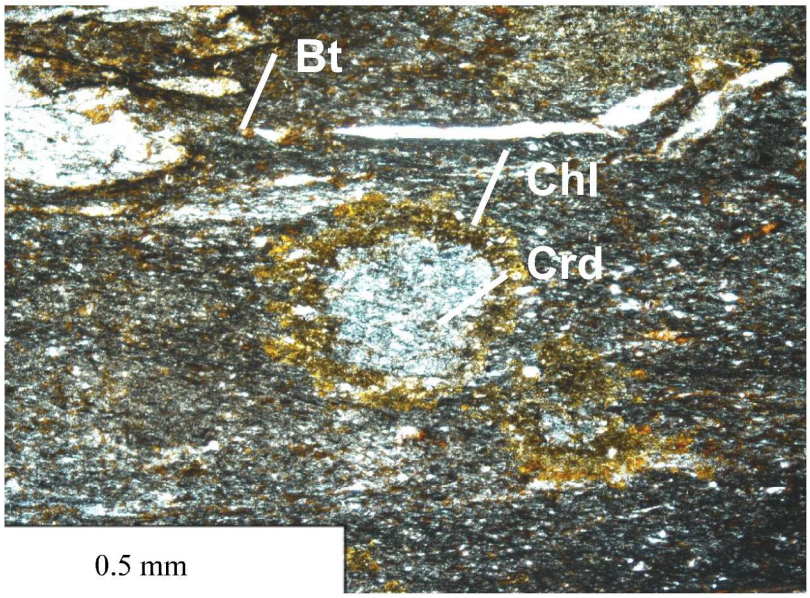

Fig. 4-2-3. Cordierite in pelitic schist in Oshima.

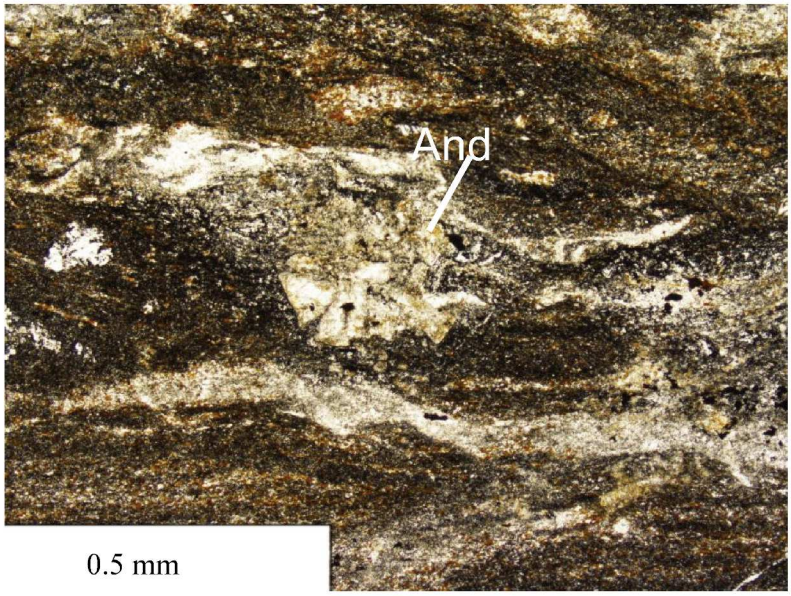

Fig. 4-2-4. Andalusite is surrounded by Muscovite in Sukumojima Island.

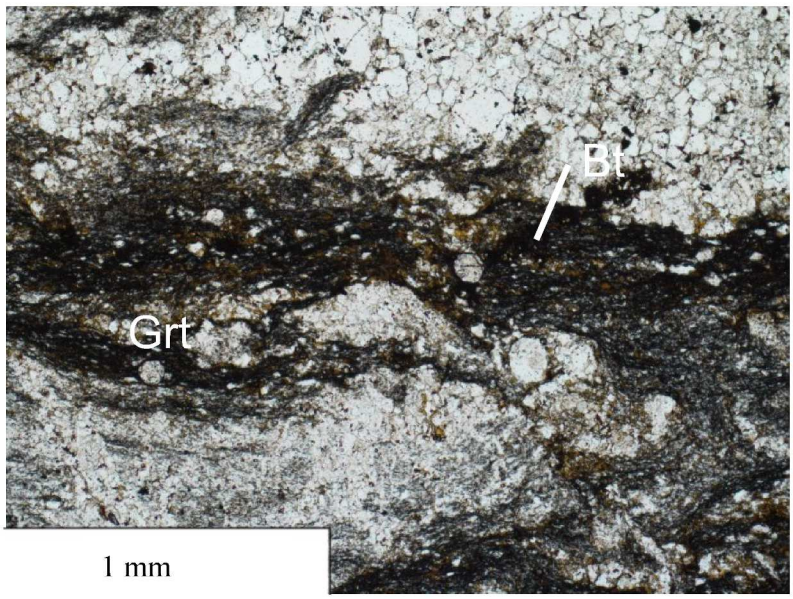

Fig. 4-2-5. Fine-grained garnet in Sukumojima Island.

4.3 Metamorphic zoning

The metamorphic zoning on Oshima peninsula is defined using the mineral parageneses of the pelitic schists. Metamorphic rocks can be spatially divided into Bt zone and And-Crd zone (Fig. 4-3-1).

Bt zone

This zone is located in the northern part of the island. The Bt zone was defined by the paragenesis of muscovite and biotite. Fine-grained chlorite occurs locally in the muscovite- and biotite-rich layers. The main mineral assemblages are as follows:

Bt + Ms ± Chl

And-Crd zone

This zone is defined by the first appearance of cordierite. In Oshima, garnet-bearing and garnet-free mineral assemblages are present, probably owing to differences in bulk-chemical compositions. The main assemblages are as follows:

Bt + Kfs + Ms + Crd + Grt

In Sukumojima, cordierite-free mineral assemblages are also present.

Bt + Ms + Grt + Kfs

Andalusite is present on the island, coexisting with cordierite.

Bt + Crd + And + Ms

The metamorphic rocks of Oshima peninsula are considered to have undergone progressive metamorphism, with grade increasing from north to south.

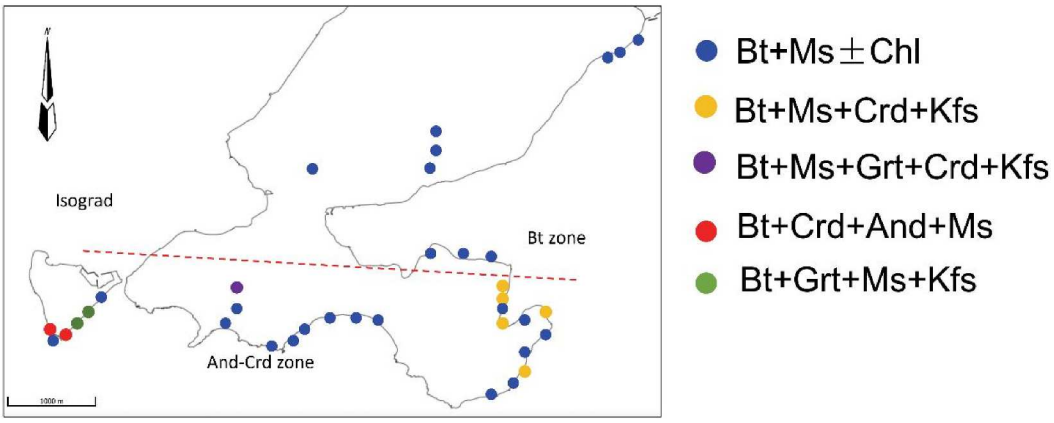

Fig. 4-3-1. The map shows the metamorphic zonation of Oshima Peninsula.

4-4 Mineral chemistry

Mineral compositions were measured by a JXA-8230 by JEOL housed at the Center for Instrumental Analyses, Yamaguchi University. The measurement conditions were 15 kV and 20 nA, and the beam diameter was normally <5 μm. To determine the metamorphic *P–T* conditions, the analyzed samples were selected from the And-Crd zone of pelitic rocks, sample 21062603 in Sukumojima Island, and sample 23043004 in Oshima.

The chemical compositions of garnet were rich in Alm (almandine) and Sps (spessartine) and poor in Prp (Pyrope) and Grs (grossular). All the garnet grains exhibited normal zoning, characterized by an increase in Fe and a decrease in Mn from the core to the rim. Figs. 4-4-1 and 4-4-2 show zoning profiles of garnets from Oshima and Sukumojima Island. They also show the normal zoning. Biotite was chemically homogenous in each zone. The chemical composition of biotite depends on the mineral combination. In the Sakurajima Island, Ti (0.1–015) is lower than in Oshima (0.15–0.25), and X_{Mg} [Mg / (Mg+Fe)] = 0.41–0.49 is also lower than those of Oshima (X_{Mg} = 0.39–0.46). The chemical compositions of plagioclase remain nearly constant as X_{Ab} [Na / (Ca+Na)] = 0.791 in Sukumojima, X_{Ab} = 0.640 in Oshima.

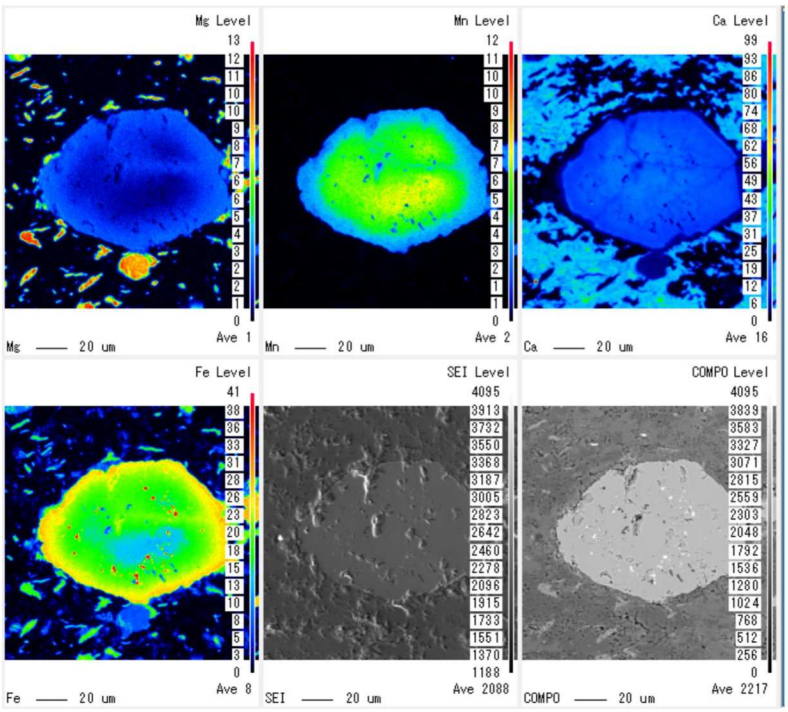

Fig. 4-4-1. Zoning profiles of garnet from (23043004) in Oshima. SEI, BSE image and elemental mapping.

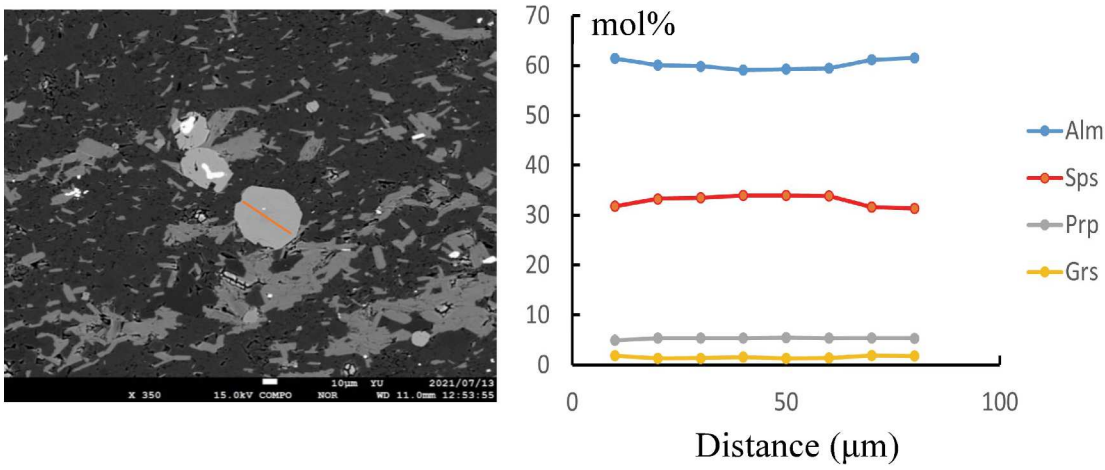

Fig. 4-4-2. Zoning profiles of garnet from (21062603) in Sukumojima Island.

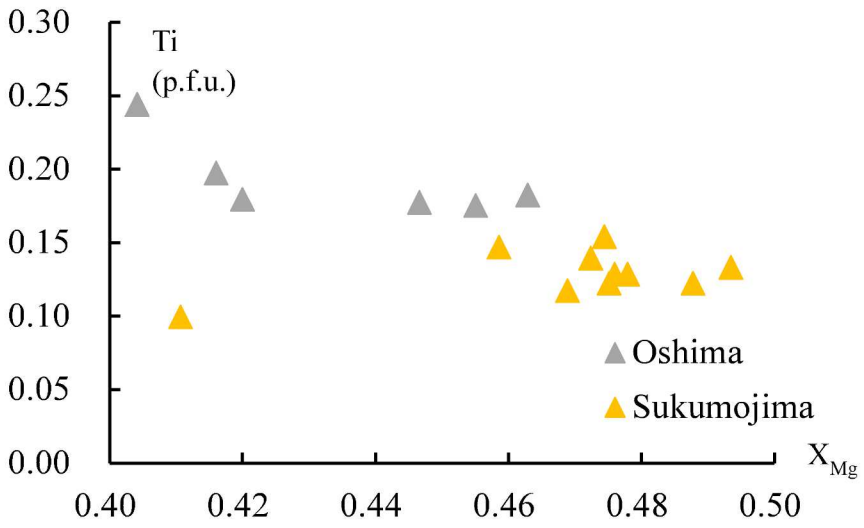

Fig. 4-4-3. Ti (O = 11, p.f.u.) vs X_{Mg} [= Mg / (Mg+Fe)] of biotite in And-Crd zone. (Oshima from 23043004; Sukumojima from 21062603.)

4-5 Metamorphic condition

Metamorphic pressure and temperature (*P-T*) conditions were estimated from the chemical composition of each mineral using conventional geothermobarometers. The chemical composition of the garnet (Figs. 4-4-1 and 4-4-2) at the low-Mn rim was regarded as peak metamorphism.

The estimated metamorphic *P-T* conditions are presented in Table 4-5-2. The Grt-Bt (Ferry and Spear, 1978 (FS); Hodges and Spear, 1982 (HS)) and the Grt-Bt-Pl-Qz (Hoisch, 1990 (H)) geothermobarometers were used for the temperature and pressure estimation, respectively. Ti in biotite geothermometer (Henry et al., 2005) is to be verified. The calculation method is explained in the chapter 2-5 of Nojima Island.

Barometers of Hoisch (1990) are used for R1 and R2, which are based on the net reactions among garnet, plagioclase, biotite, and quartz.

Table 4-5-1. Data set used for calibration.

Sample. No	K_{R1}	K_{R2}	X^{B}_{Mg}	X^{B}_{Fe}	X^{B}_{Al}	X^{B}_{Ti}	ΔV_{gr} (J/bar)
23043004	704.35	142.67	0.276	0.377	0.092	0.074	-0.302
21062602	1730.58	284.02	0.383	0.374	0.079	0.051	-0.899

Where: X^{B}_{Mg} = Mg / 3; X^{B}_{Fe} = Fe / 3 ; X^{B}_{Ti} = Ti / 3; X^{B}_{Al} = (Al + Si - 4) / 3. (O = 11, p.f.u.)

Table 4-5-2. Calculated metamorphic *P-T* conditions.

Sample. No	FS-H			HS-H		
	T (°C)	*P*(MPa)(R1)	*P*(MPa)(R2)	*T* (°C)	*P*(MPa)(R1)	*P*(MPa)(R2)
23043004	595	287	284	616	310	317
21062602	529	137	137	538	145	149

FS-H: Ferry & Spear (1978)- Hoisch (1990);
HS-H: Hodges & Spear (1982)- Hoisch (1990)

Fig.4-5-1 shows the results of Ti in biotite temperature. In Oshima, the temperature range is 650–720 ℃, slightly higher than the Grt-Bt geothermometer. In Sukuojima, the temperature range is 550–650 ℃, a little higher than the Grt-Bt geothermometer. It is possible because the biotite exhibited the characteristic of higher Ti than other areas in a similar metamorphic grade. And biotite Ti-substitution mechanisms are controlled by several factors, which also affect the result of the Ti in biotite temperatures.

The calculated metamorphic *P-T* conditions are listed in Table 4-5-2. The peak metamorphic conditions of the And-Crd zones would be 520–600 °C and 120–320 MPa, respectively, which underwent Low-*P/T* type metamorphism. These *P-T* conditions are similar to the Low-*P/T* of Kasadojima Island at 550 °C, 250 MPa (Beppu and Okudaira, 2006).

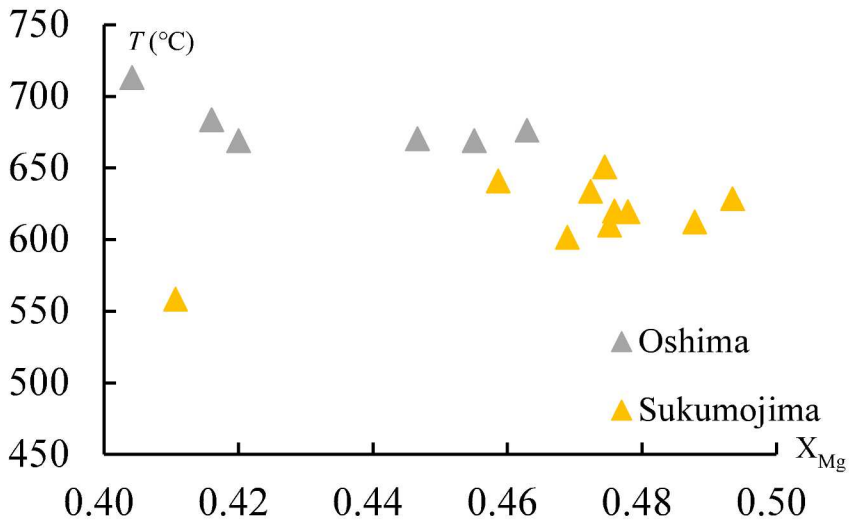

Fig. 4-5-1. Ti in biotite temperature (°C) vs X_{Mg}. (Oshima from 23043004; Sukumojima from 21062603.)

4-6 Biotite K–Ar age

The biotite K–Ar dating was performed by ACTLabs Geometallurgy-MLA Dept. The result is 90.1 ± 2.1 Ma (Table 4-6-1). The age is identified with time for passing through the closure temperature of biotite, probably at approximately 300 °C, suggesting the metamorphic rocks of Sukumojima Island were undergone by Low-*P/T* peak metamorphism at least 90 Ma.

Table 4-6-1. Biotite K–Ar age.

lithology	**location**	**K (wt%)**	**^{40}Ar rad, (ng/g)**	**^{40}Ar" air (%)**	**K-Ar age (Ma)**
Metapelite	Sukumojima	7.31 ± 0.08	46.8 ± 0.15	7.1	90.1 ± 2.1

4-7 U–Pb age

Zircon U–Pb dating was conducted for the pelitic schists from the And-Crd zone, samples 23043004 and 21062610 in Sukumojima Island and in Oshima, respectively. Zircon extraction from the samples and zircon U–Pb dating were performed by Kyoto Fission-Track Co., Ltd., Japan. In situ U-Pb dating was carried out using a New Plasma II ICP-MS (Nu instruments, Wrexham, UK), combined with a LIGHT CONVERSION laser system equipped with a 257 nm Yb: KGW femtosecond laser at the Department of Geology and Mineralogy, Kyoto University. The laser spot size of 10 μm in diameter was used. The zircon U–Pb data and analytical conditions for LA-ICP-MS are presented in the appendix. The cathodoluminescence (CL) images were obtained using a JEOL JSM-6360 scanning electron microscope at the Center for Instrumental Analyses, Yamaguchi University, Japan. The information about CL images is explained in the chapter 2-7 of Nojima Island.

Figs. 4-7-1 and 4-7-2 show CL images of the zircon grains for each sample. The zircon grains were analyzed in the core and rim parts (Figs. 4-7-1 and 4-7-2). The isotope ratios of $^{206}Pb/^{238}U$ and $^{207}Pb/^{235}U$ were statistically analyzed using Isoplot software (Ludwig, 2012). These were plotted on Concordia diagrams (Figs. 4-7-3 and 4-7-4). All data point error ellipses are 2σ (95% confidence). Following the method of Dickinson and Gehrels (2009), the weighted mean age was calculated with 13 and 7 grains that overlap in age at 2σ, using ^{238}U–^{206}Pb ages. The result of the calculated 182.9 ± 1.8 Ma in Oshima and 193.6 ± 3.9 Ma in the Sukumojima Island (Figs. 4-7-5 and 4-7-6) indicates the depositional age of the protolith.

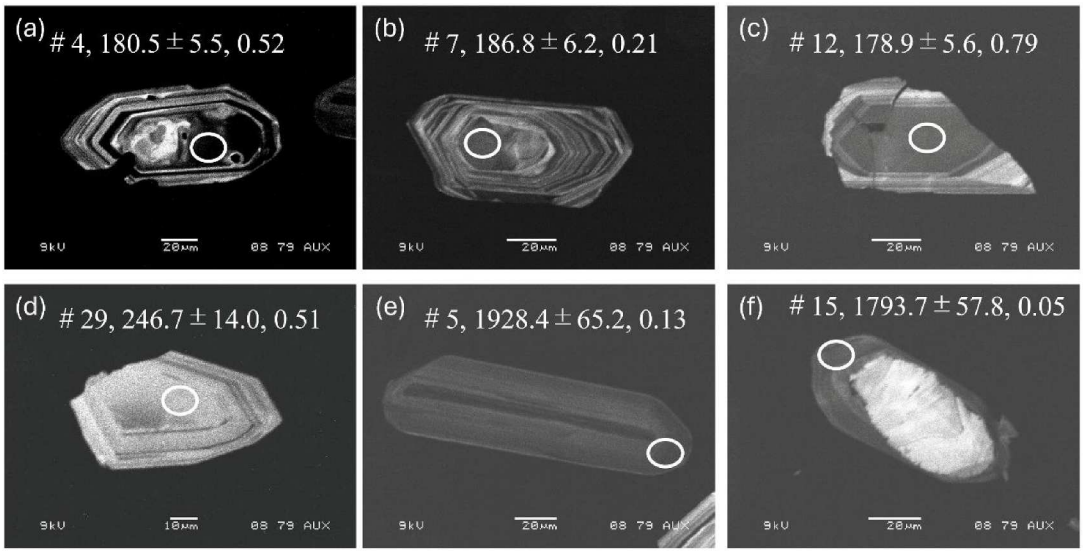

Fig. 4-7-1. Cathodoluminescence (CL) images of zircon grains in Oshima. The "#" means grain number. The values with error ranges show the ^{238}U–^{206}Pb age. The right-side values indicate Th/U ratios.

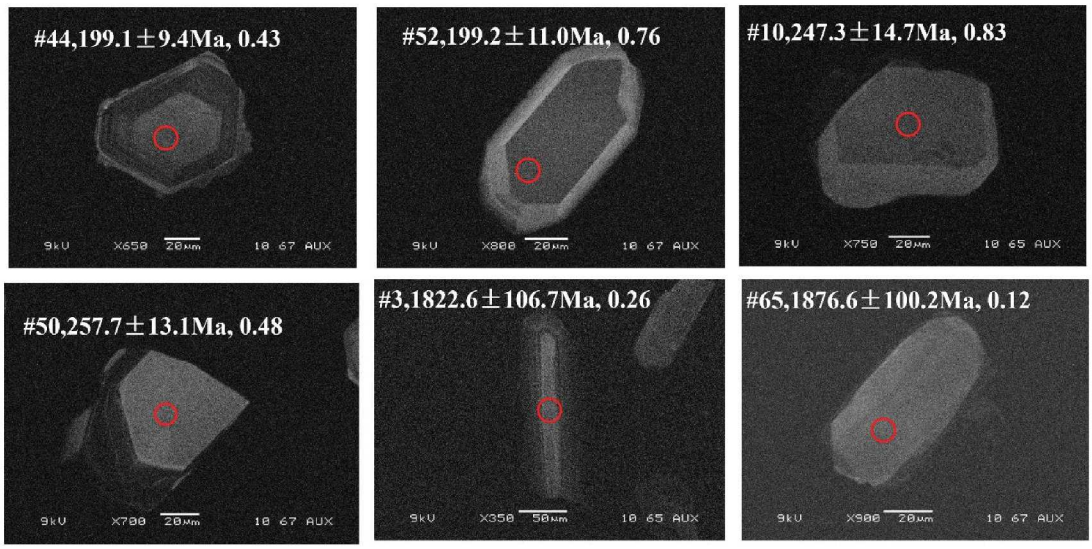

Fig. 4-7-2. Cathodoluminescence (CL) images of zircon grains in Sukumojima Island. The "#" means grain number. The values with error ranges show the ^{238}U–^{206}Pb age. The right-side values indicate Th/U ratios.

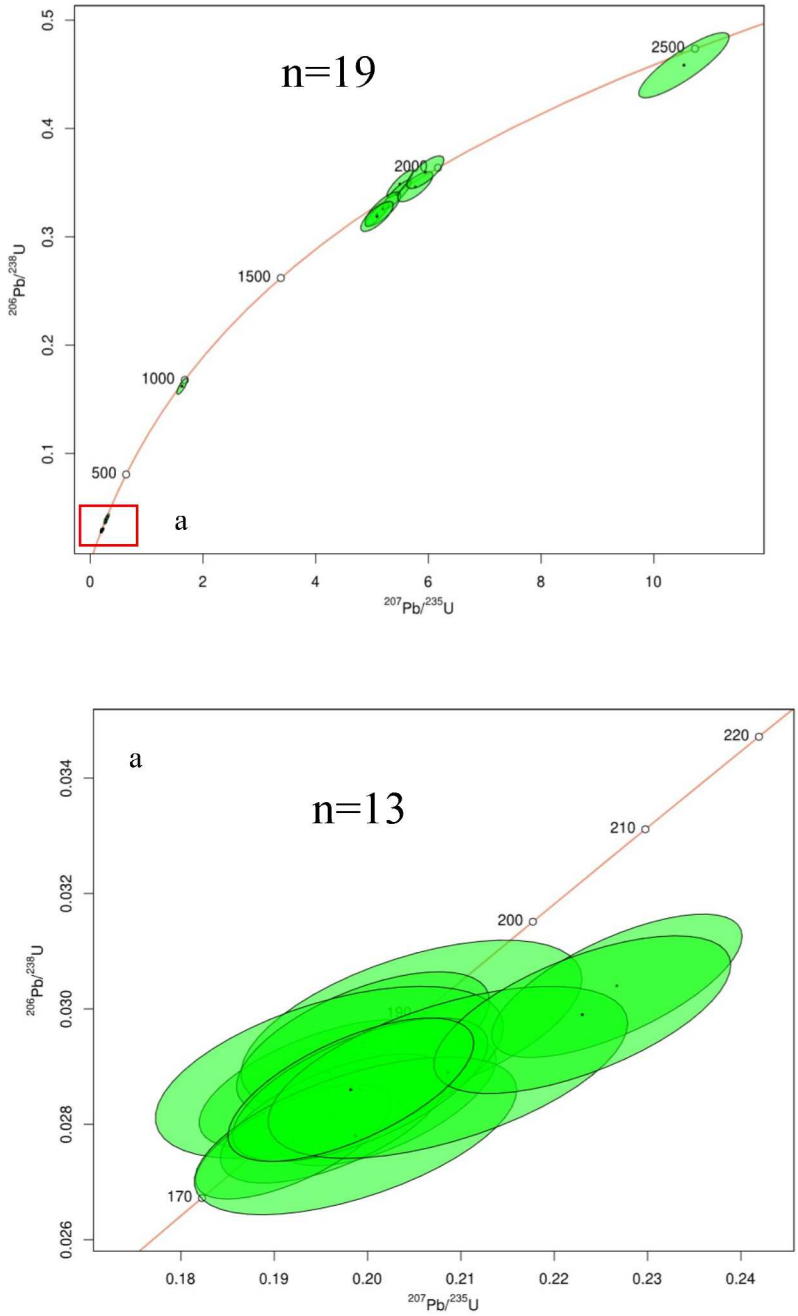

Fig. 4-7-3. Concordia diagrams for the detrital zircons in Oshima (All date point error ellipses are 2σ). a: The younger age cluster.

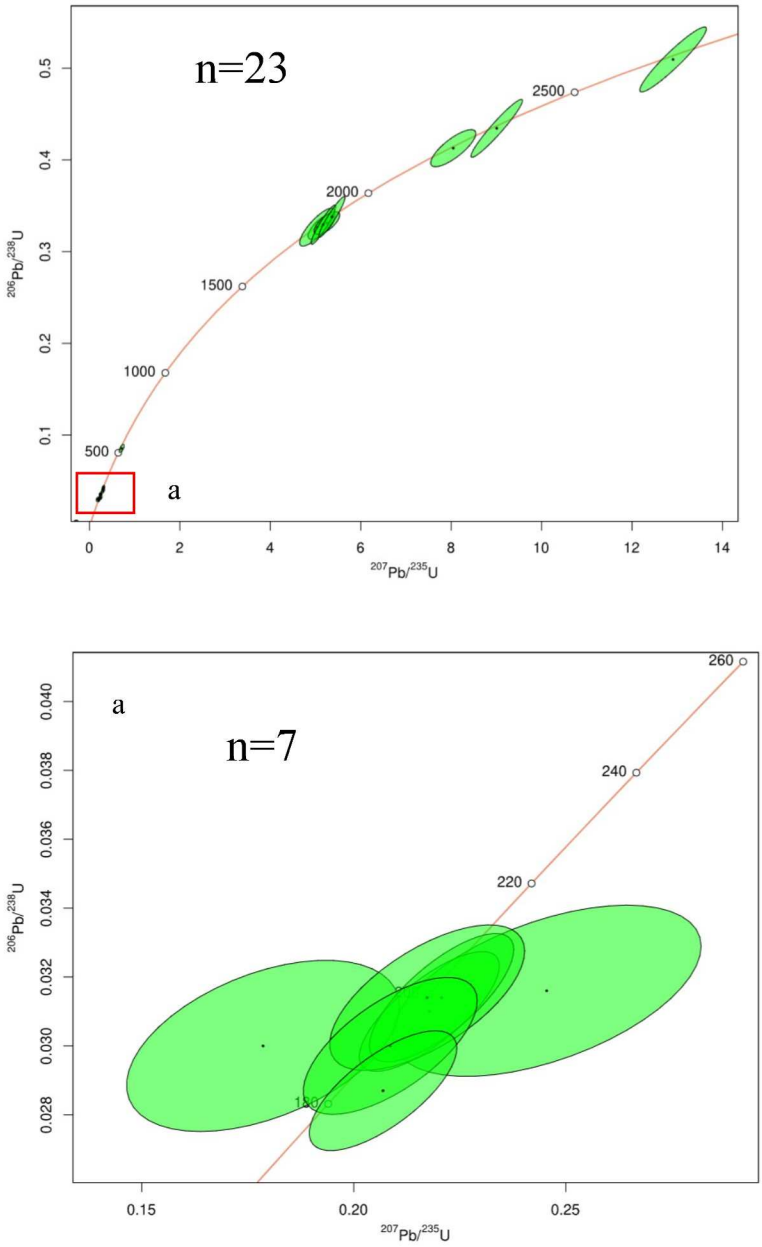

Fig. 4-7-3. Concordia diagrams for the detrital zircons in Sukumojima Island (All date point error ellipses are 2σ). a: The younger age cluster.

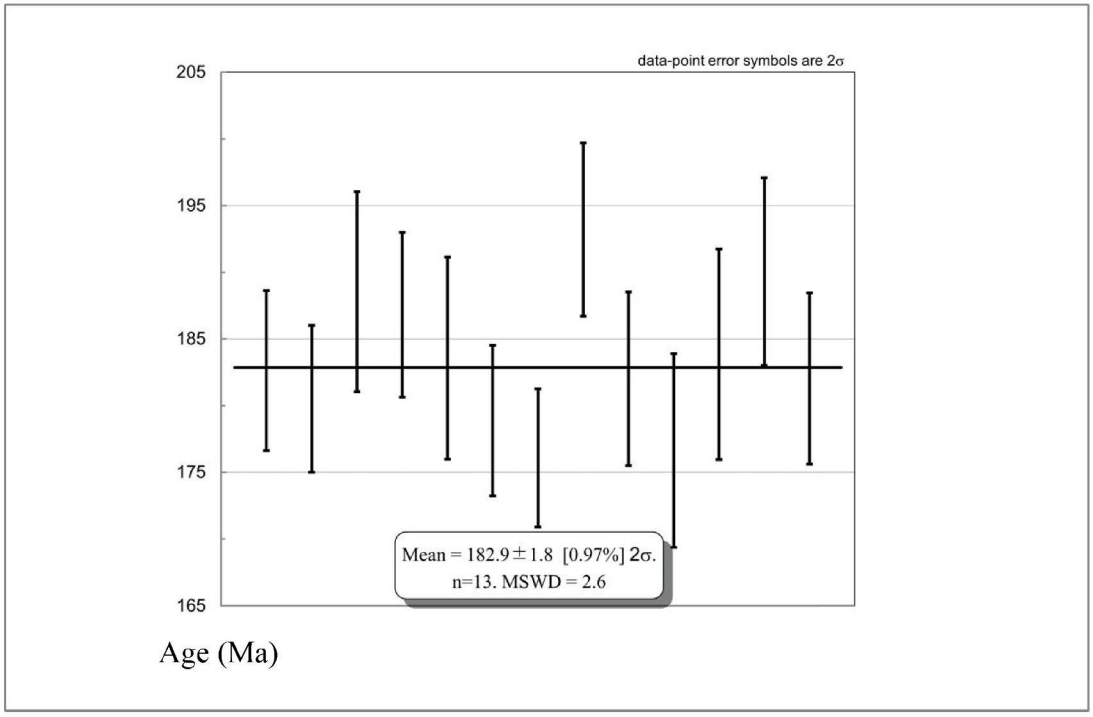

Fig. 4-7-5. The weighted mean age in Oshima.

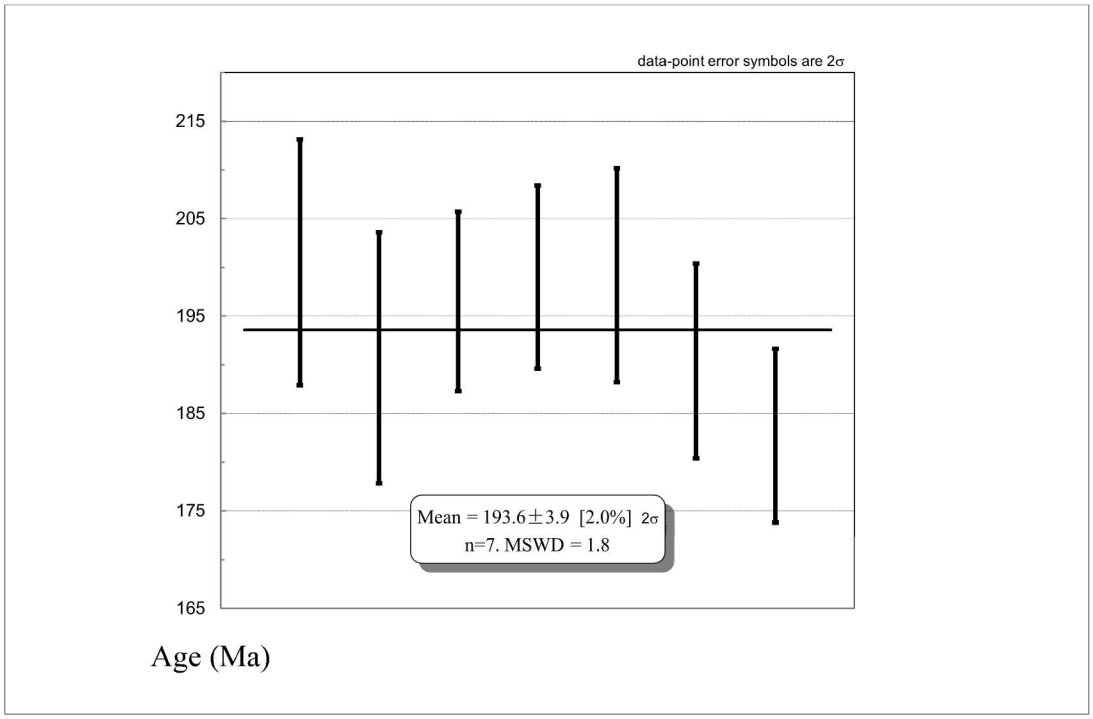

Fig. 4-7-6. The weighted mean age in Sukumojima Island.

4-8 Summary

The detrital zircon U–Pb dating revealed an age of 182.9 ± 1.8 Ma and 193.6 ± 3.9 Ma for Oshima and Sukumojima Island, respectively, as the youngest mean values. The biotite K–Ar age shows 90.1 ± 2.1 Ma in Sukumojima Island. According to this protolith age, the metamorphic rocks on Oshima and Sukumojima Island were deposited in the Jurassic. Based on mineral paragenesis and estimated *P-T* conditions, the metamorphic rocks can be divided into two metamorphic zones: Bt zone and And-Crd zone. The peak metamorphic conditions of the And-Crd zones would be 520–600 °C and 120–320 MPa, respectively, which underwent Low-*P/T* type metamorphism. According to the protolith age and metamorphic *P-T* conditions, the metamorphic rocks from Oshima Peninsula can be correlated with the Ryoke metamorphic rocks from the Iwakuni-Yanai area.

5. Kasadojima Island

To compare the metamorphism and metamorphic cooling age for the previously reported areas in this study, the author conducted sample correction and biotite K–Ar dating from the southern part of Kasadojima Island. The geological map was made by Beppu and Okudaira (2006) (Fig. 5-1-1). The sampling site for biotite K–Ar dating is marked on the geological map (Fig. 5-1-1).

5.1 Brief introduction of geology and metamorphism

According to the report of Beppu and Okudaira (2006), the Ryoke metamorphic rocks exposed on Kasadojima Island consist mainly of metapelite, metapsammite, metachert, and crystalline limestone, accompanied by massive biotite granite, and migmatitic biotite tonalite, which is formed through the injection of tonalitic melt into the pelitic gneiss. The Ryoke metamorphic rocks are divided into Bt zone and Crd zone from north to south, indicating that metamorphic grade increases toward the south. The peak metamorphic conditions for biotite zone and cordierite zone are ~470 °C (reference pressure 200 MPa) and 550 °C at 250 MPa, respectively. The biotite tonalite intruded as a deep-seated granitoid related to regional Low-*P/T* type metamorphism.

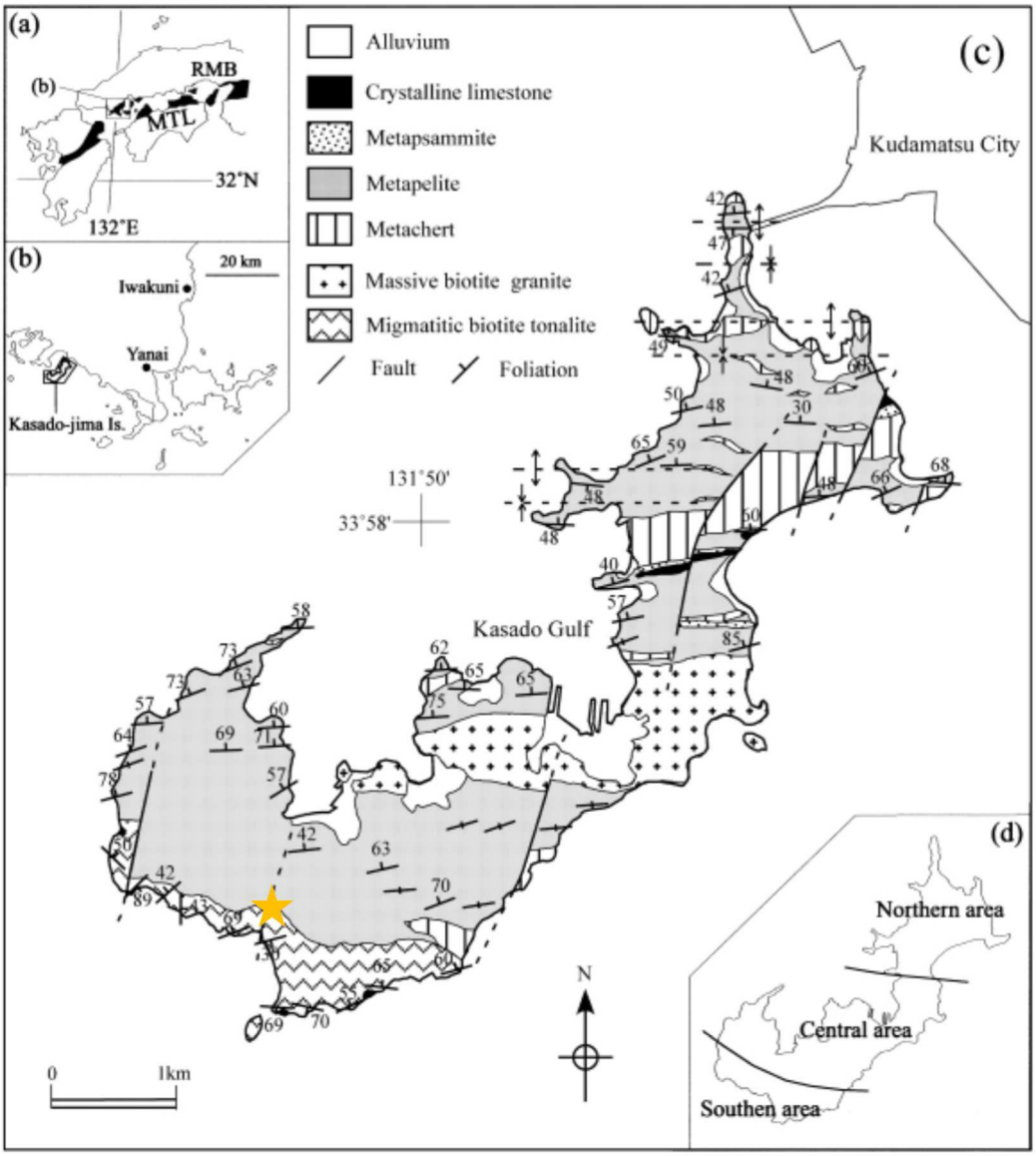

Fig. 5-1-1. Geological map of Kasadojima Island (Beppu and Okudaira, 2006). The yellow star shows the sampling location of biotite K–Ar age.

5.2 Biotite K–Ar age

The collected sample belongs to the Crd zone by Beppu and Okudaira (2006). The dating sample was collected from the southern part of Kasadojima Island, where the pelitic gneiss locally changed the lithofacies into the stromatized migmatite due to the injection of the tonalite melt within the hand-specimen size.

The biotite K–Ar age test was performed by ACTLabs Geometallurgy-MLA Dept. The result is 94 ± 2 Ma (Table 5-2-1). The age is identified with time for passing through the closure temperature of biotite, probably at approximately 300˚C, suggesting the metamorphic rocks of Kasadojima Island were undergone by Low-*P/T* peak metamorphism at least 90 Ma.

Table 5-2-1. Biotite K–Ar age.

lithology	**location**	**K (wt%)**	**^{40}Ar rad, (ng/g)**	**^{40}Ar" air (%)**	**K-Ar age (Ma)**
Migmatite	Kasadojima	7.74 ± 0.08	51.80 ± 0.17	7.1	94 ± 2

6. Discussion

6.1 Regional geothermal gradient

The detrital zircon U–Pb ages reveal depositional ages of the metamorphic rocks. Figure 6-1-1 shows the regional geological map with estimated depositional ages and the metamorphic type of each locality. In Ozushima Island, the depositional age of the low-*P/T* type metamorphic rocks is the Late Permian. Whereas, the metamorphic rocks of Nojima Island and Oshima Peninsula were deposited in the Late Triassic to the Early Jurassic (Fig.6-1-1).

In Ozushima Island, the inferred geothermal gradients from the surface to the And zone and from the And zone to the Sil zone show 80–100 °C/km and 40–50 °C/km, respectively, assuming a crustal density of 2.9 g/cm^3 (Fig. 6-1-2). Similar geothermal gradients are shown in the metamorphic rocks in Oshima Peninsula and Nojima Island (Fig. 6-1-2).

Ikeda (2004) reported the *P-T* condition of Ryoke metamorphic rocks in the Iwakuni-Yanai area. The metamorphic conditions of each metamorphic zone were estimated as follows: 492 °C, 51 MPa in the Chl-Bt zone; 451 °C, 70 MPa in the Bt zone; 519–550 °C, 68–186 MPa in the Ms-Kfs zone: 590–674 °C, 100–296 MPa in the Kfs-Crd zone; 696–755 °C, 556–653 MPa in the Sil-Kfs zone; and 784–852 °C, 430–628 MPa in the Grt-Crd zone. In addition, Skrzypek et al. (2016) complained that the ages of thermal effect of metamorphic rocks were different from each crustal level in terms of zircon U-Pb ages of the granitoids combined with metamorphic conditions and deformational processes. They interpreted the following metamorphic history: the Low-pressure segment of the metamorphic rocks (Bt and Ms-Crd zones) at 105–100 Ma and the High-pressure segment of the metamorphic rocks (Sil-Kfs zone and Grt-Crd zone) at 100–94 Ma. Furthermore, Skrzypek et al. (2018) performed numerous monazite chemical dating analyses of the

metamorphic rocks from each zone. As a result, these monazite ages (99–95 Ma) are slightly younger, but mostly overlapping, than those of peak metamorphic ages inferred from zircon U–Pb dating (103–97 Ma). Overall, they interpreted that the metamorphic period of the Ryoke Belt in the Iwakuni-Yanai area is of 105–95 Ma; then finally metamorphic field gradient in this area would be completed as a result of protracted thermal events for 10 million years (Fig. 6-1-3). The *P-T* conditions of the metamorphic rocks from Kasadojima Island, Oshima Peninsula, Ozushima Island, and Nojima Island are compiled on the *P-T* diagram (Fig.6-1-3). These data, including the *P-T* conditions of the Iwakuni-Yanai area, roughly plot along a single geothermal trend on the *P-T* diagram (Fig.6-1-3). In other words, the low-P type metamorphic rocks around the western part of the Seto Inland Sea are arranged along the coherent geothermal gradient, likely indicating that they underwent the same metamorphic process during the Cretaceous, probably due to the Cretaceous magmatic event as an active heat source.

Ikeda et al. (2017) and Yuhara et al. (2021) reported the metamorphic *P-T* conditions of pelitic rocks from the Omuta and the Chikujo areas, respectively, Kyushu Island. Their studies revealed that these metamorphic rocks underwent Low-*P/T* type metamorphism, although they belong to the Early Triassic High-*P/T* type metamorphic rocks of the Suo Belt. For example, in the Omuta area, the metamorphic conditions were estimated at 510 ± 30 °C and 300 ± 60 MPa in the Ms-And zone, 720 ± 30 °C and 620 ± 60 MPa in the Sil zone (Ikeda et al., 2017). In addition, the metamorphic age of the Omuta area was 105 Ma (Miyazaki et al., 2017). In the Tagawa metamorphic rocks of Chikujo, the metamorphic conditions were 600–650 °C and 200–300 MPa (Yuhara et al., 2021). Compared to the metamorphic *P-T* conditions among the Omuta, Chikujo, and the study areas, they are arranged in a single geothermal trend on the *P-T* diagram (Fig.6-1-4). The metamorphic ages for the Omuta, Chikujo areas and the western Chugoku area would overlap with each other in terms of previously described metamorphic ages of the above areas.

Miyazaki et al. (2004) reported the metamorphic *P-T* conditions of pelitic rocks from Higo area. The metamorphic conditions were estimated as follows: 604 °C, 290 MPa in the Bt zone; 616 °C, 300 MPa in the Sil zone; 696–818 °C, 330–500 MPa in Grt-Crd I zone; and 845 °C, 570 MPa in the Grt-Crd II zone. The age of the high-grade zone of the Higo metamorphic rocks shows 116–110 Ma (Maki et al., 2014) and 120–110 Ma (Vuong et al., 2019). Compared to the metamorphic *P-T* conditions between the Higo Belt and the study area, they also show a single geothermal trend on the *P-T* diagram, although the precise metamorphic ages of the study area are not known yet, probably younger than those of the Higo metamorphism (Fig.6-1-5).

Based on the metamorphic *P-T* conditions, the Low-*P/T* type metamorphic rocks in the western Chugoku and Kyushu areas were formed by an unusually high heat flow, having the geothermal gradient ca. 80 °C/km at the shallower crustal level in the early metamorphic stage. Then, the geothermal gradient with 50 °C/km was obtained at the middle to lower crustal level. Concludingly, the Cretaceous Low-*P/T* metamorphism was caused by advective heat flow as well as heat conduction from a deeper level regardless of any protolith ages.

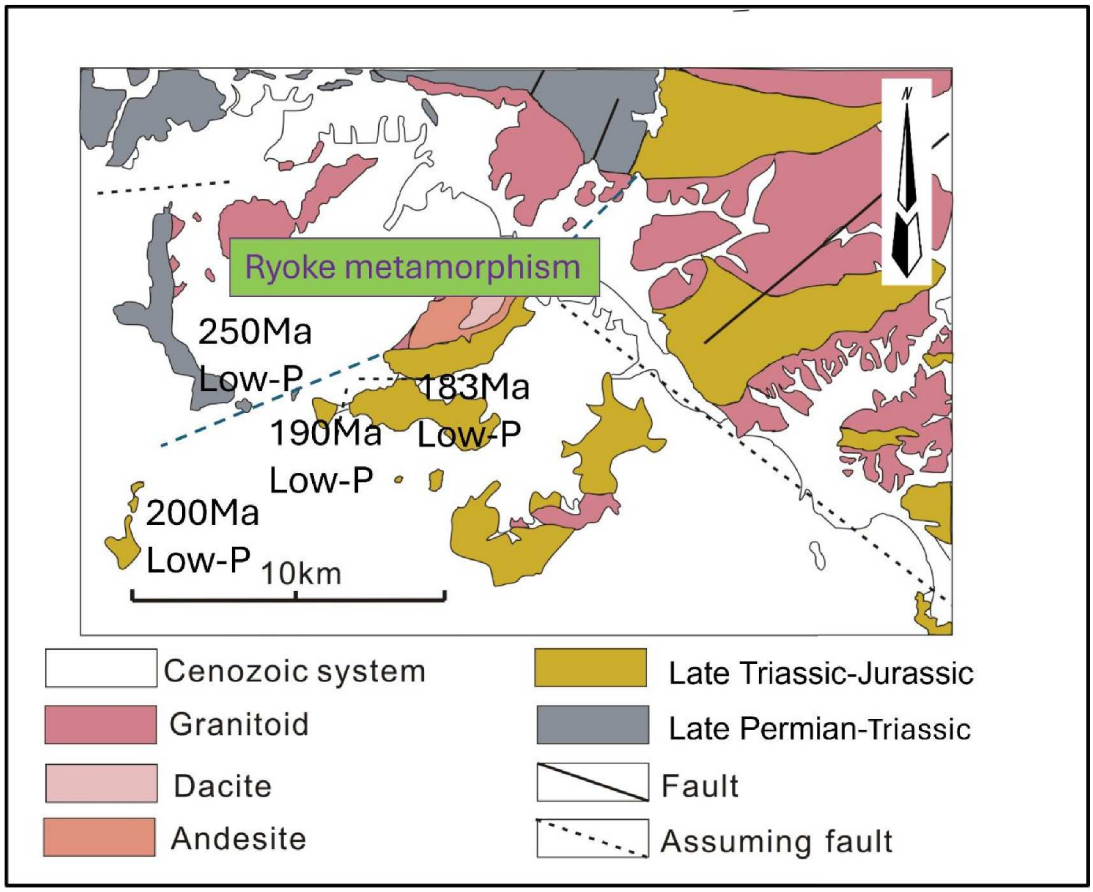

Fig. 6-1-1. Outline of geology of the study area with estimated depositional ages and the metamorphic type of each locality. Geological map is taken from Geological Survey of Japan, AIST (2024).

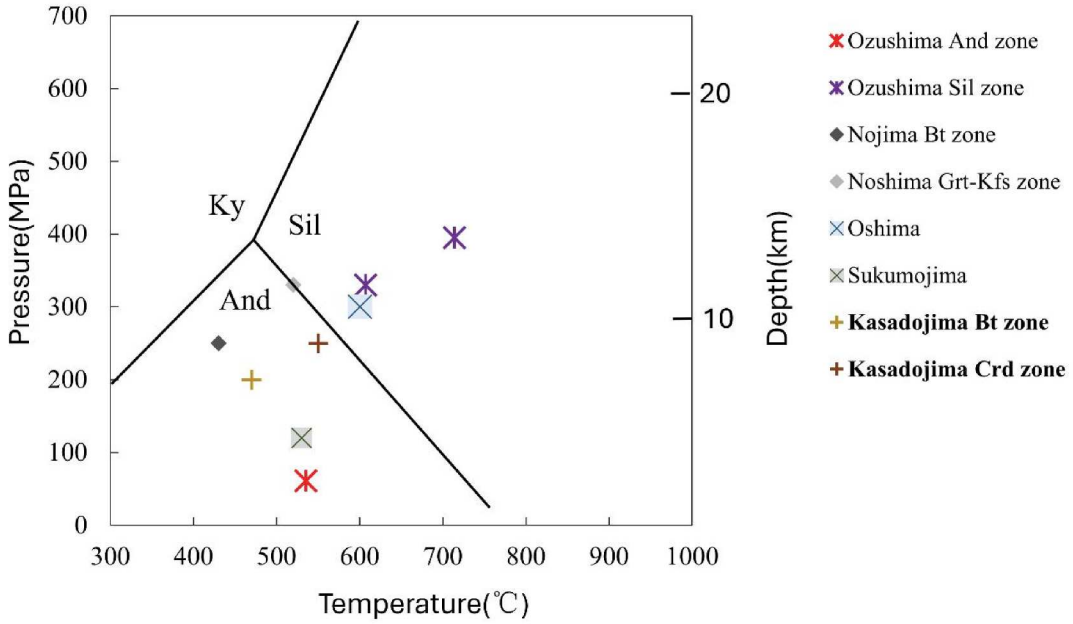

Fig. 6-1-2. The *P-T* metamorphic conditions of the study area. The data of Kasadojima Island are quoted from Beppu and Okudaira (2006).

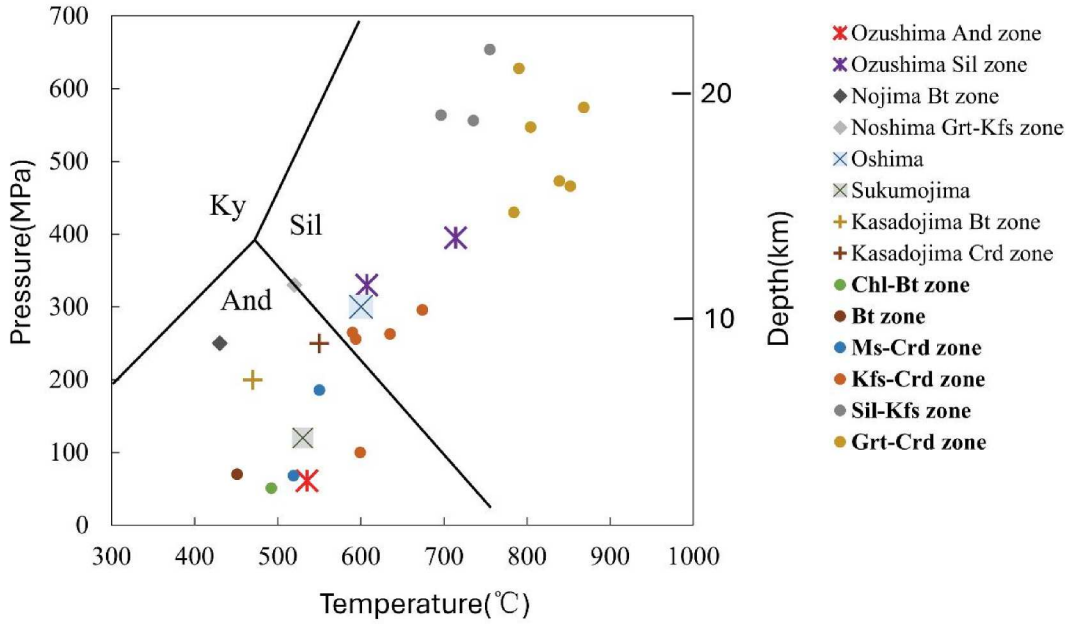

Fig. 6-1-3. The metamorphic *P-T* conditions from the study area and the Iwakuni-Yani area. The circles show data from the Iwakuni-Yanai area (after Ikeda, 2004).

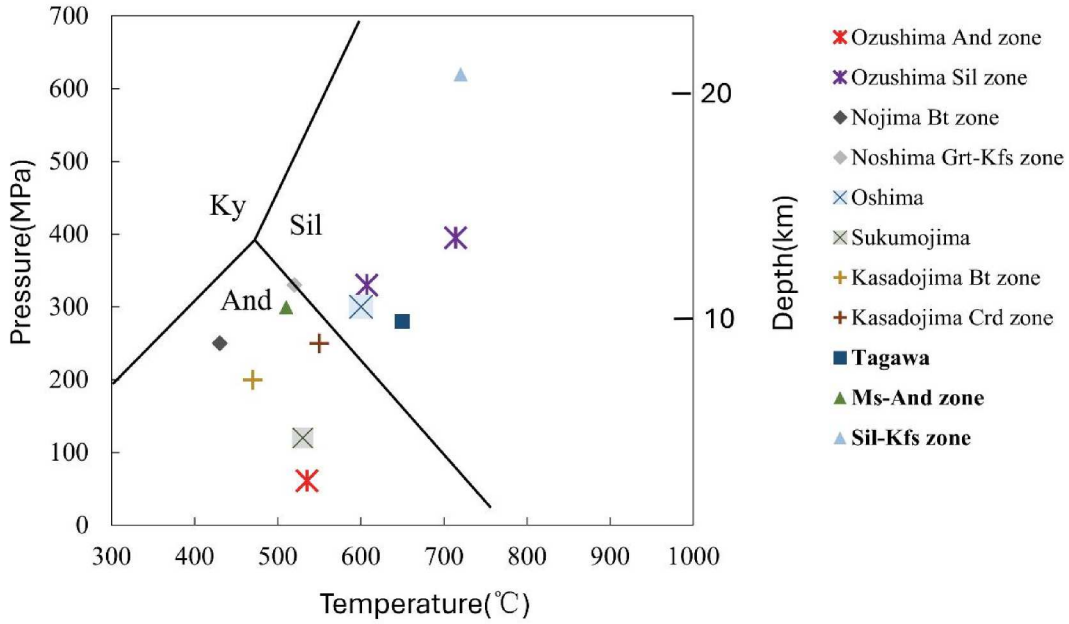

Fig. 6-1-4. The metamorphic *P*-*T* conditions of the study area, Tagawa and Omuta areas. The triangles show data from the Omuta and Tagawa areas are from Ikeda et al. (2017) and Yuhara et al. (2021).

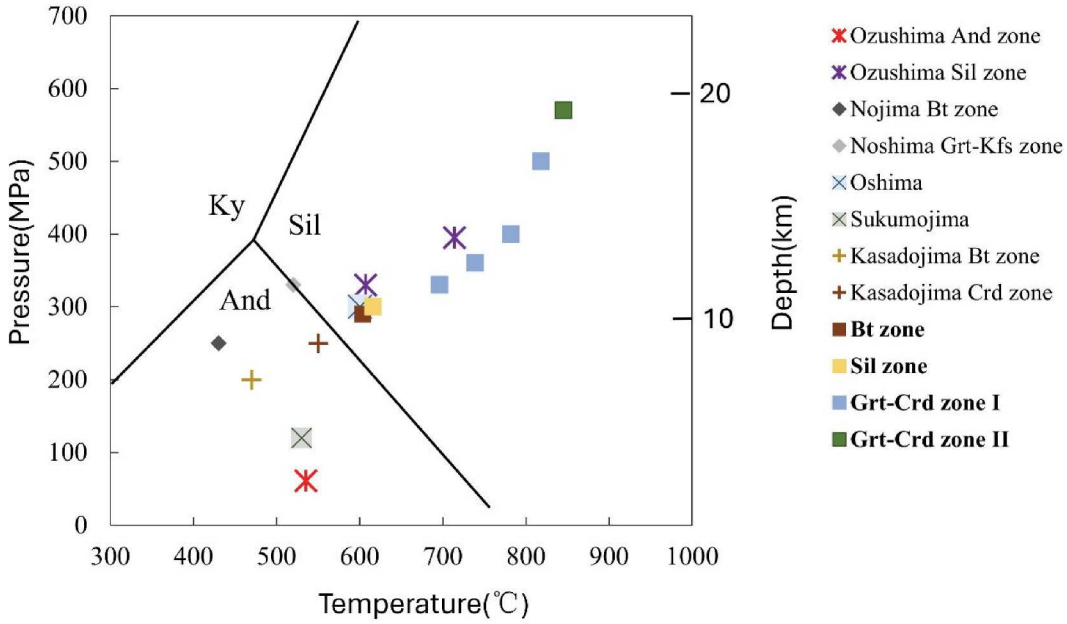

Fig. 6-1-5. The metamorphic *P-T* conditions of the study area and the Higo area. The squares show the data from the Higo Belt (Miyazaki, 2004).

6.2 Protolith of the metamorphic rocks

Figure 6-2-1 shows the KDE (kernel density estimator) plot of the detrital zircon U–Pb ages for metamorphic rocks from the Nishiki (Tsuno Group), Chikujo, Kurume, Nagasaki, Omuta and Manotani (northern Higo) areas compared to those from Ozushima Island of this study. These include the youngest detrital zircon ages of 260–250 Ma with older peaks at 1880–1800 Ma (Tsutsumi et al., 2000; Tsutsumi et al., 2003; Miyazaki et al., 2017; Suga et al., 2017; Yuhara et al., 2021; this study). Thus, the depositional ages for the compiled data are almost the same, although the youngest ages of Tsuno and Kurume metamorphic rocks are slightly older, 266–260 Ma. Detrital zircon dating revealed that the protoliths of the Ozushima Low-*P/T* type metamorphic rocks belong to the Suo belt. Based on the metamorphic *P-T* conditions and detrital zircon U–Pb ages, these metamorphic rocks from Chugoku and Kyushu areas were recognized as the same geological unit in the Late Permian-Triassic. In addition, the age spectrum of these areas reveals that these geological units were likely derived from the South China Craton (Isozaki, 2019).

Figure 6-2-2 shows the KDE plot of the detrital zircon U–Pb ages for metamorphic rocks from Nojima Island, Oshima, Sukumojima Island and Higo area (Suga et al., 2017). These include the youngest detrital zircon ages of 200–180 Ma. Although Vuong et al. (2019) reported the younger detrital zircon U-Pb age of about 130 Ma, which is similar to the Shimanto Group, it could be considered as the mixing of young-different protolith, probably the early Cretaceous, during its sedimentation. Back to this study, the protolith age of 200–180 Ma corresponds to be of the Jurassic Kuga Group, which is recognized as the protolith of the Ryoke metamorphic rocks in the Iwakuni-Yanai area. In Hime-shima, northern Kyushu, Hirayama et al. (2022) reported a gneiss xenolith with zircon U–Pb age at 195 and 188 Ma as protolith ages. They interpreted that this island is situated

within the Jurassic accretional complex (Fig. 6-2-3). Kunisaki Peninsula, south of Hime-shima Island, is also underlain by the Ryoke metamorphic rocks (Ishizuka et al., 2005). The metamorphic rocks mentioned above from Chugoku and Kyushu areas were also recognized as the same geological unit in the Late Triassic-Jurassic period.

The metamorphic rocks distributed from Chugoku to Kyushu, with a protolith age of 260–250 Ma, are located on the continental side. On the other hand, the metamorphic rocks having younger protolith ages, 200–180 Ma, are slightly situated on the ocean side (Fig. 6-2-3). This is in harmony with the geotectonic classification of the Japanese archipelago, which has been discussed mainly in terms of the formation of accretionary complexes.

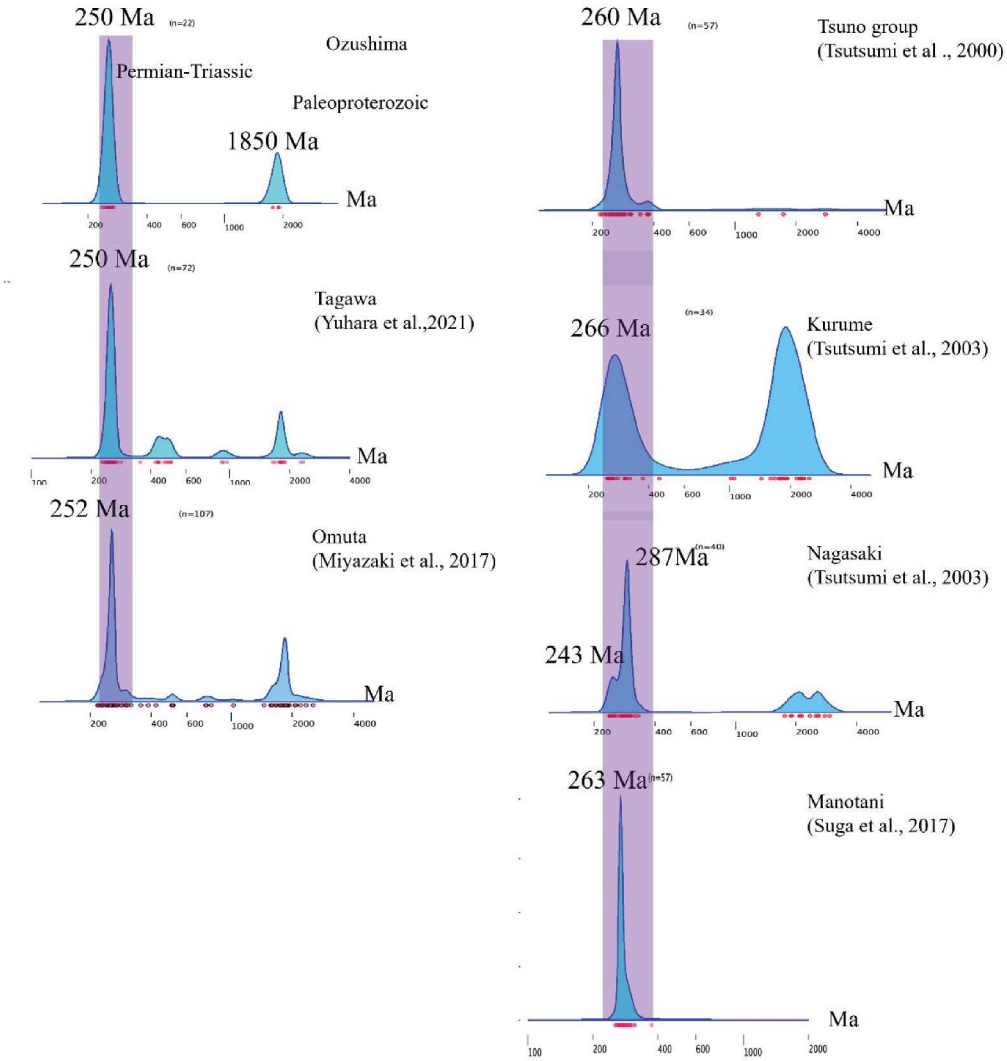

Fig. 6-2-1. KDE plots of detrital zircon ^{238}U–^{206}Pb ages from Ozushima, Nishiki (Tsuno Group), Tagawa, Kurume, Nagasaki, Omuta, and Manotani (northern Higo) areas.

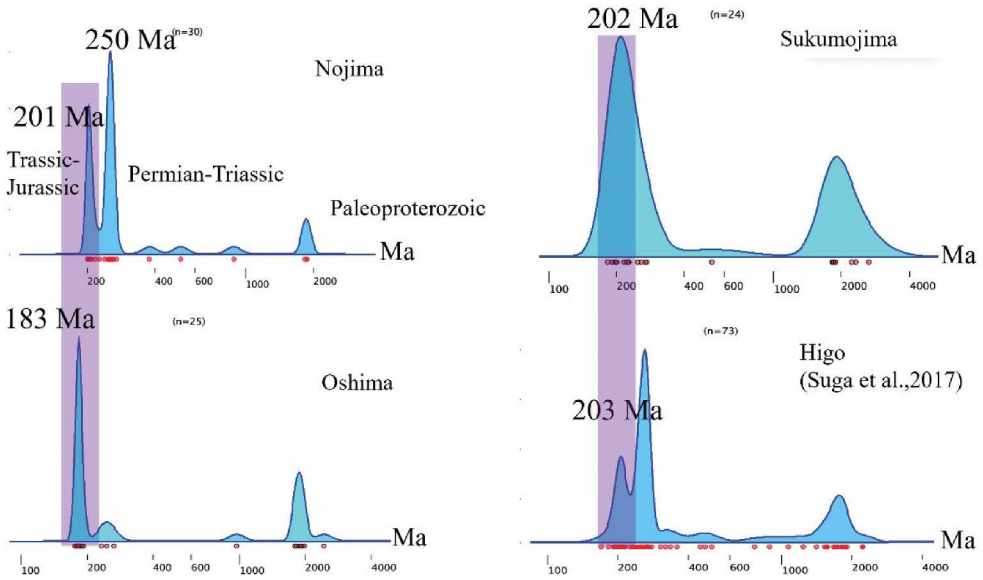

Fig. 6-2-2. KDE plots of detrital zircon ^{238}U–^{206}Pb ages from Nojima, Sukumojima, Oshima, and Higo areas.

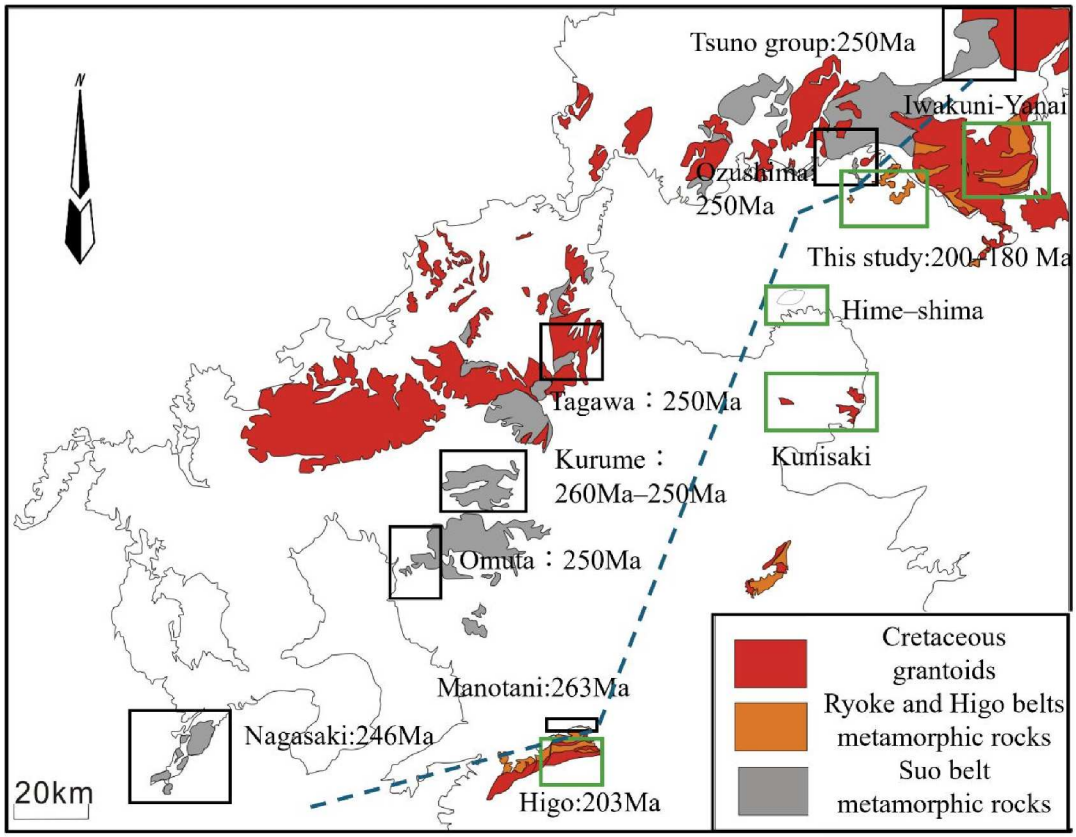

Fig. 6-2-3. Distribution map of the metamorphic rocks from the Suo Belt, Ryoke Belt, Higo Belt and the Cretaceous granitoids in the south Chugoku and north Kyushu areas. The green square indicates the areas of depositional age are Late Triassic-Jurassic. The black square indicates the areas of depositional age are Late Permian-Triassic.

6.3 Formation of Low-*P/T* type metamorphic rocks and their geotectonic implications

Based on the detrital zircon data and metamorphic field gradient, the schematic geotectonic model for the formation of Low-*P/T* metamorphic belts is shown in Fig. 6-3-1. The protoliths of the Suo Belt were deposited at 250 Ma, then underwent high pressure metamorphism at 230–210 Ma during the subduction of the oceanic plate (Nishimura, 1998). At the same time or slightly later, the Jurassic accretionary complex was beginning to deposit later than 200 Ma. Maki et al. (2014) reported that the metamorphic rocks of Higo area underwent the Cretaceous Low-*P/T* metamorphism at 116–110 Ma. In addition, the metamorphic ages of the high-grade zone of the Higo Belt could be 120–110 Ma using the method with the confirmation of HREE distribution between zircon and garnet (Vuong et al., 2019). Miyazaki et al. (2017) reported that the metamorphic rocks of Suo Belt in Omuta underwent the Cretaceous Low-*P/T* metamorphism at 105 Ma, younger than Higo area. In addition, Skrzypek et al. (2018) reported that the metamorphic age of Ryoke belt in Iwakuni-Yanai area was 103–97 Ma, the youngest metamorphic age in three areas. Although the reason was still unclear, possibly due to space position influenced by a relative plate motion at that time, it still can recognize that metamorphic rocks, which have undergone Low-pressure metamorphism distributed in the Chugoku to Kyushu areas, are inferred to have been formed by regional contact metamorphism associated with Cretaceous igneous activity as previously proposed by Skrzypek et al. (2016) and Miyazaki et al. (2017).

The Low-*P/T* type metamorphic rocks of west Chugoku and Kyushu are distributed within variable accretionary terranes and would have been affected by Cretaceous thermal events to form the Low-*P/T* type metamorphic rocks. To achieve this, these rocks should have gathered within a region affected by thermal events until the Cretaceous period. This

indicates that the Suo and Mino-Tamba Belts were juxtaposed with each other until the Cretaceous beneath the Cretaceous volcanic front.

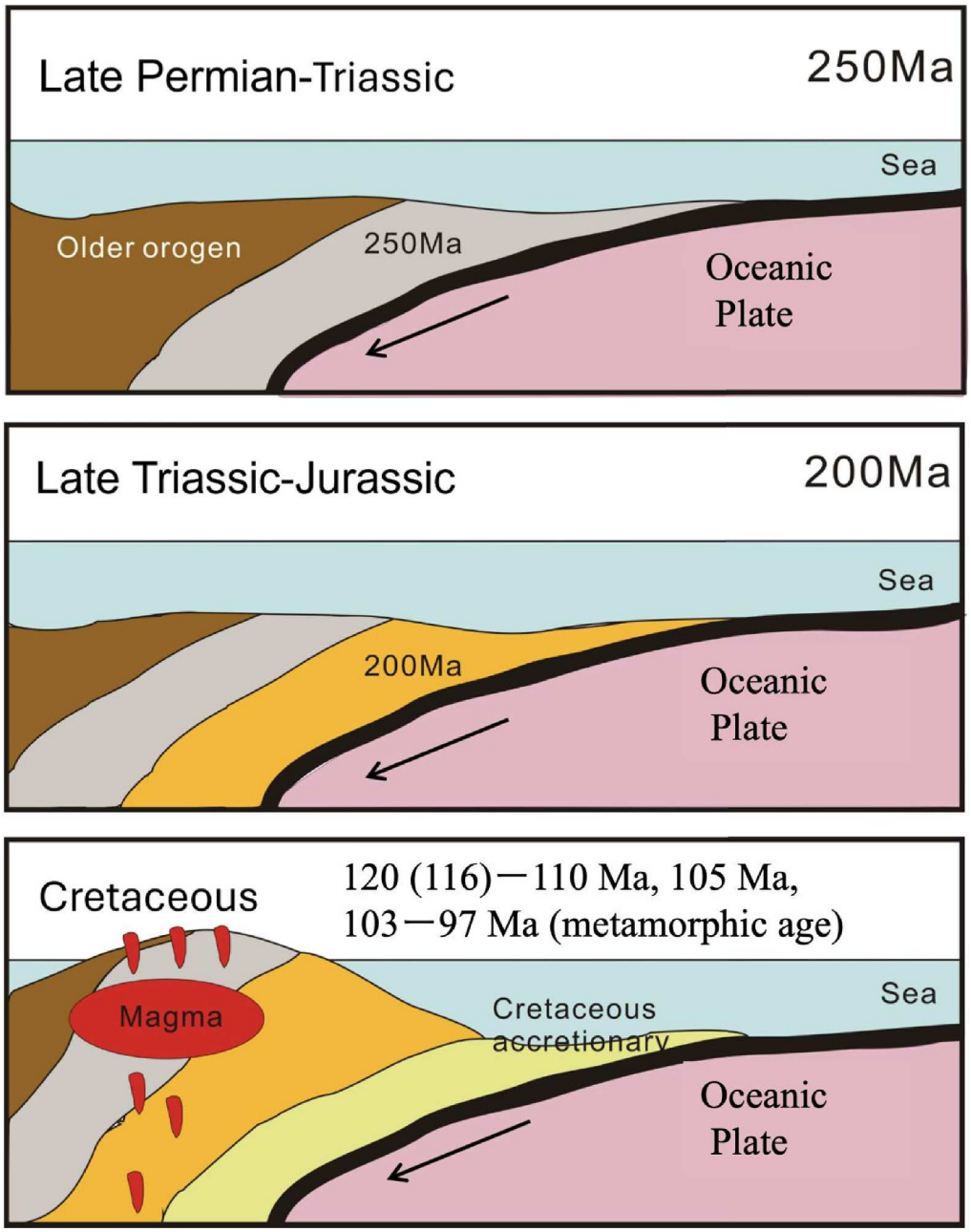

Fig. 6-3-1. Schematic tectonic model of the formation of each geological terrane from the late Permian to Cretaceous, and the Cretaceous Low-*P/T* metamorphic belt in Southwest Japan. The metamorphic ages of the Low-*P/T* metamorphic rocks are adopted from Maki et al. (2014), Miyazaki et al. (2017), Skrzypek et al. (2018), and Vuong et al. (2019).

7. Conclusions

To reveal the geotectonic boundaries of Low-*P/T* terranes, the detrital zircon U–Pb dating and compilation of metamorphic *P-T* conditions were conducted. The metamorphic rocks in Ozujima Island were deposited in the Late Permian and belong to the Suo Belt. However, the Nojima Island and Oshima Peninsula (including Sukumojima and Oshima) show detrital zircon U–Pb ages from 200 to 180 Ma as protolith ages, indicating the metamorphic rocks in Nojima Island and Oshima Peninsula were deposited in the Jurassic, probably being equivalent to the Kuga Group. In addition, the age spectrum of detrital zircon U–Pb dating reveals that the protolith of metamorphic rocks studied here would be derived from the South China Craton.

Based on mineral paragenesis and the estimated *P-T* conditions, the metamorphic field gradient of the rocks from Kasadojima Island, Oshima Peninsula, Ozujima Island, and Nojima Island is the same, forming a monotonous trend. In addition, the biotite K–Ar ages of the pelitic rocks from the study area are from 94 Ma to 90 Ma, overlapping within the analytical errors. These ages suggest that the metamorphic rocks in the study area underwent Low-*P/T* type metamorphism, and their metamorphic ages are comparable to the Cretaceous Ryoke Belt.

The inferred geothermal gradients of the Low-*P/T* metamorphic rocks are exceptionally high, not only in the study area but the western Chugoku and Kyushu areas, from surface to middle crustal level. The *P-T* conditions of the metamorphic rocks from the western Chugoku and Kyushu areas are arranged in a single geothermal trend on the *P-T* diagram and are identical with the geothermal gradient of the Iwakuni-Yanai area, which is exemplified by the Ryoke metamorphism. Thus, this study confirms that the Low-*P/T* type metamorphic rocks in western Chugoku and Kyushu area were produced by regional contact metamorphism caused by Cretaceous igneous activity.

Table 7-1. The results of this study.

Inferred/Now	Nojima	Ozushima	Oshima	Sukumojima
Depositional age (U-Pb age)	Jurassic/ Jurassic (203 Ma)	Permian/ Permian (250 Ma)	Jurassic/ Jurassic (180 Ma)	Permian/ Jurassic (190 Ma)
Type of Metamorphism	Low-*P/T*	High-*P/T* / Low-*P/T*	Low-*P/T*	High-*P/T* / Low-*P/T*
Metamorphic age (K−Ar age)	Cretaceous (92 Ma)		Cretaceous	Triassic/ Cretaceous (90 Ma)

8. Reference

Beppu, Y. & Okudaira, T. (2006). Geology and metamorphic zonation of the Ryoke Metamorphic Belt on Kasado-jima Island, SW Japan. Journal of Mineralogical and Petrological Sciences, 101, 240–253. doi:10.2465/jmps.101.240.

Dickinson, W.R. & Gehrels G.E. (2009). Use of U-Pb ages of detrital zircons to infer maximum depositional ages of strata: A test against a Colorado Plateau Mesozoic database. Earth and Planetary Science Letters, 288, 115–125. doi:10.1016/j.epsl.2009.09.013.

Ferry, J. M. & Spear, F. S. (1978). Experimental calibration of the partitioning of Fe and Mg between biotite and garnet. Contributions to Mineralogy and Petrology, 66, 113–117.

Geological Survey of Japan, AIST (2024). Seamless digital geological map of Japan V2 1:200,000, Original edition. https://gbank.gsj.jp/seamless/.

Henry, D.J., Guidotti, C.V. & Thomson J.A. (2005). The Ti-saturation surface for low-to-medium pressure metapelitic biotites: Implications for geothermometry and Ti-substitution mechanisms. American Mineralogist, 90, 316–328.

Higashimoto, S., Nureki, T., Hara, I., Tsukuda, E. & Nakajima, T. (1983). Geology of the Iwakuni district. Quadrangle Series, Scale 1:50,000, Geological Survey of Japan, 79 pp.

Hirayama, T., Shibata, T., Yoshikawa, M., Abbou–Kébir, K., Kimura, K., Osanai, Y., Das, K., Hayasaka, Y. & Takemura, K. (2022). Origin of xenoliths within the Hime–shima volcanic group, Kyushu, southwestern Japan Arc, Journal of Mineralogical and Petrological Sciences, 117. doi.org/10.2465/jmps.211217b.

Hoisch, T.D. (1990). Empirical calibration of six geobarometers for the mineral assemblage quartz + muscovite + biotite + plagioclase + garnet. Contributions to Mineralogy and Petrology, 104, 225–234. doi.org/10.1007/BF00306445.

Hodges, K. V., & Spear, F. S. (1982). Geothermometry, geobarometry and the Al_2SiO_5 triple point at Mt. Moosilauke, New Hampshire. American Mineralogist, 67, 1118–1134.

Ikeda, T. (2004). Pressure–temperature conditions of the Ryoke metamorphic rocks in Yanai district, SW Japan. Contributions to Mineralogy and Petrology, 146: 577–589. doi: 10.1007/s00410-003-0521-7.

Ikeda, T., Miyazaki, K. & Matsuura, H. (2017). Metamorphic condition of a regional metamorphic complex in the Omuta district in northern Kyushu, southwest Japan. Island Arc. doi 10.1111/iar.12204.

Ishizuka, Y., Mizuno, K., Matsuura, H. & Hoshizumi, H. (2005). Geology of the Bungo-Kitsuki District. Quadrangle Series, 1:50000, Geological Survey of Japan, AIST, 11-13.

Isozaki, Y. (2021). A visage of early Paleozoic Japan: Geotectonic and paleobiogeographical significance of Greater South China. Island Arc. doi.org/10.1111/iar.12296.

Iwano, H., Orihashi, Y., Danhara, T., Hirata, T. & Ogasawara, M. (2012). Evaluation of fission-track and U–Pb double dating method for identical zircon grains: Using homogeneous zircon grains in Kawamoto Granodiorite in Shimane prefecture, Japan. Journal of Geological Society of Japan, 118, 365–375. doi.org/10.5575/geosoc.2012.0006.

Iwano, H., Orihashi, Y., Hirata, T., Ogasawara, M., Danhara, T., Horie, K., Hasebe, N., Sueoka, S., Tamura, A., Hayasaka, Y., Katsube, A., Ito, H., Tani, K., Kimura, J.-I.,

Chang, Q., Kouchi, Y., Haruta, Y. & Yamamoto, K. (2013). Inter-laboratory evaluation of OD-3 zircon. Island Arc, 22, 382–394. doi.org/10.1111/iar.12038.

Jackson, S. E., Pearson, N. J., Griffin, W. L. & Belousova, E. A. (2004). The application of laser ablation-inductively coupled plasma-mass spectrometry to in situ U–Pb zircon geochronology. Chemical Geology, 211, 47–69.

Ludwig, K. R. (2012). User's manual for Isoplot 3.75, a geochronological toolkit for Microsoft Excel, Special Publication No. 5. Berkeley, CA: Berkeley Geochronology Center.

Lukács, R., Harangi, S., Bachmann, O., Guillogn, M., Danišik, M., Buret, Y. & Szepesi, J. (2015). Zircon geochronology and geochemistry to constrain the youngest eruption events and magma evolution of Mid-Miocene ignimbrite flare-up in the Pannonian Basin, eastern central Europe. Contributions to Mineralogy and Petrology, 170, 52. doi.org/10.1007/s00410-015-1206-8.

Maki, K., Yui, T.K., Miyazaki, K., Fukuyama, M., Wang, K.L., Martens, U., Grove, M. & Liou, J.G. (2014) Petrogenesis of metatexite and diatexite migmatites determined using zircon U–Pb age, trace element and Hf isotope data, Higo metamorphic terrane, central Kyushu, Japan. Journal of Metamorphic Geology, 32, 301–323. doi.org/10.1111/jmg.12073.

Miyashiro, A. (1973). Metamorphism and Metamorphic Belts. George Allen & Unwin Limited, London. 492pp.

Miyazaki, K. (2004). Low-P/high-T metamorphism and the role of heat transport by melt migration in the Higo Metamorphic Complex, Kyushu, Japan. Journal of Metamorphic Geology, 22, 793–809. doi.org/10.1111/j.1525-1314.2004.00550.x.

Miyazaki, K., Ikeda, T., Matsuura, H., Danhara, T., Iwano, H. & Hirata, T. (2017). A high-T metamorphic complex derived from the high-P Suo metamorphic complex in the

Omuta district, northern Kyusyu, southwest Japan. Island Arc, 26. doi: 10.1111/iar.12208.

Nishimura, Y. (1971). Regional metamorphism of the Nishiki-cho district, Southwest Japan. Journal of science of the Hiroshima University. Series C, Geology and Mineralogy, 6, 230–268.

Nishimura, Y. (1998). Geotectonic subdivision and areal extent of the Sangun belt, inner zone of southwest Japan. Journal of Metamorphic Geology, 16, 129–140.

Nishimura, Y., Imaoka, T., Kanaori, Y. & Kameya, A. (2012). Geological map of Yamaguchi Prefecture, Third edition, (1:150 000) and its explanatory text. Geological Society of Yamaguchi, 167pp. (in Japanese).

Nishimura, Y., Itaya, T., Isozaki, Y. & Kameya, A. (1989). Depositional age and metamorphic history of 220 Ma high P/T type metamorphic rocks. An example of the Nishiki-cho area, Yamaguchi Prefecture, Southwest Japan. Memoir of Geological Society of Japan, 33, 143–166.

Okudaira, T., Hayasaka, Y. & Ohtomo, Y. (2000). Cretaceous tectonics of southwest Japan in light of the studies for the Ryoke metamorphic belt. Monograph Association of Geological Collaboration Japan, 49, 67–80.

Okudaira, T., Hayasaka, Y., Himeno, O., Watanabe, K., Sakurai, Y. & Ohtomo, Y. (2001). Cooling and inferred exhumation history on the Ryoke metamorphic belt in the Yanai district, south-West Japan: Constraints from Rb-Sr and fission-track ages of gneissose granitoid and numerical modeling. Island Arc, 10, 98–115.

Skrzypek, E., Kawakami, T., Hirajima, T., Sakata, S., Hirata, T. & Ikeda, T. (2016). Revising the high temperature metamorphic field gradient of the Ryoke Belt (SW Japan): New constraints from the Iwakuni-Yanai area. Lithos, 260, 9–27. doi.org/10.1016/j.lithos.2016.04.025.

Skrzypek, E., Kato, T., Kawakami, T., Sakata, S., Hattori, K., Hirata, T. & Ikeda, T. (2018). Monazite behaviour and time-scale of metamorphic processes along a low-pressure/ high-temperature field gradient (Ryoke belt, SW Japan), Journal of Petrology, 59, 1109–1144. doi: 10.1093/petrology/egy056.

Sláma, J., Kośler, J., Condon, D. J., Crowley, J. L., Gerdes, A., Hanchar, J. M., Horstwood, M.S.A, Morris, G.A., Nasdala, L., Norberg, N., Schaltegger, U., Schoene, B., Tubrett, M.N. & Whitehouse, M. J. (2008). Plešovice zircon-a new natural reference material for U-Pb and Hf isotopic microanalysis. Chemical Geology, 249, 1–35. doi.org/10.1016/j.chemgeo.2007.11.005.

Suga, K., Yu, T.F., Miyazaki, K., Sakata, S., Hirata, T. & Fukuyama, M. (2017) A revisit to the Higo terrane, Japan: The eastern extension of the North China–South China collision zone. Journal of Asian Earth Sciences 143, 218–235.

Tsutsumi, Y., Yokoyama, K., Terada, K. & Sano, Y. (2000). SHRIMP U–Pb dating of zircons in the sedimentary rocks from the Akiyoshi and Suo zones, Southwest Japan. Journal of Mineralogical and Petrological Sciences, 95, 216–227.

Tsutsumi, Y., Yokoyama, K., Terada, K. & Sano, Y. (2003). SHRIMP U–Pb dating of detrital zircons in metamorphic rocks from northern Kyushu, western Japan. Journal of Mineralogical and Petrological Sciences, 98, 181–193. doi.org/10.2465/jmps.98.181.

Vuong Bui Thi Sinh, Osanai, Y., Nakano, N., Adachi, T. & Kitano, I. (2019) Geochronology and REE geochemistry of zircon and garnet in pelitic gneisses from the Higo metamorphic terrane, Kyushu, Japan: Constraints on the timing of high–temperature metamorphism. Journal of Mineralogical and Petrological Sciences, 114, 47–59. doi.org/10.2465/jmps.181115.

Warr, N.L. (2021). IMA-CNMNC approved mineral symbols. Mineralogical Magazine, 85, 291–320. doi.org/10.1180/mgm.2021.43.

Wiedenbeck, M., Alle, P., Corfu, F., Griffin, W. L., Meier, M., Oberli, F. & Spiegel, W. (1995). Three natural zircon standards for U–Th–Pb, Lu-Hf, trace element and REE analyses. Geostandards Newsletter, 19, 1–23.

Yuhara, M., Kiyoura, K., Hidaka, M., Hokada, T. & Hayasaka, Y. (2021). The metamorphism of the Tagawa metamorphic rocks, eastern North Kyushu. Journal of Geological Society of Japan, 127, 447–459. doi.org/10.5575/geosoc.2021.0017.

9. Appendix

9-1 Zircon U–Pb data

Table 9-1-1. Analytical conditions of zircon U–Pb dating in the LA-ICP-MS system in Nojima Island.

Laser ablation	
Model	LIGHT CONVERSION
Product name	CARBIDE
Laser tybe	Yb:KGW femtosecond laser
Pulse width	290 fs
Wave length	257 nm
Energy density	3.8 J /cm^2
Crater size	10 μm
Laser irradiation method	single- spot
Repetion rate	30 Hz
Shot count	100
Integration time	3.3 s
Carrie gas (He)	0.60 L min^{-1}
ICP-Ms	
Model	Nu Instruments
Product name	New Plasma II
ICP-MS type	Magnetic sector multi-collector ICP-MS
RF power	1300 W
Carrier gas (Ar)	0.80 L min^{-1}
ThO^+/Th Oxide formation rate	< 1%
Data Acquisition Method	Time-resolved analysis
Data acquisition time	9 s (6 s gas blank, 3 s ablation signal)
Monitor isotopes	^{202}Hg, ^{204}Pb, ^{206}Pb, ^{207}Pb, ^{208}Pb, ^{232}Th, ^{235}U
Primary standard(U-Pb)	Plešovice *1
Secondary standard (U-Pb)	OD-3 *2, 3, 4, Nancy 91500*5, GJ-1*6

(*1, Sláma et al. (2008); *2, Iwano et al. (2012); *3, Iwano et al. (2013); *4, Lukács et al. (2015), *5, Wiedenbeck et al. (1995); *6, Jackson et al. (2004))

Table 9-1-2. U–Pb isotopic data for zircon crystals determined by LA-ICP-MS in Nojiima Island.

NO.	sample name	Total count ^{206}Pb	^{207}Pb	^{208}Pb	^{232}Th	^{235}U	^{238}U	Th/U
1	LU-01 no.1	22135	3079	3927	43710	607	83635	0.90
2	LU-01 no.2	13212	786	2029	156669	3107	428385	0.63
3	LU-01 no.3	194054	11859	90654	8295456	55949	7714237	1.85
4	LU-01 no.4	89871	5609	14460	1087730	20983	2893160	0.65
5	LU-01 no.5	46820	2872	12358	926842	10700	1475327	1.08
6	LU-01 no.6	42247	2576	8980	853129	12378	1706683	0.86
7	LU-01 no.7	11515	722	2510	177207	2680	369570	0.82
8	LU-01 no.8	86718	5332	16345	1521170	25006	3447859	0.76
9	LU-01 no.9	28932	1693	4522	434400	8413	1159988	0.64
10	LU-01 no.10	83667	5062	8739	606070	19056	2627409	0.40
11	LU-01 no.11	121272	7256	23366	2189904	35467	4890128	0.77
12	LU-01 no.12	15611	997	2714	126509	2394	330061	0.66
13	LU-01 no.13	591582	80809	15429	151155	16653	2296167	0.11
14	LU-01 no.14	94830	7659	14316	305658	5914	815416	0.64
15	LU-01 no.15	358056	21867	75168	6083363	87555	12072049	0.86
16	LU-01 no.16	75013	4558	7211	524521	16860	2324648	0.39
17	LU-01 no.17	16132	1054	3493	253443	3506	483408	0.90
18	LU-01 no.18	13245	841	1753	133876	3154	434935	0.53
19	LU-01 no.19	51384	3070	3793	290634	12187	1680410	0.30
20	LU-01 no.20	14117	888	1862	149324	3368	464379	0.55
21	LU-01 no.21	51855	3167	6801	614174	14559	2007418	0.53
22	LU-01 no.22	36210	2298	6004	418401	8178	1127644	0.64
23	LU-01 no.23	47296	2894	8875	847302	13710	1890399	0.77
24	LU-01 no.24	46103	2895	7552	533987	10291	1418991	0.65
25	LU-01 no.25	71774	4210	5352	466569	19375	2671408	0.30
26	LU-01 no.26	41944	2464	7314	659045	11908	1641864	0.69
27	LU-01 no.27	36868	2292	10509	877238	9564	1318652	1.14
28	LU-01 no.28	93758	6448	27239	963386	10375	1430501	1.16
29	LU-01 no.29	2656837	362036	7940	85389	72665	10019064	0.01
30	LU-01 no.30	112763	7008	15709	1120903	25749	3550282	0.54

Standards							
91500epo 3-1	55379	5006	5298	96818	2803	386462	0.43
91500epo 3-2	55219	5056	5124	77486	2850	392944	0.33
91500epo 3-3	54267	4882	5163	80143	2808	387152	0.35
91500epo 3-4	51758	4603	4651	76013	2608	359572	0.36
91500epo 3-5	56677	5042	5337	95010	2938	405079	0.40
GJ1 3-1	148284	10439	2094	83380	14298	1971421	0.07
GJ1 3-2	145588	10403	2102	62775	14035	1935149	0.06
GJ1 3-3	150183	10906	2241	65498	14290	1970251	0.06
GJ1 3-4	145893	10687	2166	74718	14000	1930253	0.07
GJ1 3-5	148912	10695	2232	69360	14252	1965080	0.06
OD-3 3-1	11656	655	4256	2365324	21033	2900030	1.38
OD-3 3-2	12812	730	4606	2514783	23224	3202112	1.33
OD-3 3-3	11568	750	4032	2225666	20676	2850863	1.32
OD-3 3-4	27535	1576	7770	4253946	48611	6702478	1.08
OD-3 3-5	11848	635	4427	2471251	21983	3031073	1.38

Isotopic ratios												
$^{207}Pb/^{206}Pb$		Error 2σ	$^{206}Pb/^{238}U$		Error 2σ	$^{207}Pb/^{235}U$		Error 2σ	$^{208}Pb/^{232}Th$		Error 2σ	Disc.*
0.1153	±	0.0061	0.3370	±	0.0282	5.3635	±	0.4985	0.0812	±	0.0074	concordant
0.0493	±	0.0040	0.0393	±	0.0017	0.2674	±	0.0226	0.0117	±	0.0011	concordant
0.0507	±	0.0021	0.0320	±	0.0006	0.2240	±	0.0076	0.0099	±	0.0008	concordant
0.0517	±	0.0024	0.0396	±	0.0008	0.2824	±	0.0115	0.0120	±	0.0010	concordant
0.0509	±	0.0027	0.0404	±	0.0010	0.2837	±	0.0142	0.0121	±	0.0010	concordant
0.0506	±	0.0028	0.0315	±	0.0008	0.2199	±	0.0113	0.0095	±	0.0008	concordant
0.0520	±	0.0044	0.0397	±	0.0018	0.2847	±	0.0251	0.0128	±	0.0012	concordant
0.0510	±	0.0023	0.0320	±	0.0007	0.2253	±	0.0092	0.0097	±	0.0008	concordant
0.0485	±	0.0030	0.0318	±	0.0009	0.2127	±	0.0127	0.0094	±	0.0008	concordant
0.0502	±	0.0023	0.0406	±	0.0009	0.2807	±	0.0117	0.0130	±	0.0011	concordant
0.0496	±	0.0022	0.0316	±	0.0006	0.2162	±	0.0081	0.0096	±	0.0008	concordant
0.0530	±	0.0040	0.0602	±	0.0028	0.4401	±	0.0353	0.0194	±	0.0018	concordant
0.1133	±	0.0042	0.3281	±	0.0070	5.1275	±	0.1649	0.0923	±	0.0080	concordant
0.0670	±	0.0029	0.1481	±	0.0045	1.3684	±	0.0603	0.0424	±	0.0037	concordant
0.0506	±	0.0020	0.0378	±	0.0006	0.2639	±	0.0082	0.0112	±	0.0010	concordant
0.0500	±	0.0018	0.0412	±	0.0009	0.2841	±	0.0112	0.0124	±	0.0011	concordant
0.0538	±	0.0036	0.0426	±	0.0017	0.3158	±	0.0232	0.0124	±	0.0011	concordant
0.0522	±	0.0039	0.0388	±	0.0016	0.2800	±	0.0225	0.0118	±	0.0011	concordant
0.0492	±	0.0021	0.0390	±	0.0010	0.2647	±	0.0121	0.0118	±	0.0011	concordant
0.0518	±	0.0037	0.0388	±	0.0016	0.2771	±	0.0217	0.0113	±	0.0011	concordant
0.0503	±	0.0021	0.0329	±	0.0008	0.2286	±	0.0102	0.0100	±	0.0009	concordant
0.0523	±	0.0025	0.0410	±	0.0012	0.2953	±	0.0153	0.0130	±	0.0011	concordant
0.0504	±	0.0022	0.0319	±	0.0008	0.2218	±	0.0102	0.0095	±	0.0008	concordant
0.0517	±	0.0022	0.0414	±	0.0011	0.2956	±	0.0139	0.0128	±	0.0011	concordant
0.0483	±	0.0018	0.0343	±	0.0007	0.2283	±	0.0092	0.0104	±	0.0009	concordant
0.0484	±	0.0022	0.0326	±	0.0008	0.2175	±	0.0107	0.0100	±	0.0009	concordant
0.0512	±	0.0024	0.0357	±	0.0010	0.2519	±	0.0129	0.0108	±	0.0009	concordant
0.0566	±	0.0018	0.0836	±	0.0021	0.6531	±	0.0249	0.0255	±	0.0022	concordant
0.1122	±	0.0022	0.3382	±	0.0055	5.2355	±	0.1192	0.0839	±	0.0073	concordant
0.0512	±	0.0016	0.0405	±	0.0008	0.2860	±	0.0098	0.0127	±	0.0011	concordant

0.0754	±	0.0036	0.1819	±	0.0077	1.8921	±	0.1108	0.0502	±	0.0026	concordant
0.0764	±	0.0037	0.1784	±	0.0075	1.8797	±	0.1095	0.0607	±	0.0032	concordant
0.0750	±	0.0036	0.1779	±	0.0076	1.8421	±	0.1081	0.0591	±	0.0031	concordant
0.0742	±	0.0036	0.1827	±	0.0080	1.8699	±	0.1122	0.0561	±	0.0030	concordant
0.0742	±	0.0036	0.1776	±	0.0074	1.8183	±	0.1053	0.0515	±	0.0027	concordant
0.0587	±	0.0025	0.0955	±	0.0024	0.7735	±	0.0334	0.0230	±	0.0014	concordant
0.0596	±	0.0026	0.0955	±	0.0024	0.7853	±	0.0340	0.0307	±	0.0019	concordant
0.0606	±	0.0026	0.0968	±	0.0024	0.8086	±	0.0348	0.0314	±	0.0019	concordant
0.0611	±	0.0026	0.0959	±	0.0024	0.8088	±	0.0349	0.0266	±	0.0016	concordant
0.0599	±	0.0026	0.0962	±	0.0024	0.7950	±	0.0342	0.0295	±	0.0018	concordant
0.0469	±	0.0042	0.0051	±	0.0001	0.0330	±	0.0029	0.0017	±	0.0001	concordant
0.0475	±	0.0040	0.0051	±	0.0001	0.0333	±	0.0028	0.0017	±	0.0001	concordant
0.0540	±	0.0046	0.0052	±	0.0001	0.0384	±	0.0032	0.0017	±	0.0001	-3
0.0477	±	0.0031	0.0052	±	0.0001	0.0343	±	0.0021	0.0017	±	0.0001	concordant
0.0447	±	0.0040	0.0050	±	0.0001	0.0306	±	0.0027	0.0016	±	0.0001	concordant

Without correction U-Pb age (Ma)						^{232}Th-^{208}Pb age (Ma)			^{207}Pb-^{206}Pb age (Ma)				
$^{206}Pb/^{238}U$		Error 2σ	$^{207}Pb/^{235}U$		Error 2σ	$^{208}Pb/^{232}Th$		Error 2σ	$^{207}Pb/^{206}Pb$		Error 2σ	f 206%	rho
1872.4	±	179.1	1879.1	±	410.7	1578.8	±	149.2	1885.0	±	95.4	9	0.90
248.3	±	10.7	240.6	±	22.7	235.4	±	22.7	163.6	±	191.6	0	0.50
203.3	±	3.6	205.2	±	7.7	198.8	±	17.0	225.9	±	94.9	1	0.51
250.1	±	5.4	252.6	±	11.6	241.5	±	21.0	274.2	±	104.6	1	0.52
255.4	±	6.7	253.6	±	14.3	242.3	±	21.1	234.8	±	122.2	1	0.52
200.1	±	5.1	201.8	±	11.4	191.5	±	16.8	220.5	±	126.2	1	0.49
250.8	±	11.6	254.4	±	25.2	257.3	±	24.3	285.2	±	194.2	1	0.51
203.2	±	4.2	206.3	±	9.3	195.5	±	17.0	240.1	±	106.2	1	0.50
201.6	±	5.9	195.8	±	12.8	189.4	±	17.1	124.9	±	145.7	0	0.48
256.3	±	5.7	251.2	±	11.8	261.9	±	23.1	202.7	±	108.0	1	0.52
200.4	±	3.8	198.7	±	8.2	194.1	±	16.7	176.7	±	102.0	0	0.50
377.0	±	17.9	370.4	±	35.2	388.4	±	36.6	327.1	±	169.8	1	0.58
1829.1	±	45.1	1840.7	±	155.0	1784.6	±	160.9	1852.4	±	67.3	9	0.67
890.3	±	29.1	875.5	±	59.5	838.5	±	74.0	836.6	±	90.6	3	0.69
239.0	±	4.0	237.8	±	8.3	224.6	±	19.2	224.3	±	90.2	1	0.53
260.0	±	5.9	253.9	±	11.4	249.3	±	21.9	196.2	±	84.0	0	0.57
268.7	±	11.0	278.7	±	23.3	249.9	±	22.8	361.4	±	150.0	1	0.54
245.7	±	10.6	250.7	±	22.6	237.5	±	23.2	296.3	±	168.2	1	0.52
246.6	±	6.2	238.4	±	12.2	236.7	±	21.5	156.7	±	98.1	0	0.54
245.2	±	10.2	248.3	±	21.8	226.3	±	21.9	276.3	±	164.6	1	0.52
209.0	±	5.0	209.1	±	10.3	201.0	±	17.7	208.3	±	96.0	1	0.53
258.8	±	7.5	262.7	±	15.4	260.1	±	23.1	296.7	±	107.6	1	0.55
202.5	±	5.0	203.4	±	10.3	190.2	±	16.6	212.2	±	99.4	1	0.53
261.8	±	7.0	263.0	±	14.1	256.4	±	22.5	272.3	±	98.4	1	0.56
217.2	±	4.8	208.8	±	9.3	208.2	±	18.5	113.3	±	87.7	0	0.54
206.7	±	5.3	199.8	±	10.8	201.5	±	17.7	117.4	±	107.9	0	0.52
225.9	±	6.2	228.1	±	13.0	217.4	±	18.9	249.3	±	108.6	1	0.53
517.6	±	13.6	510.4	±	25.0	509.4	±	43.9	476.7	±	71.2	1	0.66
1878.2	±	35.5	1858.4	±	114.4	1629.0	±	147.8	1835.1	±	35.6	8	0.72
256.0	±	5.2	255.4	±	9.9	254.1	±	21.9	248.3	±	72.1	1	0.58

1077.4	±	49.6	1078.3	±	106.7	990.1	±	53.0	1078.8	±	96.3	4	0.73
1058.2	±	48.3	1073.9	±	105.5	1190.5	±	64.4	1104.6	±	95.8	4	0.72
1055.7	±	48.5	1060.6	±	104.2	1160.7	±	62.7	1069.3	±	96.9	4	0.72
1081.9	±	51.3	1070.5	±	108.0	1103.9	±	60.5	1045.9	±	98.4	4	0.73
1053.9	±	47.5	1052.1	±	101.7	1015.8	±	54.4	1046.8	±	96.6	4	0.72
587.9	±	15.2	581.8	±	33.4	460.5	±	29.1	556.4	±	93.6	2	0.57
588.0	±	15.3	588.5	±	33.9	611.5	±	38.8	588.8	±	93.2	2	0.57
595.4	±	15.4	601.6	±	34.7	624.7	±	39.0	623.6	±	92.2	2	0.57
590.6	±	15.3	601.8	±	34.8	530.5	±	33.3	642.5	±	92.1	2	0.58
592.1	±	15.3	594.0	±	34.2	588.1	±	36.7	599.9	±	92.7	2	0.57
32.8	±	1.0	33.0	±	2.9	33.3	±	1.8	42.7	±	212.3	0	0.33
32.7	±	0.9	33.2	±	2.8	33.9	±	1.8	74.0	±	202.1	0	0.34
33.1	±	1.0	38.3	±	3.2	33.6	±	1.8	372.8	±	189.9	1	0.35
33.5	±	0.8	34.3	±	2.2	33.8	±	1.7	85.7	±	152.2	0	0.37
31.9	±	0.9	30.6	±	2.7	33.2	±	1.8	-71.9	±	219.5	0	0.33

Table 9-1-3. Analytical conditions of zircon U–Pb dating in the LA-ICP-MS system in Ozushima Island.

Laser ablation	
Model	LIGHT CONVERSION
Product name	CARBIDE
Laser tybe	Yb:KGW femtosecond laser
Pulse width	290 fs
Wave length	257 nm
Output	30 mW
Energy density	3.8 J /cm^2
Crater size	10 μm
Laser irradiation method	single- spot
Repetion rate	10 Hz
Shot count	100
Integration time	10 s
Carrie gas (He)	0.60 L min^{-1}
ICP-Ms	
Model	Nu Instruments
Product name	New Plasma II
ICP-MS type	Magnetic sector field、double-focusing
RF power	1300 W
Carrier gas (Ar)	0.80 L min^{-1}
ThO^+/Th Oxide formation rate	< 1%
Data Acquisition Method	Time-resolved analysis
Data acquisition time	18 s (10 s gas blank, 8 s ablation signal)
Monitor isotopes	^{202}Hg, ^{204}Pb, ^{206}Pb, ^{207}Pb, ^{208}Pb, ^{232}Th, ^{235}U
Primary standard(U-Pb)	Plešovice *1
Secondary standard (U-Pb)	OD-3 *2, 3, 4, Nancy 91500*5

(*1, Sláma et al. (2008); *2, Iwano et al. (2012); *3, Iwano et al. (2013); *4, Lukács et al. (2015), *5, Wiedenbeck et al. (1995))

Table 9-1-4. U–Pb isotopic data for zircon crystals determined by LA-ICP-MS in Ozushima Island.

No.	sample name	^{206}Pb	^{207}Pb	^{232}Th	^{235}U	^{238}U	Th/U
1	2.OT-1 no.1	15854	1069	132515	3959	545850	0.37
2	2.OT-1 no.2	1595242	229417	117262	50667	6985946	0.03
3	2.OT-1 no.3	669653	97707	372148	21429	2954654	0.19
4	2.OT-1 no.4	339856	49564	106483	10025	1382192	0.12
8	2.OT-1 no.8	22589	1493	269761	5633	776633	0.53
9	2.OT-1 no.9	8300	584	196075	2275	313742	0.96
10	2.OT-1 no.10	7475	544	85822	2012	277365	0.47
12	2.OT-1 no.12	570991	82537	240486	16652	2295996	0.16
14	2.OT-1 no.14	144745	9267	692307	37112	5116982	0.21
17	2.OT-1 no.17	17996	1244	280111	4318	595299	0.72
19	2.OT-1 no.19	22756	1597	395822	5422	747620	0.82
20	2.OT-1 no.20	586555	85476	99411	17464	2407922	0.06
21	2.OT-1 no.21	167573	10677	1278471	44408	6122964	0.32
22	2.OT-1 no.22	31283	1951	628228	7868	1084804	0.89
23	2.OT-1 no.23	78740	5037	746949	20266	2794335	0.41
24	2.OT-1 no.24	31571	2042	318456	7983	1100635	0.45
26	2.OT-1 no.26	15227	1066	91457	3713	511927	0.28
27	2.OT-1 no.27	128462	8328	1564927	33273	4587652	0.53
29	2.OT-1 no.29	17145	1195	181615	4050	558481	0.50
30	2.OT-1 no.30	155634	10307	729144	38852	5356866	0.21
31	2.OT-1 no.31	436250	62975	182378	12931	1782864	0.16
32	2.OT-1 no.32	65961	4312	1005825	15898	2191948	0.71
	Standards						
	91500epo 6-3	69669	6644	130782	3773	520201	0.39
	91500epo 6-4	60325	5685	100546	3385	466697	0.33
	OD3 6-3	14547	845	2715654	28762	3965683	1.05
	OD3 6-4	12445	770	2354355	23963	3304056	1.10

Isotopic ratios												
^{207}Pb / ^{206}Pb		Error 2σ	^{206}Pb / ^{238}U		Error 2σ	^{207}Pb / ^{235}U		Error 2σ	^{208}Pb / ^{232}Th		Error 2σ	Disc.*
0.0534	±	0.0037	0.0404	±	0.0015	0.2976	±	0.0229	0.0125	±	0.0017	concordant
0.1139	±	0.0034	0.3177	±	0.0048	4.9926	±	0.1758	0.1157	±	0.0144	concordant
0.1156	±	0.0035	0.3153	±	0.0058	5.0275	±	0.1862	0.0916	±	0.0113	concordant
0.1155	±	0.0036	0.3421	±	0.0081	5.4516	±	0.2197	0.1101	±	0.0137	concordant
0.0523	±	0.0032	0.0405	±	0.0013	0.2922	±	0.0197	0.0142	±	0.0018	concordant
0.0557	±	0.0050	0.0368	±	0.0018	0.2830	±	0.0279	0.0115	±	0.0015	concordant
0.0577	±	0.0054	0.0375	±	0.0019	0.2983	±	0.0305	0.0125	±	0.0017	concordant
0.1145	±	0.0035	0.3460	±	0.0068	5.4652	±	0.2068	0.1058	±	0.0131	concordant
0.0507	±	0.0018	0.0394	±	0.0007	0.2753	±	0.0113	0.0133	±	0.0017	concordant
0.0547	±	0.0036	0.0421	±	0.0015	0.3176	±	0.0231	0.0153	±	0.0019	concordant
0.0560	±	0.0031	0.0423	±	0.0013	0.3264	±	0.0205	0.0144	±	0.0015	concordant
0.1162	±	0.0025	0.3382	±	0.0061	5.4234	±	0.1710	0.1183	±	0.0117	concordant
0.0508	±	0.0015	0.0380	±	0.0005	0.2664	±	0.0092	0.0134	±	0.0013	concordant
0.0497	±	0.0025	0.0400	±	0.0011	0.2747	±	0.0157	0.0143	±	0.0014	concordant
0.0510	±	0.0018	0.0391	±	0.0007	0.2754	±	0.0114	0.0136	±	0.0013	concordant
0.0516	±	0.0026	0.0398	±	0.0011	0.2835	±	0.0160	0.0138	±	0.0014	concordant
0.0558	±	0.0037	0.0413	±	0.0016	0.3180	±	0.0237	0.0160	±	0.0018	concordant
0.0517	±	0.0016	0.0389	±	0.0006	0.2773	±	0.0101	0.0136	±	0.0013	concordant
0.0556	±	0.0035	0.0426	±	0.0015	0.3268	±	0.0232	0.0159	±	0.0017	concordant
0.0528	±	0.0015	0.0403	±	0.0006	0.2940	±	0.0102	0.0139	±	0.0014	concordant
0.1151	±	0.0026	0.3397	±	0.0068	5.3965	±	0.1783	0.1024	±	0.0100	concordant
0.0521	±	0.0020	0.0418	±	0.0008	0.3006	±	0.0131	0.0147	±	0.0014	concordant
0.0755	±	0.0029	0.18631	±	0.00662	1.94178	±	0.10286	0.06007	±	0.00752	concordant
0.0752	±	0.0026	0.17946	±	0.00656	1.86102	±	0.09497	0.06576	±	0.00661	concordant
0.0460	±	0.0035	0.00510	±	0.00012	0.03238	±	0.00251	0.00176	±	0.00022	concordant
0.0493	±	0.0038	0.00523	±	0.00013	0.03560	±	0.00278	0.00180	±	0.00018	concordant

Without correction U-Pb age (Ma)						^{232}Th-^{208}Pb age (Ma)			^{207}Pb-^{206}Pb age (Ma)				
$^{206}Pb/^{238}U$		Error 2σ	$^{207}Pb/^{235}U$		Error 2σ	$^{208}Pb/^{232}Th$		Error 2σ	$^{207}Pb/^{206}Pb$		Error 2σ	f 206%	rho
255.3	±	9.8	264.5	±	22.9	250.4	±	33.7	345.2	±	157.5	1	0.49
1778.3	±	30.7	1818.1	±	164.5	2212.4	±	288.1	1862.7	±	53.4	9	0.43
1766.7	±	37.2	1824.0	±	173.4	1772.3	±	226.9	1888.8	±	54.0	9	0.50
1896.5	±	51.7	1893.0	±	201.6	2112.0	±	274.9	1888.0	±	55.4	9	0.58
255.7	±	8.4	260.3	±	19.8	284.6	±	36.5	300.2	±	138.9	1	0.48
233.0	±	11.6	253.1	±	28.0	230.9	±	30.4	441.9	±	201.2	1	0.49
237.3	±	12.5	265.1	±	30.5	250.4	±	35.2	517.4	±	205.2	1	0.50
1915.3	±	44.0	1895.1	±	190.9	2033.4	±	262.2	1872.0	±	54.4	9	0.52
248.8	±	4.2	246.9	±	11.4	267.2	±	33.5	227.8	±	83.7	1	0.41
265.6	±	9.7	280.1	±	23.2	306.3	±	39.2	401.7	±	146.7	1	0.49
266.8	±	8.6	286.8	±	20.6	289.5	±	29.4	451.6	±	123.8	1	0.50
1878.0	±	39.1	1888.6	±	160.3	2260.0	±	235.2	1899.0	±	39.4	9	0.57
240.4	±	3.5	239.8	±	9.3	268.2	±	26.5	232.6	±	66.3	1	0.41
253.1	±	6.9	246.5	±	15.8	287.6	±	28.8	182.8	±	118.9	0	0.47
247.4	±	4.6	247.0	±	11.5	273.4	±	27.3	241.7	±	82.2	1	0.44
251.7	±	6.9	253.4	±	16.1	277.2	±	28.5	267.4	±	115.0	1	0.47
260.9	±	10.0	280.4	±	23.8	321.7	±	36.4	444.9	±	148.2	1	0.51
245.9	±	3.9	248.6	±	10.2	273.4	±	26.9	272.5	±	70.2	1	0.43
269.1	±	9.9	287.1	±	23.3	319.6	±	33.8	435.6	±	141.0	1	0.51
254.9	±	3.8	261.7	±	10.3	279.4	±	27.9	321.0	±	65.9	1	0.42
1885.3	±	44.0	1884.3	±	166.6	1971.1	±	202.1	1882.0	±	40.3	9	0.61
263.9	±	5.4	266.8	±	13.2	294.7	±	29.2	291.6	±	85.9	1	0.46
1101	±	43	1096	±	99	1179	±	151	1083	±	78	4	0.67
1064	±	42	1067	±	92	1287	±	133	1073	±	70	4	0.72
32.8	±	0.78	32.4	±	2.55	35.5	±	4.5	-3.32	±	185	0	0.30
33.6	±	0.81	35.5	±	2.81	36.3	±	3.7	164	±	180	0	0.31

Table 9-1-5. Analytical conditions of zircon U–Pb dating in the LA-ICP-MS system in Oshima (Oshima Peninsula).

Laser ablation	
Model	LIGHT CONVERSION
Product name	CARBIDE
Laser tybe	Yb:KGW femtosecond laser
Pulse width	290 fs
Wave length	260 nm
Energy density	3.8 J /cm^2
Crater size	10 μm
Laser irradiation method	single- spot
Repetion rate	40 Hz
Shot count	100
Integration time	10 s
Carrie gas (He)	2.5 s
ICP-Ms	
Model	Nu Instruments
Product name	New Plasma II
ICP-MS type	Magnetic sector multi-collector ICP-MS
RF power	1300 W
Carrier gas (Ar)	0.85 L min^{-1}
ThO^+/Th Oxide formation rate	< 1%
Data Acquisition Method	Time-resolved analysis
Data acquisition time	9 s (6 s gas blank, 3 s ablation signal)
Monitor isotopes	^{202}Hg, ^{204}Pb, ^{206}Pb, ^{207}Pb, ^{208}Pb, ^{232}Th, ^{235}U
Primary standard(U-Pb)	Plešovice [*1]
Secondary standard (U-Pb)	OD-3 [*2, 3, 4], Nancy 91500[*5], GJ-1[*6]

(*1, Sláma et al. (2008); *2, Iwano et al. (2012); *3, Iwano et al. (2013); *4, Lukács et al. (2015); *5, Wiedenbeck et al. (1995); *6, Jackson et al. (2004))

Table 9-1-6. U–Pb isotopic data for zircon crystals determined by LA-ICP-MS in Oshima (Oshima Peninsula).

		Total count						
NO.	sample name	^{206}Pb	^{207}Pb	^{208}Pb	^{232}Th	^{235}U	^{238}U	Th/U
1	L-01 spot.01	29225	2312	5770	486057	14168	1953509	0.46
3	L-01 spot.06C	9500	813	2479	153968	3601	496509	0.58
4	L-01 spot.07	44491	3691	10220	845315	21823	3008954	0.52
5	L-01 spot.08	482447	88576	26151	190065	19271	2657068	0.13
6	L-01 spot.10	13812	1111	3171	242214	6482	893748	0.50
7	L-01 spot.12	28670	2268	2562	217099	13582	1872676	0.21
9	L-01 spot.14C	64914	10998	24109	306841	5335	735636	0.77
10	L-01 spot.18	11952	945	3761	315682	5764	794731	0.74
11	L-01 spot.22	68942	8083	9650	145909	5929	817554	0.33
12	L-01 spot.24	36033	2932	12545	1048819	17839	2459688	0.79
13	L-01 spot.25	57730	4668	5380	454380	29041	4004154	0.21
14	L-01 spot.26	259833	48613	39490	291572	10676	1472024	0.37
15	L-01 spot.27	616256	113954	11531	103404	26755	3689004	0.05
16	L-01 spot.28	114861	9897	23158	1674133	51839	7147577	0.42
17	L-01 spot.33	29212	2617	9054	680855	14011	1931774	0.63
19	L-01 spot.35C	76642	20364	17181	94408	2295	316478	0.53
20	L-01 spot.36	36409	3297	11449	880721	18036	2486791	0.63
21	L-01 spot.44	47098	3788	3981	352672	22580	3113379	0.20
22	L-01 spot.53	18329	1516	7107	603883	9059	1249083	0.86
23	L-01 spot.55	15320	1277	4059	332715	7271	1002494	0.59
24	L-01 spot.57	12001	1025	2281	121598	3937	542845	0.40
25	L-01 spot.62	36579	3153	5976	424577	16786	2314407	0.33
27	L-01 spot.67C	189324	34892	28549	228730	7983	1100683	0.37
28	L-01 spot.69	54905	4393	14655	1180084	26323	3629355	0.58
29	L-01 spot.73	7272	604	1727	100346	2559	352883	0.51
30	L-01 spot.110(1)	1642743	316358	177483	1485519	65135	8980823	0.30
31	L-01 spot.110(2)	447976	82652	6435	62641	19292	2660049	0.04
32	L-01 spot.110(3)	783093	149686	17621	125192	29898	4122334	0.05
	Standards							
	91500 4-1	20973	2505	3188	54135	1634	225326	0.44
	91500 4-2	20668	2500	3079	47483	1611	222154	0.39
	91500 4-3	21031	2541	3094	44358	1611	222154	0.37

91500 4-4	22293	2699	3339	59493	1651	227670	0.48
91500 4-5	21307	2546	3253	57372	1610	221947	0.47
91500 4-6	21150	2671	3216	45563	1766	243528	0.35
91500 4-7	19880	2489	2994	40406	1573	216914	0.35
91500 4-8	21146	2503	3240	51858	1612	222223	0.44
91500 4-9	21600	2648	3375	56479	1742	240150	0.44
91500 4-10	19996	2463	3082	45608	1615	222637	0.38
GJ1 4-1	48245	4622	1085	34133	7054	972635	0.06
GJ1 4-2	45557	4498	1038	25740	6630	914091	0.05
GJ1 4-3	49899	4786	1226	27883	7195	992010	0.05
GJ1 4-4	45987	4424	1069	27481	6846	943953	0.05
GJ1 4-5	46343	4552	1070	32280	6709	925057	0.06
GJ1 4-6	46510	4517	1049	27190	6933	955947	0.05
GJ1 4-7	46133	4619	1120	32794	7003	965600	0.06
GJ1 4-8	48327	4762	1140	34022	7026	968773	0.07
GJ1 4-9	43032	4057	993	22145	6282	866170	0.05
GJ1 4-10	47146	4611	1053	27525	6701	923886	0.06
OD-3 4-1	2652	215	1160	600132	7471	1030072	1.07
OD-3 4-2	3225	267	1504	765307	9442	1301832	1.08
OD-3 4-3	3861	284	1857	943831	10887	1501123	1.15
OD-3 4-4	1494	97	518	254804	3986	549603	0.85
OD-3 4-5	1856	144	762	385511	5076	699919	1.01
OD-3 4-6	3198	267	1283	653040	8468	1167570	1.05
OD-3 4-7	2939	240	1242	604351	8016	1105303	1.02
OD-3 4-8	4131	303	2006	1037635	11661	1607803	1.21
OD-3 4-9	4117	317	1767	834153	11273	1554357	1.00
OD-3 4-10	3174	222	1333	675364	8531	1176261	1.07

Isotopic ratios

$^{207}Pb/^{206}Pb$		Error 2σ	$^{206}Pb/^{238}U$		Error 2σ	$^{207}Pb/^{235}U$		Error 2σ	$^{208}Pb/^{232}Th$		Error 2σ	Disc.*
0.0492	±	0.0029	0.0287	±	0.0009	0.1950	±	0.0105	0.0092	±	0.0008	concordant
0.0532	±	0.0044	0.0367	±	0.0017	0.2696	±	0.0225	0.0125	±	0.0012	concordant
0.0516	±	0.0027	0.0284	±	0.0009	0.2021	±	0.0094	0.0094	±	0.0008	concordant
0.1141	±	0.0046	0.3487	±	0.0102	5.4917	±	0.1868	0.1071	±	0.0094	concordant
0.0500	±	0.0037	0.0297	±	0.0012	0.2047	±	0.0147	0.0102	±	0.0010	concordant
0.0492	±	0.0029	0.0294	±	0.0010	0.1995	±	0.0109	0.0092	±	0.0009	concordant
0.1053	±	0.0047	0.1695	±	0.0064	2.4629	±	0.1106	0.0612	±	0.0053	-10
0.0492	±	0.0038	0.0289	±	0.0012	0.1959	±	0.0150	0.0093	±	0.0009	concordant
0.0729	±	0.0034	0.1620	±	0.0060	1.6288	±	0.0742	0.0515	±	0.0046	concordant
0.0506	±	0.0028	0.0281	±	0.0009	0.1964	±	0.0098	0.0093	±	0.0008	concordant
0.0503	±	0.0025	0.0277	±	0.0008	0.1920	±	0.0084	0.0092	±	0.0008	concordant
0.1163	±	0.0047	0.3390	±	0.0108	5.4404	±	0.2007	0.1054	±	0.0092	concordant
0.1149	±	0.0046	0.3208	±	0.0090	5.0888	±	0.1679	0.0868	±	0.0077	concordant
0.0540	±	0.0017	0.0304	±	0.0010	0.2267	±	0.0108	0.0111	±	0.0016	concordant
0.0562	±	0.0026	0.0286	±	0.0011	0.2218	±	0.0133	0.0107	±	0.0015	-1
0.1665	±	0.0047	0.4584	±	0.0242	10.5341	±	0.6447	0.1458	±	0.0209	concordant
0.0568	±	0.0024	0.0277	±	0.0010	0.2170	±	0.0124	0.0104	±	0.0015	-2
0.0504	±	0.0021	0.0286	±	0.0010	0.1992	±	0.0110	0.0090	±	0.0013	concordant
0.0518	±	0.0030	0.0278	±	0.0011	0.1987	±	0.0139	0.0094	±	0.0014	concordant
0.0523	±	0.0033	0.0289	±	0.0012	0.2086	±	0.0155	0.0098	±	0.0014	concordant
0.0535	±	0.0037	0.0419	±	0.0020	0.3090	±	0.0253	0.0150	±	0.0022	concordant
0.0540	±	0.0024	0.0299	±	0.0011	0.2230	±	0.0128	0.0113	±	0.0016	concordant
0.1155	±	0.0030	0.3256	±	0.0127	5.1896	±	0.2554	0.1000	±	0.0143	concordant
0.0502	±	0.0020	0.0286	±	0.0010	0.1982	±	0.0106	0.0099	±	0.0014	concordant
0.0521	±	0.0046	0.0390	±	0.0022	0.2802	±	0.0280	0.0138	±	0.0021	concordant
0.1207	±	0.0028	0.3463	±	0.0112	5.7668	±	0.2501	0.0957	±	0.0136	concordant
0.1156	±	0.0028	0.3188	±	0.0111	5.0867	±	0.2310	0.0823	±	0.0119	concordant
0.1198	±	0.0029	0.3596	±	0.0121	5.9445	±	0.2637	0.1127	±	0.0162	concordant
0.0738	±	0.0036	0.1776	±	0.0092	1.8082	±	0.1256	0.0465	±	0.0092	concordant
0.0748	±	0.0037	0.1775	±	0.0093	1.8304	±	0.1276	0.0512	±	0.0101	concordant
0.0747	±	0.0037	0.1806	±	0.0094	1.8604	±	0.1294	0.0551	±	0.0109	concordant

0.0748	±	0.0036	0.1868	±	0.0096	1.9286	±	0.1320	0.0443	±	0.0088	concordant
0.0739	±	0.0036	0.1831	±	0.0096	1.8662	±	0.1297	0.0448	±	0.0088	concordant
0.0778	±	0.0041	0.1675	±	0.0091	1.7991	±	0.1197	0.0542	±	0.0043	concordant
0.0772	±	0.0041	0.1768	±	0.0101	1.8822	±	0.1306	0.0570	±	0.0046	concordant
0.0730	±	0.0039	0.1836	±	0.0103	1.8479	±	0.1273	0.0480	±	0.0038	concordant
0.0756	±	0.0040	0.1735	±	0.0095	1.8091	±	0.1210	0.0459	±	0.0036	concordant
0.0759	±	0.0041	0.1732	±	0.0098	1.8150	±	0.1253	0.0519	±	0.0041	concordant
0.0592	±	0.0024	0.0946	±	0.0025	0.7730	±	0.0363	0.0251	±	0.0051	concordant
0.0610	±	0.0025	0.0951	±	0.0026	0.8004	±	0.0381	0.0319	±	0.0065	concordant
0.0593	±	0.0023	0.0959	±	0.0025	0.7848	±	0.0366	0.0347	±	0.0070	concordant
0.0595	±	0.0024	0.0929	±	0.0025	0.7624	±	0.0363	0.0307	±	0.0063	concordant
0.0607	±	0.0024	0.0956	±	0.0026	0.8004	±	0.0380	0.0262	±	0.0053	concordant
0.0599	±	0.0027	0.0938	±	0.0032	0.7751	±	0.0358	0.0296	±	0.0028	concordant
0.0617	±	0.0028	0.0922	±	0.0031	0.7846	±	0.0360	0.0262	±	0.0024	concordant
0.0607	±	0.0027	0.0962	±	0.0033	0.8063	±	0.0367	0.0258	±	0.0024	concordant
0.0581	±	0.0027	0.0958	±	0.0034	0.7684	±	0.0368	0.0344	±	0.0033	concordant
0.0603	±	0.0027	0.0984	±	0.0034	0.8187	±	0.0378	0.0294	±	0.0028	concordant
0.0501	±	0.0072	0.0049	±	0.0002	0.0340	±	0.0048	0.0015	±	0.0003	concordant
0.0511	±	0.0066	0.0047	±	0.0002	0.0333	±	0.0042	0.0016	±	0.0003	concordant
0.0454	±	0.0057	0.0049	±	0.0002	0.0307	±	0.0038	0.0016	±	0.0003	concordant
0.0401	±	0.0085	0.0052	±	0.0003	0.0287	±	0.0060	0.0016	±	0.0003	concordant
0.0478	±	0.0084	0.0051	±	0.0003	0.0334	±	0.0057	0.0016	±	0.0003	concordant
0.0514	±	0.0068	0.0053	±	0.0002	0.0374	±	0.0048	0.0015	±	0.0001	concordant
0.0502	±	0.0069	0.0051	±	0.0002	0.0355	±	0.0048	0.0016	±	0.0001	concordant
0.0451	±	0.0056	0.0050	±	0.0002	0.0309	±	0.0037	0.0015	±	0.0001	concordant
0.0474	±	0.0057	0.0051	±	0.0002	0.0334	±	0.0039	0.0016	±	0.0001	concordant
0.0431	±	0.0061	0.0052	±	0.0002	0.0310	±	0.0043	0.0015	±	0.0001	concordant

Without correction U-Pb age (Ma)						^{232}Th-^{208}Pb age (Ma)				
$^{206}Pb/^{238}U$		Error 2σ	$^{207}Pb/^{235}U$		Error 2σ	$^{208}Pb/^{232}Th$		Error 2σ	f 206%	rho
182.6	±	6.0	180.9	±	10.6	185.9	±	16.9	0	0.60
232.6	±	11.0	242.4	±	22.5	251.8	±	24.1	1	0.56
180.5	±	5.5	186.9	±	9.5	189.3	±	16.8	1	0.65
1928.4	±	65.2	1899.3	±	173.9	2056.7	±	188.2	9	0.86
188.5	±	7.5	189.1	±	14.8	205.0	±	19.2	0	0.55
186.8	±	6.2	184.7	±	11.0	184.9	±	17.6	0	0.60
1009.2	±	41.4	1261.2	±	106.5	1200.0	±	107.7	8	0.85
183.6	±	7.6	181.7	±	15.1	186.6	±	17.3	0	0.53
967.6	±	38.5	981.4	±	72.6	1014.8	±	92.3	3	0.81
178.9	±	5.6	182.0	±	9.9	187.3	±	16.6	1	0.62
176.1	±	5.2	178.4	±	8.5	185.4	±	16.9	1	0.67
1881.9	±	69.5	1891.2	±	185.7	2026.1	±	184.6	9	0.87
1793.8	±	57.8	1834.2	±	157.6	1682.7	±	154.8	9	0.85
193.2	±	6.5	207.5	±	11.0	222.7	±	32.0	1	0.69
181.9	±	6.9	203.4	±	13.5	214.2	±	31.0	1	0.62
2432.7	±	154.0	2482.9	±	505.2	2750.5	±	418.3	15	0.86
176.2	±	6.5	199.4	±	12.5	209.4	±	30.2	1	0.64
182.0	±	6.5	184.5	±	11.1	181.9	±	26.7	1	0.64
176.6	±	7.3	184.0	±	14.0	189.7	±	27.5	1	0.58
183.8	±	7.9	192.3	±	15.6	196.6	±	28.8	1	0.57
264.3	±	13.0	273.4	±	25.4	301.5	±	45.1	1	0.59
190.0	±	7.0	204.4	±	13.0	226.6	±	33.0	1	0.63
1817.1	±	81.0	1850.9	±	231.0	1926.1	±	287.0	9	0.79
182.0	±	6.4	183.6	±	10.7	200.1	±	28.8	1	0.65
246.7	±	14.0	250.8	±	28.1	276.8	±	41.9	1	0.56
1916.8	±	72.0	1941.4	±	226.7	1847.3	±	273.9	9	0.75
1783.9	±	70.9	1833.9	±	211.0	1598.3	±	239.5	9	0.76
1980.3	±	77.3	1967.8	±	237.6	2159.3	±	324.1	9	0.76
1053.6	±	59.22	1048.4	±	120.10	918.9	±	185.0	4	0.75
1053.1	±	59.60	1056.4	±	121.94	1009.6	±	203.7	4	0.75
1070.1	±	60.61	1067.1	±	123.52	1083.8	±	219.0	4	0.75

1103.9	±	61.86	1091.1	±	125.86	876.6	±	176.2	4	0.75
1084.0	±	61.45	1069.2	±	123.86	885.4	±	178.0	4	0.75
998.4	±	58.39	1045.1	±	114.84	1067.7	±	87.0	4	0.82
1049.4	±	64.55	1074.8	±	124.67	1119.6	±	92.1	4	0.82
1086.3	±	66.25	1062.7	±	121.69	947.9	±	76.9	3	0.82
1031.3	±	60.75	1048.7	±	115.98	907.7	±	73.3	4	0.82
1030.0	±	62.61	1050.9	±	119.89	1023.3	±	83.7	4	0.82
582.8	±	16.27	581.5	±	36.24	501.2	±	103.2	2	0.57
585.4	±	16.81	597.1	±	38.00	633.8	±	131.1	2	0.58
590.6	±	16.34	588.2	±	36.45	690.1	±	141.9	2	0.57
572.8	±	16.22	575.4	±	36.19	611.7	±	126.3	2	0.57
588.3	±	16.80	597.0	±	37.85	522.4	±	107.6	2	0.58
578.3	±	20.56	582.7	±	35.68	590.4	±	56.6	2	0.74
568.3	±	20.15	588.1	±	35.91	523.5	±	49.4	2	0.74
592.2	±	20.99	600.4	±	36.64	514.0	±	48.3	2	0.74
589.9	±	21.59	578.8	±	36.66	684.6	±	66.7	2	0.73
605.2	±	21.74	607.3	±	37.67	585.5	±	56.1	2	0.74
31.6	±	1.45	33.9	±	4.85	30.8	±	6.3	1	0.33
30.4	±	1.27	33.3	±	4.30	31.3	±	6.3	1	0.33
31.5	±	1.21	30.7	±	3.85	31.4	±	6.3	0	0.31
33.3	±	2.04	28.7	±	6.03	32.4	±	6.9	-1	0.30
32.5	±	1.79	33.3	±	5.79	31.5	±	6.5	0	0.32
34.0	±	1.60	37.3	±	4.82	30.5	±	2.7	1	0.37
33.0	±	1.60	35.5	±	4.81	31.9	±	2.9	1	0.36
31.9	±	1.36	30.9	±	3.73	30.0	±	2.5	0	0.36
32.8	±	1.41	33.4	±	3.96	32.9	±	2.8	0	0.37
33.5	±	1.58	31.0	±	4.34	30.6	±	2.7	-6	0.34

Table 9-1-7. Analytical conditions of zircon U–Pb dating in the LA-ICP-MS system in Sukumojima (Oshima Peninsula).

Laser ablation	
Model	LIGHT Conversion, Vilnius, LITHUANIA
Product name	CARBIDE
Laser tybe	Yb:KGW femtosecond laser
Pulse width	290 fs
Wave length	260 nm
Energy density	3.8 J /cm^2
Crater size	10 μm
Laser irradiation method	single- spot
Repetion rate	1000 Hz
Shot count	100
Integration time	10 s
Carrie gas (He)	0.60 L min^{-1}
ICP-Ms	
Model	Nu Instruments
Product name	New Plasma II
ICP-MS type	Magnetic sector multi-collector ICP-MS
RF power	1300 W
Carrier gas (Ar)	0.95 L min^{-1}
ThO^+/Th Oxide formation rate	< 1%
Data Acquisition Method	Time-resolved analysis
Data acquisition time	8.5 s (6 s gas blank, 2.5 s ablation signal)
Monitor isotopes	^{202}Hg, ^{204}Pb, ^{206}Pb, ^{207}Pb, ^{208}Pb, ^{232}Th, ^{235}U
Primary standard(U-Pb)	Plešovice *1
Secondary standard (U-Pb)	Nancy 91500*2, GJ-1*3, OD-3 *4, 5, 6

(*1, Sláma et al. (2008); *2, Wiedenbeck et al. (1995); *3, Jackson et al. (2004); *4, Iwano et al. (2012); *5, Iwano et al. (2013); *6, Lukács et al. (2015))

Table 9-1-8. U–Pb isotopic data for zircon crystals determined by LA-ICP-MS in Sukumojima (Oshima Peninsula).

No.	Sample name	Total count ^{206}Pb	^{207}Pb	^{208}Pb	^{232}Th	^{235}U	^{238}U	Th/U
1	no.2	159803	29115	11332	65089	6249	861658	0.18
2	no.3	51000	9138	4431	28995	1998	275540	0.26
3	no.5	12656	981	5382	254704	4540	626039	0.99
5	no.10	5652	497	1916	86553	1850	255109	0.83
8	no.18	4220	381	2564	136261	1710	235826	1.41
9	no.23	3422	237	586	27094	1459	201214	0.33
11	no.25	23203	1870	6515	323346	8708	1200631	0.66
13	no.26	27711	2297	10816	487858	10209	1407556	0.84
14	no.28	12647	1077	2941	115325	3822	527029	0.53
15	no.32	274146	50541	27664	138059	10599	1461393	0.23
16	no.37	201406	36543	14873	79703	7970	1098943	0.18
17	no.42	23076	1876	1941	104796	9720	1340159	0.19
18	no.44	22089	1797	4294	217449	9187	1266740	0.43
19	no.46	23922	1956	4017	152539	7259	1000899	0.38
20	no.50	17450	1472	3823	149348	5579	769187	0.48
21	no.52	9844	788	3279	172355	4091	564077	0.76
22	no.65	181188	33222	8776	46170	6992	964058	0.12
23	no.68	106452	25502	18610	76303	3195	440522	0.43
25	no.70	183829	53810	71622	264702	4705	648688	1.01
27	no.74	13806	1150	3433	159694	5081	700560	0.57
28	no.85	11611	934	13064	697129	5051	696481	2.49
30	no.93	16690	1388	3437	178237	7572	1044095	0.42
32	no.105	25823	2488	7665	158851	3983	549207	0.73
33	no.106	137250	30873	48164	210872	4381	603987	0.88
	Standards							
	91500 1-1	25351	3109	3561	37779	1859	256315	0.37
	91500 1-2	21530	2656	3090	26667	1569	216383	0.31
	91500 1-3	24404	2851	3445	36049	1741	239986	0.37
	91500 1-4	26362	3113	3657	40037	1787	246387	0.40
	91500 1-5	24126	2874	3241	32820	1728	238216	0.34
	91500 2-1	32591	3900	4643	54224	2441	336628	0.40
	91500 2-2	34236	4092	4847	54341	2583	356152	0.38
	91500 2-3	37326	4422	5460	57793	2812	387650	0.37

GJ1 1-1	92334	9040	2224	36693	12191	1680924	0.05
GJ1 1-2	87589	8493	1942	34588	11489	1584121	0.05
GJ1 1-3	88765	8516	2041	35587	11817	1629328	0.05
GJ1 1-4	85972	8198	1905	39231	11345	1564298	0.06
GJ1 1-5	91889	9044	2067	24905	11857	1634867	0.04
GJ1 2-1	79650	7504	1693	34181	10829	1493086	0.06
GJ1 2-2	78360	7411	1731	38452	10656	1469253	0.07
GJ1 2-3	79572	7662	1777	36317	11044	1522734	0.06
OD-3 1-1	3334	306	1407	461125	8677	1196356	0.96
OD-3 1-2	2697	196	1157	380191	6844	943626	1.00
OD-3 1-3	3140	240	1274	428596	8074	1113262	0.96
OD-3 1-4	4865	377	1288	432250	12577	1734129	0.62
OD-3 1-5	3698	315	992	324306	8970	1236840	0.65
OD-3 2-1	4608	341	1817	589394	11994	1653758	0.89
OD-3 2-2	4211	296	1633	572681	11030	1520838	0.94
OD-3 2-3	4351	358	1733	569884	11432	1576180	0.91

Isotopic ratios

$^{207}Pb/^{206}Pb$		Error 2σ	$^{206}Pb/^{238}U$		Error 2σ	$^{207}Pb/^{235}U$		Error 2σ	$^{208}Pb/^{232}Th$		Error 2σ	Disc.*
0.1136	±	0.0028	0.3274	±	0.0113	5.1308	±	0.2395	0.0931	±	0.0111	concordant
0.1117	±	0.0035	0.3267	±	0.0167	5.0359	±	0.3121	0.0817	±	0.0099	concordant
0.0483	±	0.0034	0.0357	±	0.0015	0.2379	±	0.0190	0.0113	±	0.0014	concordant
0.0548	±	0.0053	0.0391	±	0.0023	0.2959	±	0.0319	0.0118	±	0.0015	concordant
0.0563	±	0.0061	0.0316	±	0.0020	0.2455	±	0.0293	0.0101	±	0.0012	concordant
0.0431	±	0.0059	0.0300	±	0.0020	0.1786	±	0.0259	0.0116	±	0.0017	concordant
0.0502	±	0.0026	0.0341	±	0.0012	0.2365	±	0.0150	0.0108	±	0.0013	concordant
0.0517	±	0.0025	0.0348	±	0.0011	0.2478	±	0.0147	0.0119	±	0.0014	concordant
0.0531	±	0.0036	0.0424	±	0.0018	0.3102	±	0.0244	0.0136	±	0.0017	concordant
0.1149	±	0.0027	0.3312	±	0.0100	5.2515	±	0.2264	0.1071	±	0.0127	concordant
0.1138	±	0.0026	0.3295	±	0.0150	5.1742	±	0.2193	0.1032	±	0.0106	concordant
0.0510	±	0.0027	0.0310	±	0.0014	0.2178	±	0.0133	0.0102	±	0.0011	concordant
0.0510	±	0.0027	0.0314	±	0.0015	0.2207	±	0.0137	0.0109	±	0.0011	concordant
0.0513	±	0.0026	0.0430	±	0.0020	0.304	±	0.0187	0.0146	±	0.0015	concordant
0.0529	±	0.0031	0.0408	±	0.0020	0.2977	±	0.0202	0.0142	±	0.0015	concordant
0.0502	±	0.0039	0.0314	±	0.0017	0.2173	±	0.0185	0.0105	±	0.0011	concordant
0.1150	±	0.0027	0.3379	±	0.0157	5.3621	±	0.2323	0.1051	±	0.0109	concordant
0.1503	±	0.0037	0.4345	±	0.0232	9.0077	±	0.4587	0.1348	±	0.0138	concordant
0.1836	±	0.0041	0.5095	±	0.0251	12.9074	±	0.5928	0.1496	±	0.0151	concordant
0.0523	±	0.0034	0.0354	±	0.0018	0.2555	±	0.0189	0.0119	±	0.0013	concordant
0.0504	±	0.0036	0.0300	±	0.0016	0.2086	±	0.0165	0.0104	±	0.0011	concordant
0.0522	±	0.0031	0.0287	±	0.0014	0.2069	±	0.0140	0.0107	±	0.0011	concordant
0.0605	±	0.0031	0.0854	±	0.0036	0.7131	±	0.0455	0.0274	±	0.0016	concordant
0.1413	±	0.0045	0.4128	±	0.0163	8.0458	±	0.4018	0.1298	±	0.0071	concordant
0.0758	±	0.0030	0.1735	±	0.0087	1.8144	±	0.1140	0.0513	±	0.0064	concordant
0.0762	±	0.0033	0.1745	±	0.0094	1.836	±	0.1240	0.0630	±	0.0079	concordant
0.0722	±	0.0030	0.1784	±	0.0092	1.7769	±	0.1153	0.0520	±	0.0065	concordant
0.0730	±	0.0029	0.1877	±	0.0095	1.8897	±	0.1200	0.0497	±	0.0062	concordant
0.0736	±	0.0031	0.1777	±	0.0092	1.8043	±	0.1171	0.0537	±	0.0067	concordant
0.0752	±	0.0034	0.1759	±	0.0086	1.8237	±	0.1170	0.0487	±	0.0030	concordant
0.0751	±	0.0033	0.1746	±	0.0083	1.8087	±	0.1141	0.0507	±	0.0031	concordant
0.0744	±	0.0032	0.1749	±	0.0081	1.7956	±	0.1104	0.0537	±	0.0033	concordant
0.0605	±	0.0016	0.0964	±	0.0023	0.8043	±	0.0287	0.0330	±	0.0042	concordant

0.0599	±	0.0016	0.0970	±	0.0024	0.8018	±	0.0292	0.0305	±	0.0039	concordant
0.0593	±	0.0016	0.0956	±	0.0023	0.7817	±	0.0283	0.0312	±	0.0040	concordant
0.0589	±	0.0016	0.0964	±	0.0023	0.7838	±	0.0288	0.0264	±	0.0034	concordant
0.0608	±	0.0016	0.0986	±	0.0024	0.8274	±	0.0297	0.0451	±	0.0058	concordant
0.0592	±	0.0023	0.0969	±	0.0031	0.7911	±	0.0384	0.0281	±	0.0021	concordant
0.0594	±	0.0023	0.0969	±	0.0031	0.794	±	0.0386	0.0256	±	0.0019	concordant
0.0605	±	0.0023	0.0949	±	0.0030	0.792	±	0.0383	0.0278	±	0.0020	concordant
0.0568	±	0.0068	0.0049	±	0.0002	0.0383	±	0.0045	0.0017	±	0.0002	-3
0.0450	±	0.0067	0.0050	±	0.0002	0.0311	±	0.0046	0.0017	±	0.0002	concordant
0.0472	±	0.0064	0.0049	±	0.0002	0.0322	±	0.0043	0.0016	±	0.0002	concordant
0.0479	±	0.0052	0.0049	±	0.0002	0.0325	±	0.0035	0.0016	±	0.0002	concordant
0.0526	±	0.0062	0.0052	±	0.0002	0.0381	±	0.0045	0.0017	±	0.0002	concordant
0.0464	±	0.0054	0.0051	±	0.0002	0.0324	±	0.0038	0.0018	±	0.0001	concordant
0.0441	±	0.0055	0.0050	±	0.0002	0.0306	±	0.0038	0.0016	±	0.0001	concordant
0.0516	±	0.0059	0.0050	±	0.0002	0.0357	±	0.0041	0.0017	±	0.0001	concordant

Without correction U-Pb age (Ma)						^{232}Th-^{208}Pb age (Ma)				
$^{206}Pb/^{238}U$		Error 2σ	$^{207}Pb/^{235}U$		Error 2σ	$^{208}Pb/^{232}Th$		Error 2σ	f 206%**	rho
1825.8	±	72.5	1841	±	218	1799.1	±	222.9	9	0.74
1822.6	±	106.7	1825	±	275.8	1587.6	±	200	8	0.82
226.1	±	9.5	216.7	±	19.1	227.1	±	27.5	0	0.52
247.3	±	14.7	263.2	±	31.9	237.8	±	30.2	1	0.54
200.5	±	12.6	222.9	±	29.3	202.3	±	25.2	1	0.52
190.7	±	12.9	166.8	±	26	232.6	±	33.7	0	0.46
216.3	±	7.5	215.5	±	15.1	216.6	±	26.1	1	0.54
220.2	±	7.3	224.8	±	14.9	238.2	±	28.5	1	0.55
267.5	±	11.9	274.3	±	24.4	273.7	±	33.9	1	0.55
1844	±	64.4	1861	±	207.2	2057.3	±	254.2	9	0.7
1836	±	96.1	1848	±	201.3	1984.6	±	212.2	9	1.08
196.5	±	9.2	200	±	13.4	206	±	22.9	1	0.76
199	±	9.4	202.5	±	13.8	219.5	±	23.2	1	0.75
271.2	±	13.2	269.5	±	18.8	292.2	±	31.1	1	0.78
257.7	±	13.1	264.6	±	20.3	284.1	±	30.3	1	0.74
199.2	±	11	199.7	±	18.6	211.5	±	22.7	1	0.64
1876.6	±	100.2	1879	±	212.1	2019.8	±	218.4	9	1.07
2325.8	±	147.7	2339	±	383.4	2556.7	±	276.2	13	1.05
2654.5	±	159.9	2673	±	472.6	2817.8	±	303.3	17	1.07
224.5	±	11.7	231	±	19	238.8	±	25.6	1	0.7
190.4	±	10	192.4	±	16.6	208.3	±	21.4	1	0.66
182.7	±	8.9	191	±	14.1	214.4	±	22.9	1	0.71
528.3	±	23.2	546.6	±	45.1	546.9	±	32.4	2	0.66
2227.7	±	104.3	2236	±	342.9	2467.2	±	142.7	12	0.79
1031.4	±	55.7	1051	±	109.6	1010.4	±	128.8	4	0.8
1037.1	±	60.6	1058	±	118.7	1235.2	±	159.3	4	0.8
1058.2	±	59	1037	±	110.8	1024	±	130.7	3	0.79
1108.9	±	61.2	1078	±	115	979.9	±	124.7	3	0.8
1054.2	±	59	1047	±	112.5	1057.2	±	135.4	4	0.8
1044.4	±	55.1	1054	±	112.3	960.6	±	60.6	4	0.76
1037.5	±	53.6	1049	±	109.7	999.5	±	62.8	4	0.76
1039.1	±	52.1	1044	±	106.3	1057.3	±	65.7	4	0.75

593.1	±	14.8	599.3	±	28.8	655.6	±	84.7	2	0.67
596.8	±	15.1	597.9	±	29.2	608	±	79.1	2	0.67
588.4	±	14.8	586.5	±	28.4	620.9	±	80.6	2	0.66
593.4	±	15.1	587.6	±	28.8	526.9	±	68.5	2	0.66
606.2	±	15.2	612.2	±	29.7	892.1	±	116.5	2	0.67
596.3	±	20.1	591.8	±	38.2	561.1	±	41.6	2	0.66
596.1	±	20.2	593.4	±	38.5	510.6	±	37.6	2	0.66
584.6	±	19.6	592.3	±	38.1	554.4	±	40.6	2	0.66
31.4	±	1.4	38.2	±	4.6	33.5	±	4.4	1	0.36
32.2	±	1.5	31.1	±	4.6	33.4	±	4.5	0	0.32
31.8	±	1.4	32.2	±	4.3	32.6	±	4.3	0	0.33
31.7	±	1.2	32.5	±	3.5	32.7	±	4.3	0	0.34
33.7	±	1.4	38	±	4.5	33.6	±	4.6	1	0.36
32.6	±	1.4	32.4	±	3.8	35.4	±	2.5	0	0.37
32.3	±	1.4	30.6	±	3.8	32.7	±	2.4	0	0.35
32.2	±	1.4	35.6	±	4.1	34.9	±	2.5	1	0.38

9.2 Mineral chemistry

Table 9-2-1. EPMA data of Nojima Island.

sample No 19081002A														
Comment	Garnet	Garnet	Garnet	Garnet	Garnet	Garnet	Garnet	Garnet	Garnet	Garnet	Garnet	Garnet	Garnet	Garnet
SiO_2	36.97	36.23	36.04	35.81	36.32	36.05	36.04	36.06	36.03	36.17	36.01	35.86	35.87	35.86
TiO_2	0.05	0.09	0.21	0.08	0.19	0.18	0.21	0.12	0.09	0.13	0.26	0.20	0.12	0.03
Al_2O_3	20.86	20.81	20.58	20.70	20.83	20.84	20.74	20.73	20.64	20.68	20.80	20.76	20.63	20.88
Cr_2O_3	0.00	0.02	0.00	0.03	0.00	0.03	0.00	0.03	0.09	0.03	0.00	0.02	0.02	0.01
FeO	25.76	22.52	20.15	17.98	19.08	19.54	18.46	18.81	17.95	16.96	17.70	18.50	23.11	27.01
MnO	15.41	18.21	20.67	23.21	21.35	20.87	21.62	21.78	22.63	23.65	24.11	22.37	17.58	14.63
MgO	1.29	0.99	0.80	0.61	0.73	0.76	0.69	0.70	0.59	0.54	0.54	0.56	1.08	1.34
CaO	0.89	1.18	1.48	1.60	1.86	1.79	1.78	1.77	1.75	1.67	1.56	1.56	1.12	0.40
Na_2O	0.01	0.01	0.00	0.02	0.01	0.02	0.01	0.01	0.00	0.03	0.02	0.02	0.01	0.02
K_2O	0.00	0.00	0.00	0.02	0.00	0.01	0.00	0.00	0.00	0.00	0.00	0.00	0.01	0.00
Total	101.24	100.07	99.93	100.04	100.38	100.07	99.55	100.01	99.78	99.86	101.00	99.86	99.54	100.19
O=	12	12	12	12	12	12	12	12	12	12	12	12	12	12
Si	2.990	2.969	2.964	2.949	2.967	2.956	2.967	2.961	2.967	2.973	2.941	2.953	2.959	2.945
Ti	0.003	0.006	0.013	0.005	0.012	0.011	0.013	0.007	0.005	0.008	0.016	0.013	0.007	0.002
Al	1.988	2.010	1.994	2.009	2.005	2.014	2.012	2.007	2.002	2.003	2.002	2.015	2.006	2.020
Cr	0.000	0.001	0.000	0.002	0.000	0.002	0.000	0.002	0.006	0.002	0.000	0.002	0.001	0.001
Fe	1.742	1.543	1.385	1.238	1.303	1.340	1.271	1.292	1.236	1.166	1.209	1.274	1.594	1.854
Mn	1.057	1.266	1.442	1.621	1.480	1.452	1.509	1.517	1.580	1.649	1.670	1.562	1.230	1.019
Mg	0.155	0.121	0.098	0.074	0.089	0.093	0.085	0.086	0.073	0.067	0.066	0.068	0.133	0.165
Ca	0.077	0.104	0.131	0.141	0.162	0.158	0.157	0.156	0.154	0.147	0.136	0.138	0.099	0.035
Na	0.002	0.001	0.000	0.004	0.002	0.002	0.001	0.001	0.001	0.005	0.003	0.003	0.001	0.003
K	0.000	0.000	0.000	0.002	0.000	0.001	0.000	0.000	0.000	0.000	0.000	0.000	0.001	0.000
Total	8.014	8.020	8.027	8.044	8.020	8.027	8.015	8.028	8.024	8.019	8.043	8.028	8.031	8.044

Biotite	Biotite	Biotite	Biotite	Biotite	Biotite	Biotite	Plagioclase	Plagioclase	Plagioclase	Plagioclase	Plagioclase	Plagioclase	K-feldspar
33.93	34.11	33.66	34.56	34.66	34.52	34.59	66.54	63.45	62.45	63.96	65.47	64.92	64.64
1.28	1.51	1.52	1.40	1.57	1.45	1.68	0.06	0.02	0.00	0.09	0.00	0.02	0.05
19.58	19.88	19.20	20.03	19.59	19.82	18.96	20.68	23.09	23.93	22.41	22.49	22.14	18.85
0.00	0.00	0.05	0.03	0.00	0.00	0.07	0.02	0.00	0.06	0.05	0.01	0.00	0.00
22.83	22.03	21.97	22.30	22.76	21.76	21.99	0.17	0.17	0.23	0.36	0.12	0.11	0.24
0.28	0.35	0.33	0.29	0.41	0.36	0.26	0.03	0.01	0.04	0.04	0.01	0.00	0.13
7.74	7.22	7.55	7.72	7.67	7.57	7.77	0.00	0.00	0.00	0.00	0.00	0.00	0.01
0.01	0.00	0.03	0.00	0.00	0.00	0.00	1.07	3.82	4.69	3.15	2.53	2.41	0.00
0.05	0.03	0.04	0.08	0.05	0.11	0.04	10.50	9.47	8.65	10.27	10.18	10.26	0.25
9.04	9.05	9.66	8.99	10.08	9.10	9.63	0.10	0.07	0.10	0.09	0.20	0.09	16.54
94.75	94.19	94.02	95.39	96.79	94.68	94.99	99.16	100.10	100.15	100.42	101.01	99.94	100.72
11	11	11	11	11	11	11	8	8	8	8	8	8	8
2.645	2.662	2.649	2.660	2.654	2.675	2.686	2.936	2.801	2.761	2.820	2.854	2.859	2.975
0.075	0.089	0.090	0.081	0.090	0.084	0.098	0.002	0.001	0.000	0.003	0.000	0.001	0.002
1.799	1.829	1.781	1.817	1.769	1.811	1.735	1.075	1.201	1.246	1.165	1.155	1.149	1.023
0.000	0.000	0.003	0.002	0.000	0.000	0.004	0.001	0.000	0.002	0.002	0.000	0.000	0.000
1.489	1.438	1.446	1.436	1.458	1.410	1.428	0.006	0.006	0.009	0.013	0.004	0.004	0.009
0.018	0.023	0.022	0.019	0.027	0.023	0.017	0.001	0.000	0.001	0.002	0.001	0.000	0.005
0.900	0.840	0.886	0.886	0.876	0.875	0.899	0.000	0.000	0.000	0.000	0.000	0.000	0.001
0.001	0.000	0.003	0.000	0.000	0.000	0.000	0.051	0.181	0.222	0.149	0.118	0.114	0.000
0.008	0.005	0.007	0.012	0.007	0.016	0.005	0.898	0.810	0.741	0.878	0.860	0.876	0.022
0.899	0.901	0.970	0.883	0.985	0.899	0.954	0.006	0.004	0.006	0.005	0.011	0.005	0.971
7.834	7.787	7.857	7.796	7.867	7.793	7.826	4.976	5.005	4.988	5.036	5.004	5.006	5.008

Garnet	Garnet	Garnet	Garnet	Garnet	Garnet	Garnet	Garnet	Garnet	Biotite	Biotite	Biotite	Biotite	Biotite	Biotite	Biotite	Biotite
36.50	36.31	36.13	36.16	36.11	36.35	36.01	36.12	36.53	37.93	34.37	33.52	33.99	34.81	34.57	34.32	34.83
0.12	0.07	0.17	0.15	0.37	0.09	0.10	0.06	0.08	1.66	1.67	1.33	1.59	1.45	1.47	1.43	1.46
20.72	20.77	20.58	20.78	20.72	20.95	20.94	20.80	20.36	18.62	19.37	19.50	19.30	19.83	19.76	19.64	19.81
0.03	0.00	0.04	0.03	0.00	0.07	0.01	0.07	0.00	0.02	0.00	0.03	0.00	0.04	0.05	0.00	0.01
25.11	24.31	24.06	24.49	25.28	23.56	23.52	24.40	26.11	21.22	22.39	22.78	22.71	22.29	22.22	22.27	22.32
15.74	16.38	17.23	15.77	14.40	17.13	16.96	16.55	15.03	0.35	0.21	0.32	0.31	0.49	0.36	0.32	0.21
1.24	1.15	1.16	1.17	1.19	1.17	1.12	1.14	1.27	6.71	7.44	8.06	7.46	7.56	7.57	7.55	7.73
0.76	0.98	1.10	1.14	1.53	1.22	1.10	0.94	0.81	0.05	0.01	0.03	0.03	0.01	0.04	0.00	0.02
0.02	0.00	0.04	0.03	0.06	0.00	0.02	0.02	0.05	0.07	0.04	0.09	0.08	0.08	0.14	0.14	0.08
0.00	0.01	0.01	0.01	0.00	0.00	0.02	0.00	0.01	9.22	8.77	8.71	9.22	9.38	9.44	8.62	9.05
100.24	99.97	100.53	99.73	99.66	100.53	99.79	100.11	100.24	95.85	94.28	94.36	94.69	95.94	95.62	94.30	95.51
12	12	12	12	12	12	12	12	12	11	11	11	11	11	11	11	11
2.982	2.976	2.956	2.968	2.963	2.963	2.957	2.961	2.991	2.870	2.678	2.624	2.654	2.672	2.665	2.672	2.677
0.008	0.004	0.011	0.009	0.023	0.005	0.006	0.004	0.005	0.095	0.098	0.078	0.093	0.084	0.085	0.084	0.085
1.995	2.006	1.985	2.010	2.004	2.012	2.027	2.010	1.965	1.661	1.780	1.798	1.777	1.794	1.795	1.802	1.795
0.002	0.000	0.003	0.002	0.000	0.005	0.001	0.004	0.000	0.001	0.000	0.002	0.000	0.003	0.003	0.000	0.001
1.715	1.666	1.646	1.681	1.735	1.606	1.615	1.673	1.787	1.343	1.460	1.491	1.483	1.431	1.432	1.449	1.435
1.091	1.139	1.196	1.098	1.002	1.184	1.181	1.151	1.044	0.023	0.014	0.021	0.020	0.032	0.024	0.021	0.014
0.151	0.140	0.141	0.144	0.146	0.143	0.137	0.140	0.156	0.758	0.865	0.941	0.869	0.865	0.870	0.876	0.886
0.066	0.086	0.097	0.100	0.134	0.106	0.097	0.083	0.071	0.004	0.000	0.002	0.003	0.001	0.003	0.000	0.001
0.003	0.000	0.007	0.005	0.009	0.000	0.004	0.003	0.007	0.010	0.007	0.013	0.012	0.012	0.020	0.022	0.012
0.000	0.001	0.001	0.001	0.000	0.000	0.002	0.000	0.001	0.890	0.872	0.870	0.918	0.919	0.928	0.856	0.887
8.013	8.018	8.043	8.020	8.016	8.024	8.026	8.029	8.026	7.654	7.773	7.840	7.829	7.812	7.825	7.782	7.791

Plagioclase	Plagioclase	Plagioclase	Plagioclase	Plagioclase	Plagioclase	Garnet	Garnet	Garnet	Garnet	Garnet	Garnet	Garnet
65.37	64.47	63.33	64.84	64.93	64.36	38.63	37.46	36.76	36.36	36.75	36.53	36.16
0.00	0.00	0.01	0.02	0.07	0.02	0.03	0.19	0.22	0.31	0.22	0.14	0.05
22.15	22.13	23.24	22.27	22.84	22.37	22.03	20.84	20.54	20.40	20.48	20.45	20.51
0.00	0.06	0.00	0.00	0.09	0.02	0.19	0.00	0.04	0.00	0.00	0.00	0.03
0.17	0.17	0.30	0.17	0.22	0.16	21.18	17.57	15.65	10.60	11.18	19.00	21.10
0.00	0.02	0.03	0.04	0.02	0.00	18.71	16.98	19.58	24.89	24.17	16.96	18.33
0.01	0.01	0.01	0.00	0.01	0.00	1.14	1.22	0.87	0.30	0.29	1.38	1.63
2.43	2.74	3.89	2.69	3.18	3.10	0.57	5.90	5.41	6.02	6.07	4.64	1.25
9.85	10.16	9.22	9.65	9.60	9.09	0.02	0.03	0.01	0.01	0.01	0.00	0.03
0.09	0.15	0.38	0.08	0.11	0.09	0.07	0.02	0.00	0.00	0.01	0.00	0.02
100.07	99.91	100.42	99.76	101.06	99.19	102.59	100.20	99.08	98.87	99.17	99.10	99.12
8	8	8	8	8	8	12	12	12	12	12	12	12
2.869	2.846	2.793	2.857	2.832	2.850	3.041	3.011	3.001	2.986	3.004	2.988	2.979
0.000	0.000	0.000	0.001	0.002	0.001	0.002	0.012	0.013	0.019	0.014	0.009	0.003
1.146	1.152	1.208	1.157	1.174	1.168	2.044	1.974	1.976	1.975	1.973	1.971	1.990
0.000	0.002	0.000	0.000	0.003	0.001	0.012	0.000	0.002	0.000	0.000	0.000	0.002
0.006	0.006	0.011	0.006	0.008	0.006	1.394	1.181	1.068	0.728	0.764	1.299	1.453
0.000	0.001	0.001	0.002	0.001	0.000	1.249	1.158	1.355	1.734	1.675	1.176	1.281
0.001	0.001	0.000	0.000	0.001	0.000	0.134	0.146	0.106	0.036	0.035	0.169	0.201
0.114	0.130	0.184	0.127	0.148	0.147	0.048	0.508	0.473	0.530	0.531	0.406	0.111
0.839	0.870	0.788	0.824	0.811	0.780	0.003	0.004	0.002	0.002	0.001	0.000	0.005
0.005	0.008	0.021	0.004	0.006	0.005	0.007	0.002	0.000	0.000	0.001	0.000	0.002
4.980	5.016	5.007	4.978	4.986	4.958	7.935	7.994	7.998	8.009	7.997	8.018	8.026

Biotite	Biotite	Biotite	Biotite	Biotite	Biotite	Plagioclase	Plagioclase	Plagioclase	Plagioclase	Plagioclase	Plagioclase
35.58	35.84	34.82	35.33	35.14	35.62	62.35	63.06	62.31	62.64	63.29	60.66
1.77	1.65	1.75	1.60	1.67	1.56	0.00	0.02	0.02	0.02	0.00	0.02
20.04	19.72	18.86	19.42	19.64	19.68	22.66	22.72	22.94	23.28	23.29	23.31
0.00	0.05	0.01	0.04	0.07	0.02	0.04	0.00	0.02	0.02	0.00	0.12
17.63	17.26	17.80	17.65	17.83	17.59	0.23	0.29	0.27	0.40	0.35	0.71
0.58	0.57	0.50	0.65	0.48	0.45	0.03	0.12	0.06	0.12	0.19	0.31
10.03	10.31	10.79	10.38	9.87	10.11	0.04	0.01	0.01	0.07	0.01	0.00
0.03	0.03	0.02	0.02	0.03	0.09	3.53	3.50	3.94	3.88	3.86	4.70
0.15	0.14	0.13	0.15	0.12	0.25	10.43	9.32	9.34	9.00	8.94	8.91
9.13	8.65	8.73	9.52	10.00	8.74	0.13	0.13	0.10	0.15	0.14	0.11
94.94	94.22	93.40	94.75	94.86	94.12	99.43	99.17	99.01	99.57	100.08	98.86
11	11	11	11	11	11	8	8	8	8	8	12
2.691	2.718	2.683	2.690	2.681	2.712	2.786	2.810	2.787	2.784	2.795	2.737
0.101	0.094	0.101	0.092	0.096	0.090	0.000	0.001	0.001	0.001	0.000	0.001
1.787	1.763	1.713	1.743	1.766	1.766	1.193	1.193	1.209	1.219	1.213	1.240
0.000	0.003	0.001	0.003	0.004	0.001	0.001	0.000	0.001	0.001	0.000	0.004
1.115	1.094	1.147	1.124	1.138	1.120	0.009	0.011	0.010	0.015	0.013	0.027
0.037	0.037	0.033	0.042	0.031	0.029	0.001	0.005	0.002	0.004	0.007	0.012
1.131	1.165	1.239	1.178	1.123	1.148	0.003	0.001	0.001	0.005	0.001	0.000
0.002	0.002	0.002	0.002	0.003	0.007	0.169	0.167	0.189	0.185	0.183	0.227
0.022	0.021	0.019	0.022	0.017	0.037	0.903	0.805	0.810	0.775	0.766	0.779
0.881	0.837	0.858	0.925	0.974	0.849	0.007	0.007	0.006	0.009	0.008	0.006
7.767	7.734	7.797	7.819	7.833	7.758	5.072	4.999	5.015	4.997	4.985	5.033

sample No.20103004B													
Comment	Garnet	Garnet	Garnet	Garnet	Garnet	Garnet	Garnet	Biotite	Biotite	Biotite	Biotite	Plagioclase	Plagioclase
SiO_2	35.93	36.15	36.10	35.78	35.92	35.96	36.03	34.43	33.94	33.79	33.94	59.14	61.53
TiO_2	0.15	0.24	0.12	0.09	0.11	0.13	0.00	1.74	1.80	1.53	1.43	0.12	0.00
Al_2O_3	21.34	21.48	21.21	21.56	21.25	21.24	21.31	20.07	19.65	19.69	19.73	22.67	23.93
Cr_2O_3	0.00	0.00	0.05	0.00	0.01	0.01	0.04	0.04	0.03	0.06	0.02	0.08	0.00
FeO	27.24	24.64	23.25	22.11	22.93	24.85	27.72	21.39	22.09	21.65	21.84	1.34	1.36
MnO	13.96	15.27	16.39	15.85	16.72	15.24	13.89	0.20	0.13	0.30	0.31	0.02	0.07
MgO	1.12	1.11	1.02	1.05	0.98	1.09	1.10	8.15	8.39	8.47	8.23	0.12	0.07
CaO	1.34	2.24	2.73	3.35	2.64	2.14	1.06	0.00	0.01	0.00	0.03	3.53	3.78
Na_2O	0.04	0.01	0.03	0.11	0.03	0.03	0.03	0.06	0.10	0.07	0.02	11.77	11.98
K_2O	0.02	0.01	0.00	0.00	0.00	0.01	0.00	11.12	11.18	10.62	10.77	0.13	0.16
Total	101.12	101.15	100.90	99.89	100.58	100.69	101.17	97.21	97.31	96.18	96.31	98.91	102.88
O=	12	12	12	12	12	12	12	11	11	11	11	8	8
Si	2.922	2.926	2.932	2.921	2.928	2.929	2.931	2.623	2.598	2.607	2.617	2.700	2.698
Ti	0.009	0.015	0.007	0.006	0.007	0.008	0.000	0.100	0.103	0.089	0.083	0.004	0.000
Al	2.045	2.049	2.030	2.074	2.041	2.039	2.042	1.803	1.774	1.790	1.794	1.220	1.237
Cr	0.000	0.000	0.003	0.000	0.001	0.001	0.003	0.003	0.002	0.004	0.001	0.003	0.000
Fe	1.852	1.667	1.579	1.510	1.562	1.692	1.886	1.363	1.414	1.397	1.408	0.051	0.050
Mn	0.963	1.048	1.129	1.097	1.156	1.053	0.958	0.013	0.008	0.020	0.020	0.001	0.003
Mg	0.136	0.134	0.124	0.127	0.119	0.132	0.134	0.926	0.957	0.974	0.946	0.008	0.005
Ca	0.117	0.194	0.238	0.293	0.230	0.186	0.092	0.000	0.001	0.000	0.002	0.173	0.178
Na	0.006	0.002	0.004	0.017	0.005	0.004	0.004	0.009	0.014	0.010	0.003	1.041	1.019
K	0.002	0.001	0.000	0.000	0.000	0.001	0.000	1.080	1.092	1.045	1.059	0.007	0.009
Total	8.051	8.036	8.046	8.045	8.047	8.046	8.049	7.919	7.964	7.935	7.934	5.209	5.197

Table 9-2-2. EPMA data of Ozushima Island.

Sample No 21080704														
Comment	Garnet	Garnet	Garnet	Garnet	Garnet	Garnet	Garnet	Garnet	Garnet	Garnet	Garnet	Garnet	Garnet	Garnet
SiO_2	35.58	35.74	35.80	35.34	35.22	34.82	35.61	35.20	35.81	35.80	35.48	35.70	35.75	35.64
TiO_2	0.60	0.30	0.57	0.55	0.48	0.50	0.46	0.66	0.39	0.07	0.25	0.05	0.06	0.02
Al_2O_3	19.77	20.38	19.82	19.78	19.75	19.50	20.14	19.96	20.16	19.91	20.10	20.23	20.27	20.37
Cr_2O_3	0.00	0.00	0.00	0.01	0.01	0.02	0.01	0.00	0.01	0.00	0.00	0.00	0.02	0.01
FeO	23.48	19.27	15.64	18.53	19.69	18.06	18.91	23.29	21.89	27.03	28.58	28.54	29.71	30.36
MnO	12.48	17.83	18.49	15.51	14.72	17.48	16.30	14.50	14.19	12.86	12.75	12.80	11.63	11.61
MgO	0.92	0.63	0.45	0.59	0.68	0.52	0.60	0.90	0.82	1.12	1.14	1.16	1.21	1.12
CaO	3.41	2.75	5.00	4.88	4.60	4.17	5.45	2.79	3.98	1.50	1.00	0.68	0.53	0.27
Na_2O	0.02	0.04	0.02	0.02	0.01	0.02	0.02	0.02	0.01	0.03	0.01	0.00	0.07	0.02
K_2O	0.00	0.00	0.00	0.01	0.01	0.00	0.00	0.00	0.00	0.01	0.00	0.01	0.01	0.00
Total	96.26	96.92	95.80	95.22	95.16	95.08	97.51	97.33	97.26	98.33	99.31	99.18	99.24	99.42
O=	12	12	12	12	12	12	12	12	12	12	12	12	12	12
Si	3.001	2.997	3.019	3.002	2.998	2.983	2.969	2.958	2.990	2.989	2.949	2.966	2.967	2.959
Ti	0.038	0.019	0.036	0.035	0.031	0.032	0.029	0.042	0.024	0.004	0.016	0.003	0.004	0.001
Al	1.965	2.014	1.970	1.980	1.981	1.969	1.979	1.976	1.984	1.959	1.969	1.981	1.983	1.993
Cr	0.000	0.000	0.000	0.001	0.001	0.001	0.000	0.000	0.001	0.000	0.000	0.000	0.001	0.001
Fe	1.656	1.351	1.103	1.316	1.401	1.294	1.318	1.637	1.529	1.887	1.986	1.983	2.062	2.108
Mn	0.893	1.268	1.323	1.117	1.062	1.270	1.153	1.033	1.005	0.911	0.899	0.902	0.819	0.818
Mg	0.115	0.079	0.056	0.075	0.086	0.066	0.075	0.112	0.102	0.139	0.141	0.144	0.150	0.138
Ca	0.308	0.247	0.452	0.444	0.419	0.383	0.487	0.251	0.356	0.134	0.089	0.061	0.047	0.024
Na	0.004	0.006	0.003	0.003	0.002	0.003	0.003	0.004	0.002	0.005	0.002	0.000	0.011	0.003
K	0.000	0.000	0.000	0.001	0.001	0.000	0.000	0.000	0.000	0.001	0.000	0.001	0.001	0.000
Total	7.980	7.981	7.961	7.974	7.982	8.001	8.014	8.014	7.994	8.030	8.052	8.041	8.043	8.044

Biotite	Biotite	Plagioclase	Plagioclase	Plagioclase	Plagioclase	Biotite	Biotite	Biotite	Biotite
33.50	32.87	63.92	64.00	62.35	65.03	31.90	34.79	34.00	34.19
1.93	2.06	0.15	0.07	0.25	0.00	1.38	1.37	1.52	1.43
18.94	19.01	21.60	21.23	21.08	22.10	18.80	19.16	19.28	19.54
0.02	0.03	0.02	0.01	0.00	0.03	0.05	0.05	0.03	0.05
25.33	22.48	0.47	0.42	1.73	0.15	22.12	19.47	19.58	19.42
0.78	0.63	0.10	0.00	0.09	0.00	1.08	0.74	0.74	0.82
5.76	7.17	0.00	0.01	0.32	0.00	9.63	8.36	8.15	8.17
0.00	0.00	1.85	1.79	1.80	2.49	0.03	0.01	0.01	0.01
0.05	0.03	11.02	11.22	9.73	10.84	0.06	0.07	0.07	0.07
8.83	8.77	0.19	0.24	0.68	0.10	8.43	12.03	11.63	11.82
95.12	93.07	99.32	98.98	98.02	100.74	93.49	96.05	95.00	95.52
11	11	8	8	8	8	11	11	11	11
2.641	2.617	2.848	2.861	2.832	2.850	2.535	2.682	2.651	2.651
0.114	0.124	0.005	0.002	0.009	0.000	0.083	0.079	0.089	0.084
1.760	1.784	1.134	1.118	1.128	1.141	1.761	1.741	1.773	1.786
0.001	0.002	0.001	0.000	0.000	0.001	0.003	0.003	0.002	0.003
1.670	1.497	0.018	0.016	0.066	0.006	1.470	1.255	1.277	1.259
0.052	0.043	0.004	0.000	0.003	0.000	0.073	0.049	0.049	0.054
0.677	0.851	0.000	0.001	0.022	0.000	1.141	0.961	0.947	0.944
0.000	0.000	0.088	0.086	0.088	0.117	0.003	0.000	0.001	0.001
0.008	0.005	0.952	0.972	0.856	0.921	0.009	0.010	0.010	0.010
0.888	0.891	0.011	0.014	0.039	0.006	0.855	1.183	1.158	1.169
7.812	7.814	5.061	5.070	5.043	5.042	7.932	7.963	7.956	7.961

Sample No 21051407													
Comment	Garnet	Garnet	Garnet	Garnet	Garnet	Garnet	Garnet	Garnet	Garnet	Garnet	Biotite	Biotite	Plagioclase
SiO_2	35.82	35.58	35.88	35.63	35.59	35.66	35.64	35.63	36.06	35.05	33.59	33.61	64.23
TiO_2	0.21	0.06	0.03	0.15	0.11	0.04	0.06	0.23	0.17	0.06	2.63	2.75	0.00
Al_2O_3	21.11	20.92	20.83	20.89	20.75	20.37	20.83	20.91	20.77	20.55	19.55	19.76	21.04
Cr_2O_3	0.00	0.00	0.01	0.00	0.00	0.03	0.00	0.00	0.00	0.04	0.03	0.03	0.01
FeO	26.56	26.02	24.21	23.09	22.69	22.77	23.61	24.44	25.64	26.89	22.43	22.83	0.54
MnO	13.85	14.87	16.50	17.69	18.61	17.70	17.00	16.46	15.30	13.94	0.56	0.61	0.02
MgO	1.29	1.27	1.18	1.06	1.07	1.11	1.14	1.22	1.32	1.34	5.64	5.46	0.14
CaO	0.56	0.51	0.48	0.49	0.47	0.47	0.49	0.51	0.54	0.58	0.04	0.01	3.12
Na_2O	0.00	0.00	0.16	0.00	0.02	0.09	0.14	0.12	0.08	0.03	0.13	0.12	12.08
K_2O	0.01	0.00	0.00	0.01	0.01	0.00	0.01	0.00	0.01	0.02	10.61	9.53	0.17
Total	99.40	99.24	99.28	99.00	99.32	98.20	98.92	99.51	99.89	98.46	95.23	94.72	101.33
O=	12	12	12	12	12	12	12	12	12	12	11	11	8
Si	2.949	2.944	2.963	2.952	2.947	2.977	2.955	2.940	2.961	2.930	2.633	2.635	2.831
Ti	0.013	0.004	0.002	0.009	0.007	0.002	0.004	0.014	0.010	0.004	0.155	0.162	0.000
Al	2.049	2.040	2.027	2.040	2.025	2.004	2.036	2.033	2.010	2.025	1.807	1.827	1.093
Cr	0.000	0.000	0.000	0.000	0.000	0.002	0.000	0.000	0.000	0.002	0.002	0.002	0.000
Fe	1.828	1.800	1.672	1.600	1.571	1.590	1.637	1.686	1.760	1.880	1.471	1.497	0.020
Mn	0.967	1.043	1.156	1.243	1.307	1.254	1.196	1.152	1.066	0.988	0.037	0.040	0.001
Mg	0.158	0.157	0.146	0.131	0.133	0.138	0.140	0.149	0.161	0.167	0.659	0.639	0.009
Ca	0.050	0.045	0.043	0.043	0.041	0.042	0.043	0.045	0.048	0.052	0.003	0.001	0.147
Na	0.000	0.000	0.025	0.000	0.003	0.015	0.022	0.018	0.013	0.005	0.020	0.018	1.032
K	0.001	0.000	0.000	0.001	0.001	0.000	0.001	0.000	0.001	0.002	1.061	0.953	0.009
Total	8.014	8.033	8.034	8.019	8.036	8.024	8.035	8.038	8.030	8.055	7.848	7.774	5.143

Garnet	Garnet	Garnet	Garnet	Garnet	Garnet	Garnet	Garnet	Garnet	Garnet	Garnet	Biotite	Biotite	Biotite	Biotite	Biotite	Biotite
36.04	35.92	35.57	35.56	35.84	35.65	35.84	35.95	35.74	35.74	35.32	33.08	33.30	33.64	33.64	33.51	33.65
0.00	0.09	0.28	0.18	0.22	0.27	0.02	0.33	0.02	0.14	0.07	2.56	2.80	2.82	2.25	2.59	2.34
21.10	21.04	21.02	20.92	20.72	20.89	20.98	20.81	20.99	20.73	20.70	19.34	18.83	19.76	19.10	19.11	19.35
0.01	0.04	0.04	0.00	0.00	0.00	0.03	0.01	0.01	0.00	0.01	0.08	0.03	0.08	0.12	0.05	0.05
27.18	24.72	23.32	22.10	21.39	21.15	21.05	22.00	23.12	24.43	26.91	23.39	23.64	22.64	23.10	23.52	23.34
13.87	16.08	17.96	19.06	19.55	20.15	20.18	19.83	18.49	16.30	13.94	0.59	0.69	0.48	0.51	0.72	0.56
1.26	1.21	1.09	1.01	1.00	0.93	0.96	1.02	1.04	1.24	1.26	5.76	5.77	5.57	5.78	5.59	5.73
0.54	0.51	0.48	0.46	0.58	0.51	0.51	0.53	0.55	0.48	0.53	0.06	0.03	0.04	0.02	0.04	0.01
0.10	0.14	0.00	0.07	0.00	0.13	0.15	0.01	0.00	0.03	0.00	0.19	0.03	0.13	0.08	0.27	0.11
0.02	0.01	0.00	0.01	0.01	0.01	0.01	0.00	0.00	0.00	0.01	10.44	10.49	11.13	10.63	10.63	10.57
100.10	99.72	99.72	99.37	99.32	99.68	99.69	100.47	99.95	99.07	98.74	95.40	95.58	96.21	95.09	95.97	95.67
12	O=	12	12	12	12	12	12	12	12	12	11	11	11	11	11	11
2.953	2.952	2.931	2.941	2.961	2.941	2.952	2.944	2.942	2.958	2.941	2.602	2.619	2.616	2.647	2.624	2.634
0.000	0.005	0.017	0.011	0.014	0.017	0.001	0.020	0.001	0.008	0.004	0.152	0.165	0.165	0.133	0.152	0.138
2.038	2.038	2.041	2.039	2.018	2.030	2.037	2.009	2.037	2.022	2.031	1.793	1.746	1.811	1.771	1.764	1.786
0.001	0.003	0.003	0.000	0.000	0.000	0.002	0.001	0.001	0.000	0.001	0.005	0.002	0.005	0.007	0.003	0.003
1.863	1.699	1.607	1.528	1.478	1.459	1.450	1.507	1.591	1.691	1.873	1.538	1.555	1.472	1.520	1.540	1.528
0.964	1.121	1.255	1.337	1.370	1.410	1.410	1.378	1.291	1.144	0.984	0.040	0.046	0.031	0.034	0.048	0.037
0.154	0.148	0.134	0.124	0.123	0.115	0.117	0.125	0.128	0.153	0.156	0.676	0.677	0.646	0.678	0.652	0.669
0.047	0.045	0.042	0.041	0.051	0.045	0.045	0.046	0.048	0.042	0.047	0.005	0.003	0.003	0.001	0.004	0.001
0.015	0.022	0.000	0.012	0.000	0.020	0.024	0.001	0.000	0.005	0.000	0.029	0.004	0.020	0.012	0.041	0.016
0.002	0.001	0.000	0.001	0.001	0.001	0.001	0.000	0.000	0.000	0.001	1.047	1.053	1.105	1.067	1.062	1.056
8.036	8.034	8.030	8.035	8.017	8.038	8.039	8.031	8.039	8.024	8.040	7.886	7.870	7.874	7.870	7.891	7.870

Sample No 22032013													
Comment	Garnet	Garnet	Garnet	Garnet	Garnet	Garnet	Garnet	Garnet	Garnet	Garnet	Garnet	Garnet	Garnet
SiO_2	36.57	36.53	36.39	36.44	36.36	36.54	35.39	36.30	36.83	36.58	36.54	36.80	36.34
TiO_2	0.05	0.10	0.00	0.00	0.17	0.10	0.10	0.09	0.08	0.04	0.00	0.00	0.02
Al_2O_3	20.28	19.68	20.09	20.32	20.41	20.15	19.09	19.69	20.11	19.83	19.75	20.19	19.79
Cr_2O_3	0.00	0.00	0.00	0.02	0.04	0.06	0.06	0.03	0.00	0.05	0.02	0.04	0.00
FeO	32.06	30.71	29.69	27.60	26.72	25.69	26.68	27.80	29.17	31.07	32.49	33.64	33.02
MnO	7.83	9.43	10.74	12.39	13.89	14.23	13.70	12.46	11.33	9.35	7.94	7.29	7.06
MgO	2.64	2.41	2.21	2.02	1.81	1.70	1.68	1.94	2.22	2.52	2.66	2.63	2.26
CaO	0.84	0.77	0.82	0.73	0.63	0.86	0.66	0.73	0.78	0.85	0.83	0.78	0.75
Na_2O	0.02	0.05	0.02	0.00	0.03	0.03	0.00	0.02	0.01	0.01	0.00	0.02	0.01
K_2O	0.00	0.00	0.00	0.01	0.00	0.00	0.00	0.00	0.00	0.01	0.01	0.01	0.04
Total	100.29	99.68	99.97	99.51	100.05	99.36	97.35	99.06	100.52	100.32	100.24	101.39	99.29
O=	12	12	12	12	12	12	12	12	12	12	12	12	12
Si	2.978	2.999	2.982	2.991	2.976	3.004	2.993	3.002	2.997	2.988	2.988	2.975	2.997
Ti	0.003	0.006	0.000	0.000	0.010	0.006	0.006	0.006	0.005	0.002	0.000	0.000	0.001
Al	1.946	1.905	1.940	1.966	1.968	1.952	1.903	1.919	1.929	1.909	1.903	1.924	1.924
Cr	0.000	0.000	0.000	0.001	0.003	0.004	0.004	0.002	0.000	0.003	0.001	0.003	0.000
Fe	2.183	2.109	2.035	1.894	1.828	1.766	1.887	1.922	1.985	2.122	2.221	2.274	2.277
Mn	0.541	0.657	0.747	0.862	0.964	0.992	0.983	0.874	0.782	0.648	0.550	0.500	0.494
Mg	0.320	0.295	0.270	0.247	0.221	0.208	0.212	0.239	0.269	0.307	0.324	0.317	0.278
Ca	0.073	0.068	0.072	0.064	0.055	0.076	0.059	0.065	0.068	0.075	0.073	0.068	0.066
Na	0.003	0.007	0.004	0.000	0.005	0.005	0.001	0.003	0.001	0.002	0.001	0.003	0.002
K	0.000	0.000	0.000	0.001	0.000	0.000	0.000	0.000	0.000	0.001	0.001	0.001	0.004
Total	8.047	8.046	8.050	8.026	8.030	8.014	8.048	8.033	8.035	8.056	8.061	8.064	8.043

Biotite	Biotite	Biotite	Biotite	Biotite	Biotite	Plagioclase	Plagioclase	Plagioclase	Cordierite	Biotite	Biotite	Biotite	Biotite	Biotite	Biotite	Biotite
34.44	34.51	34.95	34.88	35.10	33.73	62.79	62.51	62.66	47.01	32.74	32.79	32.84	33.22	33.29	32.78	32.88
2.96	3.16	2.95	3.10	2.91	3.13	0.00	0.05	0.00	0.02	3.68	3.68	3.92	3.83	3.70	3.80	2.97
18.82	18.55	18.96	18.90	18.73	18.27	23.24	24.20	24.26	32.52	17.51	17.38	17.27	17.35	17.55	17.30	18.34
0.09	0.13	0.08	0.01	0.07	0.09	0.02	0.00	0.02	0.04	0.06	0.06	0.08	0.06	0.04	0.06	0.01
22.65	22.61	22.69	22.70	23.10	23.65	0.60	0.26	0.08	11.99	23.30	22.51	23.20	22.59	23.00	23.72	23.06
0.63	0.65	0.65	0.56	0.56	0.55	0.04	0.05	0.03	0.87	0.22	0.21	0.27	0.26	0.20	0.32	0.22
7.06	7.04	6.99	7.05	7.14	7.31	0.00	0.02	0.00	6.36	5.87	5.89	6.08	5.98	5.85	5.96	6.02
0.05	0.01	0.00	0.04	0.02	0.06	4.17	4.49	4.58	0.01	0.05	0.00	0.01	0.00	0.00	0.02	0.00
0.12	0.15	0.16	0.16	0.12	0.12	9.34	9.29	8.76	0.25	0.07	0.09	0.11	0.11	0.11	0.09	0.10
8.71	8.89	9.20	9.25	9.20	9.01	0.14	0.22	0.25	0.01	12.33	11.48	12.25	12.13	12.20	12.19	12.36
95.53	95.69	96.62	96.67	96.95	95.90	100.33	101.08	100.63	99.08	95.83	94.07	96.03	95.54	95.94	96.24	95.94
11	11	11	11	11	11	8	8	8	18	11	11	11	11	11	11	11
2.659	2.664	2.671	2.666	2.677	2.620	2.778	2.746	2.756	4.917	2.601	2.631	2.602	2.632	2.630	2.598	2.600
0.172	0.184	0.170	0.178	0.167	0.183	0.000	0.002	0.000	0.002	0.220	0.222	0.233	0.229	0.220	0.227	0.177
1.713	1.688	1.708	1.702	1.684	1.673	1.212	1.253	1.258	4.009	1.639	1.644	1.613	1.620	1.634	1.616	1.710
0.005	0.008	0.005	0.001	0.004	0.006	0.001	0.000	0.001	0.003	0.004	0.004	0.005	0.004	0.003	0.004	0.000
1.463	1.460	1.450	1.451	1.474	1.536	0.022	0.009	0.003	1.049	1.548	1.510	1.537	1.497	1.519	1.572	1.525
0.041	0.043	0.042	0.036	0.036	0.036	0.001	0.002	0.001	0.077	0.015	0.014	0.018	0.018	0.013	0.021	0.014
0.813	0.810	0.796	0.803	0.812	0.846	0.000	0.001	0.000	0.991	0.695	0.704	0.718	0.707	0.689	0.704	0.709
0.004	0.001	0.000	0.004	0.002	0.005	0.197	0.211	0.216	0.001	0.004	0.000	0.001	0.000	0.000	0.001	0.000
0.018	0.022	0.024	0.024	0.017	0.019	0.801	0.791	0.747	0.051	0.011	0.014	0.017	0.016	0.017	0.014	0.015
0.858	0.875	0.897	0.902	0.895	0.893	0.008	0.012	0.014	0.001	1.250	1.175	1.238	1.226	1.230	1.233	1.247
7.747	7.754	7.763	7.767	7.768	7.814	5.020	5.028	4.995	11.101	7.987	7.918	7.983	7.948	7.955	7.990	7.999

Table 9-2-3. EPMA data of Oshima (Oshima Peninsula).

Sample No 23043004																
Comment	Garnet	Garnet	Garnet	Garnet	Garnet	Garnet	Garnet	Garnet	Garnet	Garnet	Garnet	Garnet	Garnet	Biotite	Plagioclase	Plagioclase
SiO_2	36.39	35.90	35.20	35.20	35.11	35.43	35.37	35.30	34.94	34.98	35.28	35.09	35.36	33.05	59.53	57.54
TiO_2	0.03	0.16	0.24	0.19	0.28	0.27	0.20	0.22	0.21	0.25	0.23	0.27	0.11	3.00	0.01	0.00
Al_2O_3	21.17	20.41	19.94	20.04	20.03	20.22	20.13	20.04	19.75	19.91	19.88	19.89	20.10	18.16	25.01	25.60
Cr_2O_3	0.07	0.00	0.03	0.05	0.03	0.04	0.08	0.00	0.00	0.04	0.01	0.00	0.00	0.08	0.19	0.00
FeO	28.11	23.63	17.58	15.56	15.25	15.07	14.60	13.87	12.86	13.86	16.63	21.74	26.44	19.85	1.19	0.06
MnO	9.43	11.88	17.28	19.88	19.43	18.58	20.34	19.69	21.42	21.73	18.51	13.40	10.41	0.27	0.06	0.00
MgO	1.96	1.62	0.93	0.63	0.65	0.71	0.55	0.51	0.39	0.49	0.76	1.41	1.97	8.07	0.00	0.01
CaO	0.92	2.82	3.59	3.85	3.84	4.14	3.75	3.96	4.10	3.33	3.31	3.25	1.35	0.12	6.48	7.32
Na_2O	0.01	0.01	0.00	0.00	0.00	0.00	0.00	0.00	0.01	0.02	0.02	0.00	0.04	0.19	8.39	9.41
K_2O	0.07	0.01	0.00	0.00	0.02	0.01	0.00	0.01	0.01	0.00	0.00	0.00	0.03	10.49	0.11	0.09
Total	98.16	96.44	94.78	95.41	94.65	94.47	95.03	93.60	93.68	94.60	94.63	95.06	95.81	93.20	100.97	100.03
O=	12	12	12	12	12	12	12	12	12	12	12	12	12	11	8	8
Si	2.995	3.004	3.003	2.993	3.000	3.017	3.009	3.033	3.016	3.000	3.016	2.989	2.993	2.621	2.650	2.594
Ti	0.002	0.010	0.015	0.012	0.018	0.017	0.013	0.014	0.014	0.016	0.015	0.018	0.007	0.179	0.000	0.000
Al	2.053	2.012	2.005	2.008	2.018	2.029	2.019	2.030	2.009	2.012	2.003	1.997	2.005	1.698	1.312	1.360
Cr	0.004	0.000	0.002	0.004	0.002	0.003	0.006	0.000	0.000	0.003	0.001	0.000	0.000	0.005	0.007	0.000
Fe	1.935	1.653	1.254	1.106	1.090	1.073	1.039	0.997	0.928	0.994	1.189	1.549	1.871	1.317	0.044	0.002
Mn	0.659	0.843	1.251	1.434	1.408	1.342	1.468	1.435	1.568	1.581	1.342	0.968	0.748	0.018	0.002	0.000
Mg	0.241	0.202	0.118	0.079	0.083	0.091	0.069	0.065	0.050	0.063	0.097	0.179	0.248	0.954	0.000	0.001
Ca	0.081	0.253	0.328	0.351	0.352	0.378	0.342	0.365	0.379	0.306	0.303	0.296	0.122	0.010	0.309	0.354
Na	0.002	0.002	0.001	0.000	0.000	0.000	0.000	0.000	0.002	0.004	0.003	0.000	0.006	0.028	0.724	0.823
K	0.007	0.001	0.000	0.000	0.002	0.001	0.000	0.001	0.001	0.000	0.000	0.000	0.003	1.062	0.006	0.005
Total	7.979	7.981	7.978	7.988	7.973	7.950	7.966	7.939	7.967	7.978	7.969	7.995	8.002	7.893	5.055	5.140

Garnet	Garnet	Garnet	Garnet	Garnet	Garnet	Garnet	Garnet	Garnet	Biotite	Biotite	Biotite	Biotite	Plagioclase	K-feldspar	K-feldspar
35.53	34.85	35.00	35.37	35.68	35.41	34.78	34.57	34.93	33.26	33.07	32.98	33.26	58.60	63.94	64.25
0.11	0.22	0.18	0.04	0.00	0.07	0.19	0.27	0.13	4.51	4.32	4.38	4.00	0.02	0.00	0.00
20.36	19.96	19.93	20.55	20.54	20.81	19.90	20.18	20.06	17.13	17.17	16.90	17.39	24.88	18.89	18.37
0.00	0.01	0.03	0.00	0.00	0.01	0.00	0.05	0.00	0.07	0.11	0.15	0.13	0.00	0.00	0.00
23.08	20.56	16.04	34.01	34.11	32.47	17.38	19.58	23.28	20.23	20.31	21.00	20.39	0.34	0.21	0.15
13.76	16.16	20.66	1.33	1.64	4.34	17.83	16.90	14.15	0.32	0.28	0.44	0.30	0.01	0.05	0.02
1.41	1.20	0.77	4.30	4.17	3.68	1.07	1.22	1.47	7.27	7.57	6.73	7.73	0.01	0.00	0.00
2.92	3.19	4.19	1.16	1.16	1.20	4.54	3.30	2.85	0.03	0.01	0.03	0.04	6.71	0.23	0.04
0.04	0.00	0.00	0.03	0.00	0.03	0.01	0.04	0.03	0.06	0.08	0.11	0.06	7.47	1.83	0.97
0.00	0.00	0.01	0.02	0.00	0.00	0.00	0.01	0.04	9.44	10.04	9.69	9.98	0.22	13.92	16.26
97.22	96.15	96.80	96.79	97.30	98.03	95.71	96.12	96.93	92.31	92.94	92.41	93.27	98.25	99.07	100.05
12	12	12	12	12	12	12	12	12	11	11	11	11	8	8	8
2.972	2.957	2.956	2.940	2.952	2.923	2.957	2.934	2.946	2.654	2.634	2.650	2.637	2.663	2.967	2.980
0.007	0.014	0.011	0.003	0.000	0.004	0.012	0.017	0.008	0.271	0.259	0.265	0.239	0.001	0.000	0.000
2.007	1.996	1.983	2.013	2.003	2.025	1.994	2.019	1.994	1.612	1.612	1.601	1.625	1.332	1.033	1.004
0.000	0.001	0.002	0.000	0.000	0.001	0.000	0.003	0.000	0.005	0.007	0.010	0.008	0.000	0.000	0.000
1.614	1.459	1.132	2.364	2.359	2.241	1.236	1.390	1.642	1.350	1.353	1.412	1.352	0.013	0.008	0.006
0.977	1.163	1.479	0.093	0.115	0.304	1.286	1.217	1.012	0.021	0.019	0.030	0.020	0.000	0.002	0.001
0.176	0.151	0.097	0.532	0.514	0.453	0.136	0.154	0.185	0.866	0.898	0.806	0.913	0.000	0.000	0.000
0.262	0.290	0.379	0.103	0.103	0.106	0.413	0.300	0.258	0.002	0.001	0.002	0.003	0.327	0.011	0.002
0.007	0.001	0.000	0.005	0.000	0.005	0.001	0.007	0.005	0.010	0.012	0.016	0.009	0.658	0.165	0.087
0.000	0.000	0.001	0.002	0.000	0.000	0.000	0.001	0.004	0.961	1.021	0.993	1.009	0.013	0.824	0.962
8.021	8.031	8.041	8.054	8.046	8.063	8.035	8.041	8.054	7.752	7.815	7.785	7.816	5.006	5.011	5.042

Garnet	Garnet	Garnet	Garnet	Garnet	Garnet	Garnet	Garnet	Garnet	Garnet	Garnet	Garnet	Biotite	Biotite	Biotite	Plagioclase	Plagioclase	Plagioclase
37.33	37.22	38.13	36.76	37.00	36.65	36.56	36.82	36.51	36.48	36.70	36.24	35.19	34.79	35.37	61.33	50.77	59.25
0.08	0.09	0.25	0.20	0.26	0.23	0.06	0.02	0.24	0.22	0.20	0.07	3.18	2.97	3.12	0.03	1.09	0.00
20.51	20.03	19.53	20.00	20.00	20.18	20.07	19.99	19.95	19.96	19.93	19.68	18.07	17.62	18.40	23.71	22.33	24.94
0.04	0.05	0.00	0.05	0.01	0.01	0.02	0.02	0.06	0.00	0.05	0.00	0.03	0.07	0.09	0.01	0.02	0.00
26.02	21.21	17.68	14.30	14.24	17.86	20.69	18.76	15.16	15.72	19.50	25.87	18.62	18.39	19.37	0.64	6.49	0.45
10.97	14.13	18.05	21.58	20.68	16.92	17.18	19.23	19.00	19.71	16.75	11.28	0.23	0.38	0.30	0.15	0.11	0.04
2.16	1.43	0.95	0.53	0.58	1.02	1.18	0.98	0.68	0.67	1.17	2.09	9.00	8.62	8.77	0.00	4.32	0.00
1.04	3.04	3.18	3.52	4.11	4.09	1.41	1.43	4.59	3.97	3.01	1.16	0.04	0.02	0.10	5.81	4.14	6.81
0.04	0.01	0.02	0.00	0.00	0.03	0.00	0.01	0.02	0.01	0.02	0.04	0.10	0.09	0.42	8.36	4.89	7.43
0.06	0.04	0.01	0.03	0.00	0.01	0.01	0.02	0.01	0.00	0.02	0.03	12.48	10.34	11.79	0.17	4.79	0.16
98.22	97.24	97.80	96.95	96.89	96.99	97.17	97.27	96.22	96.75	97.35	96.45	96.95	93.29	97.72	100.21	98.93	99.09
12	12	12	12	12	12	12	12	12	12	12	12	11	11	11	8	8	8
3.057	3.076	3.132	3.062	3.073	3.043	3.050	3.068	3.054	3.046	3.048	3.042	2.680	2.723	2.672	2.730	2.434	2.669
0.005	0.006	0.015	0.012	0.016	0.014	0.003	0.001	0.015	0.014	0.012	0.004	0.182	0.175	0.177	0.001	0.039	0.000
1.979	1.951	1.890	1.963	1.958	1.974	1.973	1.963	1.967	1.964	1.950	1.947	1.622	1.625	1.638	1.244	1.262	1.324
0.002	0.003	0.000	0.003	0.001	0.000	0.002	0.001	0.004	0.000	0.003	0.000	0.002	0.004	0.005	0.000	0.001	0.000
1.782	1.466	1.215	0.996	0.989	1.240	1.443	1.307	1.060	1.098	1.354	1.816	1.186	1.204	1.223	0.024	0.260	0.017
0.762	0.990	1.257	1.524	1.457	1.192	1.216	1.359	1.348	1.396	1.180	0.803	0.015	0.025	0.019	0.006	0.005	0.002
0.263	0.177	0.116	0.065	0.072	0.126	0.146	0.121	0.085	0.083	0.144	0.261	1.022	1.005	0.987	0.000	0.308	0.000
0.091	0.269	0.280	0.314	0.366	0.364	0.126	0.127	0.412	0.355	0.268	0.104	0.003	0.002	0.008	0.277	0.212	0.329
0.006	0.001	0.004	0.000	0.000	0.005	0.000	0.001	0.003	0.002	0.004	0.006	0.015	0.013	0.062	0.721	0.454	0.649
0.006	0.004	0.001	0.003	0.000	0.001	0.001	0.003	0.001	0.000	0.002	0.003	1.213	1.033	1.136	0.010	0.293	0.009
7.953	7.944	7.910	7.944	7.932	7.959	7.960	7.951	7.947	7.959	7.966	7.985	7.940	7.810	7.928	5.013	5.269	4.998

Garnet	Garnet	Garnet	Garnet	Garnet	Garnet	Garnet	Garnet	Garnet	Biotite	Biotite	Biotite	Biotite	Plagioclase	Plagioclase	Plagioclase	Plagioclase
38.15	37.15	36.83	36.36	36.75	36.42	37.96	36.48	36.52	34.59	34.14	34.22	33.79	59.00	58.99	57.99	59.03
0.08	0.17	0.14	0.19	0.17	0.06	0.22	0.21	0.04	4.20	3.78	3.35	4.50	0.02	0.03	0.00	0.00
20.93	19.93	20.13	19.72	19.88	20.22	20.42	19.82	19.80	17.67	17.50	17.58	17.41	25.63	25.88	25.94	25.97
0.02	0.02	0.01	0.02	0.07	0.00	0.00	0.00	0.01	0.05	0.10	0.12	0.13	0.01	0.00	0.00	0.02
23.80	16.34	14.20	12.46	15.82	32.47	20.27	19.61	22.11	19.24	19.69	19.12	19.30	0.13	0.15	0.13	0.14
13.16	19.65	21.38	22.33	17.11	4.33	14.84	16.52	12.74	0.43	0.43	0.35	0.36	0.00	0.04	0.04	0.00
1.64	0.79	0.55	0.38	0.97	2.97	1.22	1.12	1.32	7.32	7.12	7.64	7.15	0.01	0.00	0.02	0.01
1.70	3.41	3.78	4.56	5.16	1.01	3.92	3.20	4.06	0.00	0.00	0.00	0.00	7.46	7.69	7.93	7.77
0.00	0.00	0.01	0.03	0.03	0.01	0.00	0.00	0.00	0.11	0.09	0.11	0.06	7.35	7.26	6.99	6.89
0.06	0.02	0.01	0.01	0.00	0.00	0.02	0.01	0.00	13.11	13.00	12.61	13.02	0.11	0.17	0.20	0.23
99.53	97.48	97.02	96.06	95.96	97.49	98.87	96.98	96.59	96.70	95.85	95.10	95.73	99.73	100.20	99.23	100.05
12	12	12	12	12	12	12	12	12	11	11	11	11	8	8	8	8
3.076	3.075	3.062	3.057	3.068	3.014	3.079	3.044	3.049	2.668	2.666	2.679	2.640	2.642	2.632	2.615	2.634
0.005	0.011	0.009	0.012	0.011	0.003	0.013	0.013	0.002	0.244	0.222	0.197	0.265	0.001	0.001	0.000	0.000
1.989	1.944	1.972	1.953	1.956	1.972	1.952	1.948	1.949	1.606	1.611	1.622	1.604	1.352	1.361	1.379	1.366
0.001	0.002	0.000	0.001	0.004	0.000	0.000	0.000	0.001	0.003	0.006	0.008	0.008	0.000	0.000	0.000	0.001
1.605	1.131	0.987	0.876	1.105	2.247	1.375	1.368	1.544	1.241	1.286	1.252	1.261	0.005	0.005	0.005	0.005
0.900	1.379	1.507	1.592	1.212	0.304	1.021	1.169	0.902	0.028	0.028	0.023	0.024	0.000	0.001	0.001	0.000
0.197	0.097	0.068	0.048	0.121	0.367	0.148	0.139	0.164	0.842	0.829	0.891	0.833	0.001	0.000	0.002	0.000
0.147	0.303	0.336	0.411	0.462	0.089	0.341	0.286	0.363	0.000	0.000	0.000	0.000	0.358	0.367	0.383	0.371
0.000	0.000	0.001	0.004	0.005	0.001	0.000	0.000	0.000	0.016	0.014	0.016	0.010	0.638	0.628	0.611	0.596
0.006	0.002	0.001	0.002	0.000	0.000	0.002	0.001	0.000	1.290	1.295	1.260	1.298	0.006	0.010	0.011	0.013
7.927	7.943	7.944	7.956	7.943	7.997	7.932	7.969	7.974	7.937	7.958	7.947	7.943	5.003	5.005	5.007	4.987

Table 9-2-4! EPMA data of Sukumojima (Oshima Peninsula).

Sample No 21062603													
Comment	Garnet	Garnet	Garnet	Garnet	Garnet	Garnet	Garnet	Garnet	Biotite	Biotite	Biotite	Plagioclase	Plagioclase
SiO_2	36.65	36.18	36.06	35.86	35.73	34.97	35.10	34.87	34.58	34.47	35.34	62.87	62.40
TiO_2	0.06	0.12	0.07	0.07	0.19	0.20	0.14	0.00	2.64	2.53	2.09	0.00	0.08
Al_2O_3	20.40	20.76	20.51	20.50	20.49	19.87	19.90	19.43	17.07	17.04	17.21	22.51	22.61
Cr_2O_3	0.03	0.05	0.00	0.04	0.01	0.09	0.03	0.01	0.05	0.03	0.02	0.00	0.00
FeO	25.98	25.43	25.31	24.97	25.21	25.57	25.89	26.19	19.66	20.42	19.16	0.23	0.43
MnO	13.46	14.07	14.15	14.36	14.44	14.54	13.38	13.33	0.52	0.39	0.31	0.04	0.13
MgO	2.10	2.27	2.25	2.27	2.33	2.29	2.28	2.26	9.96	9.70	9.73	0.00	0.03
CaO	0.78	0.54	0.57	0.67	0.57	0.59	0.79	0.76	0.02	0.02	0.16	3.72	3.98
Na_2O	0.00	0.04	0.02	0.05	0.05	0.02	0.02	0.00	0.11	0.11	0.22	9.11	8.34
K_2O	0.00	0.01	0.01	0.00	0.01	0.02	0.03	0.01	10.60	11.60	9.31	0.10	0.10
Total	99.45	99.46	98.95	98.80	99.01	98.16	97.55	96.86	95.20	96.30	93.55	98.59	98.09
O=	12	12	12	12	12	12	12	12	11	11	11	8	8
Si	3.000	2.964	2.971	2.961	2.948	2.929	2.948	2.957	2.679	2.665	2.750	2.815	2.808
Ti	0.003	0.007	0.005	0.005	0.012	0.013	0.009	0.000	0.154	0.147	0.122	0.000	0.003
Al	1.968	2.004	1.992	1.995	1.992	1.961	1.969	1.942	1.559	1.552	1.578	1.188	1.199
Cr	0.002	0.003	0.000	0.003	0.001	0.006	0.002	0.001	0.003	0.002	0.001	0.000	0.000
Fe	1.778	1.742	1.743	1.724	1.739	1.791	1.818	1.857	1.274	1.320	1.247	0.008	0.016
Mn	0.935	0.978	0.989	1.006	1.010	1.033	0.953	0.959	0.034	0.026	0.021	0.002	0.005
Mg	0.256	0.277	0.276	0.280	0.286	0.286	0.286	0.285	1.150	1.118	1.128	0.000	0.002
Ca	0.069	0.047	0.051	0.059	0.050	0.053	0.071	0.069	0.002	0.002	0.013	0.178	0.192
Na	0.000	0.007	0.003	0.007	0.008	0.004	0.003	0.000	0.016	0.016	0.033	0.791	0.727
K	0.000	0.001	0.001	0.000	0.001	0.002	0.003	0.002	1.048	1.144	0.925	0.006	0.006
Total	8.011	8.030	8.030	8.039	8.048	8.077	8.061	8.072	7.918	7.991	7.817	4.989	4.957

Garnet	Garnet	Garnet	Garnet	Garnet	Garnet	Biotite	Biotite	Biotite	Plagioclase	Plagioclase	Plagioclase
36.03	36.18	36.94	36.16	36.42	35.78	35.26	34.98	34.19	64.10	63.38	62.79
0.06	0.25	0.10	0.18	0.17	0.09	2.24	2.21	2.01	0.01	0.00	0.03
20.64	20.70	20.59	20.30	20.75	20.23	17.20	16.83	17.52	22.26	22.41	22.52
0.00	0.03	0.01	0.00	0.03	0.00	0.06	0.05	0.05	0.01	0.04	0.00
26.65	26.33	24.50	26.43	26.64	26.12	19.90	19.86	19.89	0.52	0.28	0.19
12.84	13.17	10.46	12.73	12.95	12.85	0.38	0.31	0.36	0.06	0.03	0.01
2.28	2.31	2.11	2.21	2.16	2.01	10.14	10.20	9.85	0.01	0.00	0.00
0.66	0.60	4.80	0.55	0.71	0.76	0.04	0.03	0.03	3.61	3.73	3.76
0.01	0.05	0.03	0.06	0.05	0.00	0.15	0.13	0.14	7.54	9.34	9.42
0.00	0.02	0.01	0.02	0.02	0.04	12.08	11.47	11.94	0.06	0.07	0.11
99.16	99.65	99.55	98.64	99.90	97.88	97.43	96.06	95.98	98.17	99.28	98.83
12	12	12	12	12	12	11	11	11	8	8	8
2.963	2.959	2.992	2.986	2.971	2.981	2.687	2.697	2.651	2.860	2.820	2.809
0.003	0.016	0.006	0.011	0.011	0.006	0.129	0.128	0.117	0.000	0.000	0.001
2.000	1.996	1.966	1.976	1.995	1.987	1.545	1.530	1.602	1.171	1.175	1.187
0.000	0.002	0.001	0.000	0.002	0.000	0.003	0.003	0.003	0.000	0.001	0.000
1.833	1.801	1.660	1.825	1.817	1.819	1.268	1.281	1.290	0.019	0.011	0.007
0.895	0.914	0.719	0.892	0.896	0.908	0.025	0.020	0.024	0.002	0.001	0.001
0.279	0.282	0.255	0.272	0.263	0.250	1.151	1.172	1.139	0.001	0.000	0.000
0.059	0.053	0.416	0.049	0.062	0.067	0.003	0.003	0.002	0.172	0.178	0.180
0.002	0.008	0.004	0.009	0.007	0.000	0.022	0.020	0.021	0.652	0.806	0.817
0.000	0.002	0.001	0.002	0.002	0.005	1.174	1.128	1.181	0.003	0.004	0.006
8.034	8.031	8.021	8.021	8.025	8.023	8.008	7.982	8.030	4.881	4.996	5.008

Garnet	Garnet	Garnet	Garnet	Garnet	Garnet	Garnet	Garnet	Biotite	Biotite	Biotite	Biotite	Plagioclase	Plagioclase	Plagioclase	Plagioclase	Plagioclase
36.28	36.14	35.94	35.48	35.84	35.42	35.45	35.34	37.12	35.15	34.64	34.90	65.80	68.06	67.38	65.17	65.53
0.06	0.00	0.15	0.10	0.13	0.18	0.16	0.09	2.49	2.29	1.69	2.10	0.00	0.00	0.00	0.00	0.04
20.96	20.79	20.55	20.54	20.66	20.29	20.29	20.44	18.33	16.93	17.65	17.00	22.16	21.21	22.83	23.22	22.63
0.00	0.00	0.01	0.02	0.02	0.00	0.02	0.05	0.07	0.07	0.08	0.06	0.02	0.01	0.00	0.00	0.03
25.95	25.86	25.12	25.16	24.42	25.11	25.20	25.87	19.14	19.30	21.01	19.80	0.07	2.14	0.47	0.20	0.13
13.94	14.02	14.85	14.83	14.77	14.91	14.70	13.63	0.39	0.41	3.39	0.36	0.00	0.00	0.06	0.05	0.00
2.13	2.35	2.47	2.49	2.44	2.44	2.42	2.27	9.61	10.55	8.21	10.57	0.00	0.00	0.34	0.00	0.00
0.77	0.71	0.54	0.52	2.20	0.47	0.49	0.78	0.19	0.14	0.29	0.09	3.38	2.40	3.00	3.75	3.47
0.01	0.03	0.01	0.02	0.03	0.03	0.04	0.02	0.91	0.36	0.12	0.22	9.14	6.96	6.97	8.56	9.04
0.03	0.01	0.01	0.00	0.00	0.00	0.01	0.01	9.11	9.16	7.46	9.50	0.08	0.05	0.20	0.09	0.05
100.13	99.89	99.65	99.16	100.51	98.83	98.79	98.50	97.36	94.37	94.54	94.59	100.63	100.83	101.26	101.04	100.91
12	12	12	12	12	12	12	12	11	11	11	11	8	8	8	8	8
2.957	2.954	2.948	2.929	2.918	2.936	2.939	2.936	2.759	2.716	2.703	2.702	2.871	2.947	2.895	2.834	2.853
0.003	0.000	0.009	0.006	0.008	0.011	0.010	0.006	0.139	0.133	0.099	0.122	0.000	0.000	0.000	0.000	0.001
2.013	2.002	1.986	1.998	1.982	1.982	1.982	2.001	1.605	1.543	1.623	1.551	1.139	1.082	1.156	1.190	1.161
0.000	0.000	0.001	0.002	0.001	0.000	0.001	0.003	0.004	0.005	0.005	0.004	0.001	0.000	0.000	0.000	0.001
1.769	1.767	1.722	1.737	1.662	1.740	1.747	1.797	1.189	1.248	1.371	1.282	0.002	0.078	0.017	0.007	0.005
0.964	0.972	1.033	1.038	1.020	1.048	1.034	0.960	0.025	0.027	0.224	0.023	0.000	0.000	0.002	0.002	0.000
0.259	0.286	0.301	0.306	0.296	0.301	0.299	0.281	1.064	1.215	0.955	1.220	0.000	0.000	0.022	0.000	0.000
0.067	0.062	0.048	0.046	0.192	0.042	0.044	0.070	0.015	0.012	0.024	0.007	0.158	0.112	0.138	0.175	0.162
0.001	0.004	0.002	0.004	0.004	0.004	0.006	0.003	0.131	0.054	0.018	0.032	0.773	0.584	0.581	0.722	0.763
0.003	0.001	0.001	0.000	0.000	0.000	0.001	0.001	0.864	0.903	0.742	0.939	0.004	0.002	0.011	0.005	0.003
8.036	8.048	8.051	8.066	8.085	8.064	8.063	8.058	7.795	7.856	7.764	7.884	4.948	4.805	4.822	4.934	4.948